Exhibit DD

Exhibit D-6

Invalidity of U.S. Patent No. 6,922,632 ("'632 Patent") under Pre-AIA Section 102 or Section 103 in view of Welch et al., "High-Performance Wide-Area Optical Tracking: The HiBall Tracking System," PRESENCE, Vol. 10, No. 1, February 2001 ("Welch 2001")[1]

Welch 2001 was published in February 2001. Plaintiffs belatedly asserted a priority date of June 13, 2001 for the '632 Patent on December 22, 2021, 71 days after the Court's deadline. Defendants have reviewed Plaintiffs' alleged evidence of the purported June 13, 2001 priority date, and maintain that the '632 Patent is not entitled to this priority date. *See* Defendants' March 15, 2022 Supplemental Invalidity Contentions. Defendants reserve their objections to Plaintiffs' belated assertion of the new priority date and expressly reserve all rights to challenge this alleged new priority date. As such, Defendants assume for the sake of these invalidity contentions, that the priority date for the '632 Patent is August 9, 2002 based on the first filed Provisional Application from which the '632 Patent claims priority. (Defendants do not concede nor agree that Plaintiffs are even entitled to this date.) Assuming this priority date, Welch 2001 qualifies as prior art under at least pre-AIA Sections 102(a) and (b).

As described herein, the asserted claims of the '632 Patent are invalid (a) under one or more sections of 35 U.S.C. § 102 as anticipated expressly or inherently by Welch 2001 (including the documents incorporated into Welch 2001 by reference), and (b) under 35 U.S.C. § 103 as obvious in view of Welch 2001 standing alone, and additionally, in combination with the knowledge of one of ordinary skill in the art, and/or other prior art, including but not limited to the prior art identified in Defendants' Invalidity Contentions and the prior art described in the claim charts attached in Exhibits D-1 – D-22. With respect to the proposed modifications to Welch 2001, as of the priority date of the '632 Patent, such modification would have been obvious to try, an obvious combination of prior art elements according to known methods to yield predictable results, a simple substitution of one known element for another to obtain predictable results, a use of known techniques to improve a similar device or method in the same way, an application of a known technique to a known device or method ready for improvement to yield predictable results, a variation of a known work in one field of endeavor for use in either the same field or a different one based on design incentives or other market forces with variations that are predictable to one of ordinary skill in the art, and/or obvious in view of teachings, suggestions, and motivations in the prior art that would have led one of ordinary skill to modify or combine the prior art references.

All cross-references should be understood to include material that is cross-referenced within the cross-reference. Where a particular figure is cited, the citation should be understood to encompass the caption and description of the figure as well as any text relating to or

[1] Discovery in this case is ongoing and, accordingly, this invalidity chart is not to be considered final. Defendants have conducted the invalidity analysis herein without having fully undergone claim construction and a *Markman* hearing. By charting the prior art against the claim(s) herein, Defendants are not admitting nor agreeing to Plaintiffs' interpretation of the claims at issue in this case. Additionally, these charts provide representative examples of portions of the charted references that disclose the indicated limitations under Plaintiffs' application of the claims; additional portions of these references other than the representative examples provided herein may also disclose the indicated limitation(s) and Defendants contend that the asserted claim(s) are invalid in light of the charted reference(s) as a whole. Defendants reserve the right to rely on additional citations or sources of evidence that also may be applicable, or that may become applicable in light of claim construction, changes in Plaintiffs' infringement contentions, and/or information obtained during discovery as the case progresses. Further, by submitting these invalidity contentions, Defendants do not waive and hereby expressly reserve their right to raise other invalidity defenses, including but not limited to defenses under Sections 101 and 112. Defendants reserve the right to amend or supplement this claim chart at a later date, including after the Court's order construing disputed claim terms.

describing the figure. Conversely, where particular text referring to a figure is cited, the citation should be understood to include the figure as well.

A. INDEPENDENT CLAIM 1

CLAIM 1	Welch 2001
[1.pre] A method for tracking an object comprising:	At least under Plaintiffs' apparent infringement theory, Welch 2001 discloses, either expressly or inherently, a method for tracking an object. No party has yet asserted that the preamble is limiting, nor has the Court construed the preamble as limiting. However, to the extent that the preamble is limiting, it is disclosed by Welch 2001. In the alternative, this element would be obvious over Welch 2001 in light of the other references disclosed in Defendants' Invalidity Contentions and/or the knowledge of one of ordinary skill in the art. *See, e.g.*: We present results and a complete description of our most recent electro-optical system, the HiBall Tracking System. In particular, we discuss motivation for the geometric configuration and describe the novel optical, mechanical, electronic, and algorithmic aspects that enable unprecedented speed, resolution, accuracy, robustness, and flexibility. Welch 2001 at Abstract. **Systems for head tracking for interactive computer graphics have been explored for more than thirty years.** Welch 2001 at Section 1. As part of his 1984 dissertation on Self-Tracker, Bishop put forward **the idea of outward-looking tracking systems based on user-mounted sensors that estimate user pose by observing landmarks in the environment** (Bishop, 1984). He described two kinds of landmarks: high signal-to-noise-ratio beacons such as light-emitting diodes (LEDs) and low signal-to-noise- ratio landmarks such as naturally occurring features. Bishop designed and demonstrated custom VLSI chips (figure 2) that combined image sensing and processing on a single chip (Bishop & Fuchs, 1984). The idea was to combine multiple instances of these chips into an outward-looking cluster that estimated cluster motion by observing natural features in the unmodified environment. Integrating the resulting motion to estimate pose is prone to accumulating error, so further development required a complementary system

Exhibit D-6

CLAIM 1	Welch 2001
	based on easily detectable landmarks (LEDs) at known locations. Welch 2001 at Section 1.2. 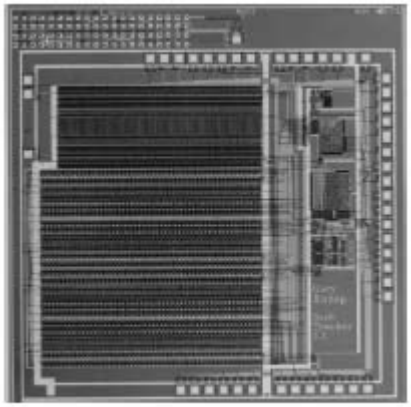 Figure 2. **In 1991, we demonstrated a working, scalable, electro-optical head-tracking system** in the Tomorrow's Realities gallery at that year's ACM SIGGRAPH conference (Wang et al., 1990; Wang, Chi, & Fuchs, 1990; Ward et al., 1992). **The system (figure 3) used four, head-worn, lateral-effect photodiodes that looked upward at a regular array of infrared LEDs installed in precisely machined ceiling panels. A user-worn backpack contained electronics that digitized and communicated the photo-coordinates of the sighted LEDs. Photo-grammetric techniques were used to compute a user's head pose using the known LED positions and the corresponding measured photo-coordinates from each LEPD sensor** (Azuma & Ward, 1991). Welch 2001 at Section 1.2.

Exhibit D-6

CLAIM 1	Welch 2001
	

Exhibit D-6

CLAIM 1	Welch 2001
	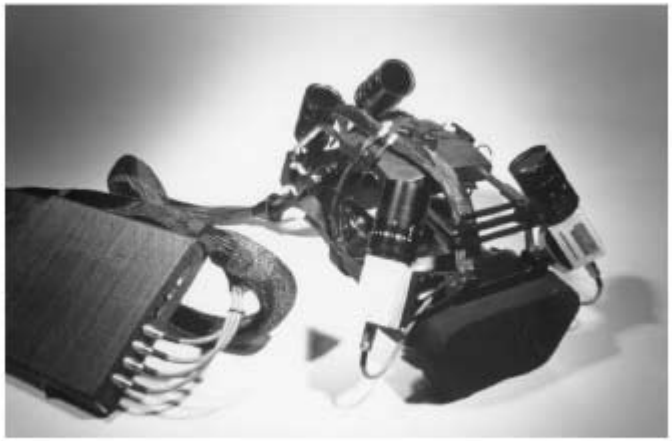 Figure 3. *See also* Defendants' Invalidity Contentions for further discussion.
[1.a] coupling a sensor subsystem to an estimation subsystem, said sensor subsystem enabling measurement related to relative locations or orientations of sensing elements;	At least under Plaintiffs' apparent infringement theory, Welch 2001 discloses, either expressly or inherently, coupling a sensor subsystem to an estimation subsystem, said sensor subsystem enabling measurement related to relative locations or orientations of sensing elements. In the alternative, this element would be obvious over Welch 2001 in light of the other references disclosed in Defendants' Invalidity Contentions and/or the knowledge of one of ordinary skill in the art. *See, e.g.*: Thanks to significant improvements in hardware and software, this HiBall system offers unprecedented speed, resolution, accuracy, robustness, and flexibility. The bulky and heavy sensors and backpack of the previous system have been replaced by a small HiBall unit (figure 4, bottom). In addition, the precisely machined LED ceiling panels of the previous system have been replaced by looser-tolerance panels that are relatively inexpensive to make and simple to install (figure 4, top; figure 10). Finally, we are using an unusual **Kalman-filter-based algorithm that generates very accurate pose estimates at a high rate with low latency, and that**

Exhibit D-6

CLAIM 1	Welch 2001
	simultaneously self-calibrates the system. Welch 2001 at Section 1.3.  Figure 4. In all of the optical systems we have developed (see section 1.2), **we have chosen what we call an inside-looking-out configuration, in which the optical sensors are on the (moving) user and the landmarks (for instance, the LEDs) are fixed in the laboratory.** The corresponding outside-looking-in alternative would be to place the landmarks on the user and to fix the optical sensors in the laboratory. (One can think about similar

Exhibit D-6

CLAIM 1	Welch 2001
	outside-in and inside-out distinctions for acoustic and magnetic technologies.) The two configurations are depicted in figure 5. Welch 2001 at Section 2. 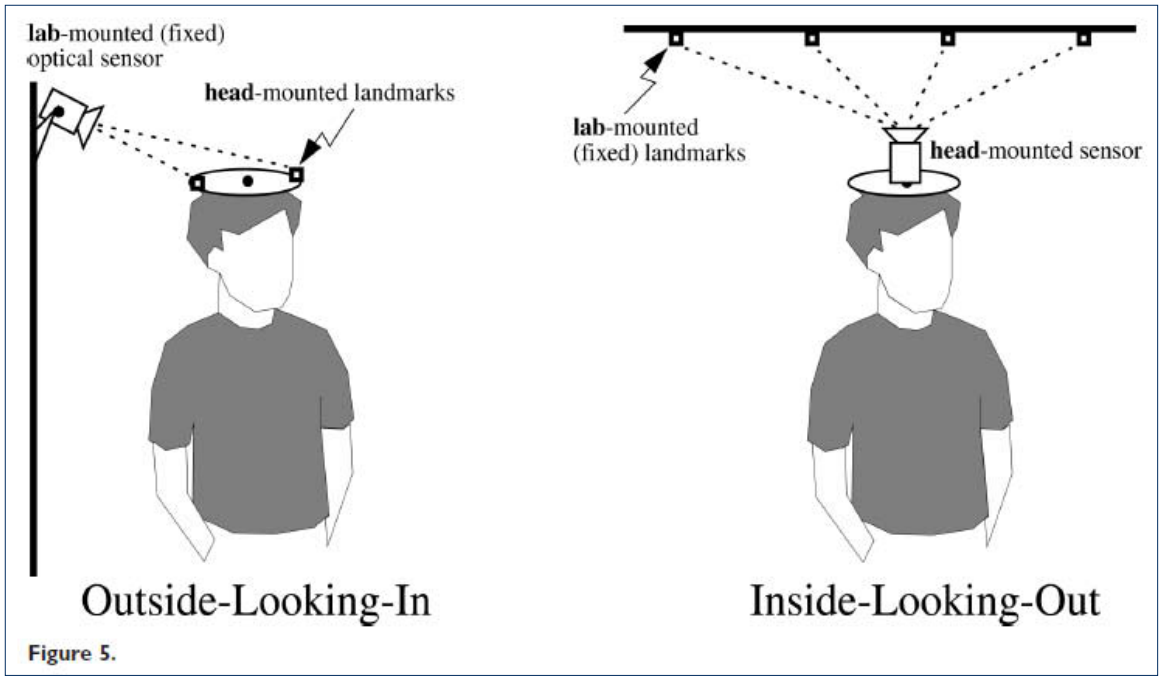 Figure 5. **Each HiBall observes LEDs through multiple sensor-lens views that are distributed over a large solid angle. LEDs are sequentially flashed (one at a time) such that they are seen via a diverse set of views for each HiBall. Initial acquisition is performed using a brute-force search through LED space, but, once initial lock is made, the selection of LEDs to flash is tailored to the views of the active HiBall units. Pose estimates are maintained using a Kalman-filter-based prediction-correction approach known as single-constraint-at-a-time (SCAAT) tracking.** This technique has been extended to provide self-calibration of the ceiling, concurrent with HiBall tracking. Welch 2001 at Section 3.

Exhibit D-6

CLAIM 1	Welch 2001
	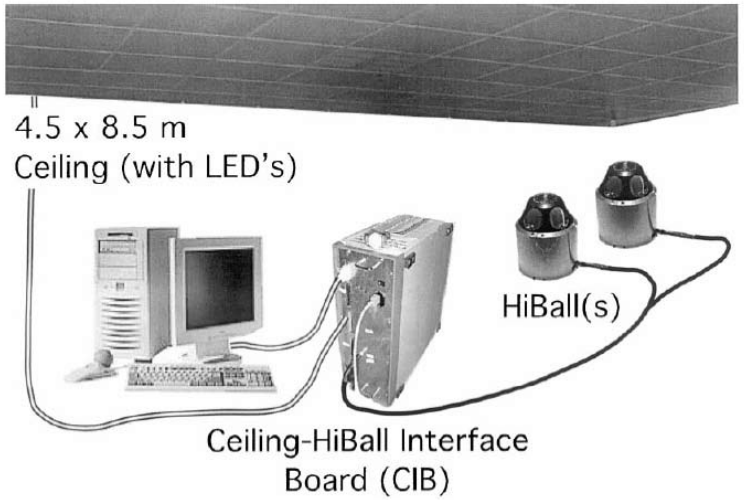 Figure 6. HiBall sensor unit was designed as a single, rigid, hollow ball having dodecahedral symmetry, with lenses in the upper six faces and LEPDs on the insides of the opposing six lower faces (figure 7). This immediately gives six primary "camera" views uniformly spaced by 57 deg. The views efficiently share the same internal air space and are rigid with respect to each other. In addition, light entering any lens sufficiently off-axis can be seen by a neighboring LEPD, giving rise to five secondary views through the top or central lens, and three secondary views through the five other lenses. Overall, this provides 26 fields of view that are used to sense widely separated groups of LEDs in the environment. Welch 2001 at Section 4.1.

Exhibit D-6

CLAIM 1	Welch 2001
	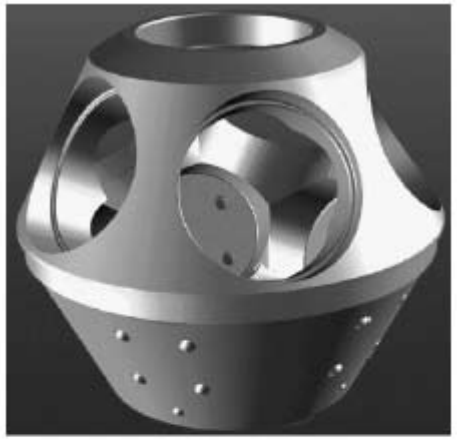  **Figure 7.** The LEPDs themselves are not imaging devices; rather, they detect the centroid of the luminous flux incident on the detector. The x-position of the centroid determines the ratio of two output y-position determines the ratio of two other output currents. The total output current of each pair are commensurate and are proportional to the total incident flux. Consequently, focus is not an issue, so the simple fixed-focus lenses work well over a range of LED distances from about half a meter to infinity. The LEPDs and associated electronic components are mounted on a custom rigid-flex printed circuitboard (figure 8). This arrangement makes efficient use of the internal HiBall volume while maintaining isolation between analog and digital circuitry, and increasing reliability by alleviating

CLAIM 1	Welch 2001
	the need for intercomponent mechanical connectors. Welch 2001 at Section 4.1. 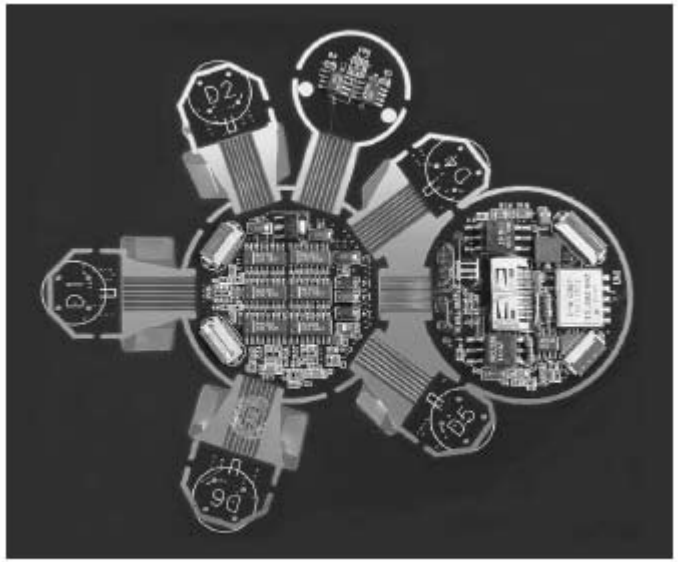 Figure 8. Figure 9 shows the physical arrangement of the folded electronics in the HiBall. Each LEPD has four transimpedance amplifiers (shown together as one "Amp" in figure 9), the analog outputs of which are multiplexed with those of the other LEPDs, then sampled, held, and converted by four 16-bit Delta-Sigma analog-to-digital (A/D) converters. Multiple samples are integrated via an accumulator. The digitized LEPD data are organized into packets for communication back to the CIB. The packets also contain information to assist in error detection. The communication protocol is simple, and, while presently implemented by wire, the modulation scheme is amenable to a wireless implementation. Welch 2001 at Section 4.1.

Exhibit D-6

CLAIM 1	Welch 2001

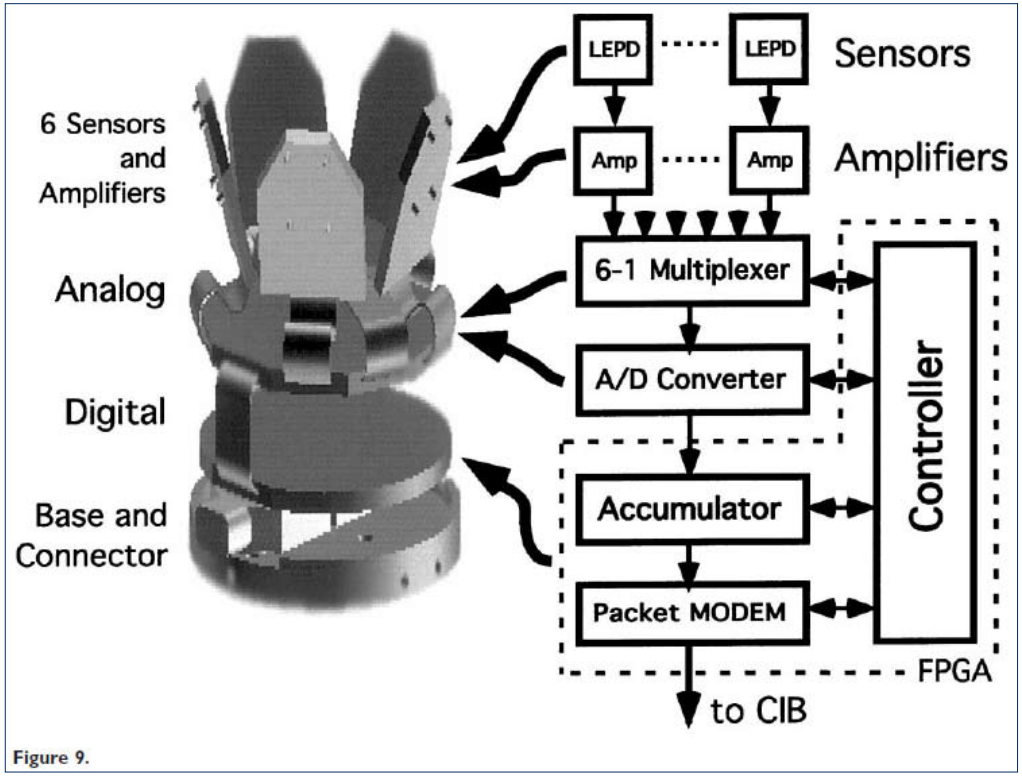

Figure 9.

The design results in a ceiling with a rectangular LED pattern with periods of 7.6 cm and 15.2 cm. T**his spacing is used for the initial estimates of the LED positions in the lab; then, during normal operation, the SCAAT algorithm continually refines the LED position estimates (section 5.4).** The SCAAT autocalibration not only relaxes design and installation constraints, but provides greater precision in the face of initial and ongoing uncertainty in the ceiling structure.
Welch 2001 at Section 4.2.

The CIB comprises analog drive and receive components as well as digital logic components. The digital components implement store and forward in both directions and synchronize the timing of the LED "on" interval within the HiBall dark-light-dark intervals (section 5.2). The protocol supports full-duplex flow control. The data

Exhibit D-6

CLAIM 1	Welch 2001
	are arranged into packets that incorporate error detection. Welch 2001 at Section 4.3. After each HiBall is assembled, we perform an off- line calibration procedure to determine the correspondence between image-plane coordinates and rays in space. This involves more than just determining the view transform for each of the 26 views. Nonlinearities in the silicon sensor and distortions in the lens (such as spherical aberration) cause significant deviations from a simple pinhole camera model. We dealt with all of these issues through the use of a two-part camera model. The first part is a standard pinhole camera represented by a 3 X 4 matrix. The second part is a table mapping real image-plane coordinates to ideal image-plane coordinates. Welch 2001 at Section 5.1. Both parts of the camera model are determined using a calibration procedure that relies on a goniometer (an angular positioning system) of our own design. This device consists of two servo motors mounted together such that one motor provides rotation about the vertical axis while the second motor provides rotation about an axis orthogonal to vertical. An important characteristic of the goniometer is that the rotational axes of the two motors intersect at a point at the center of the HiBall optical sphere; this point is defined as the origin of the HiBall. . . . The rotational positioning motors were rated to provide twenty arc-second precision; we further calibrated them to six arc seconds using a laboratory grade theodolite—an angle measuring system. Welch 2001 at Section 5.1. The online measurements (section 5.2) are used to estimate the pose of the HiBall during operation. The 1991 system collected a group of diverse measurements for a variety of LEDs and sensors, and then used a method of simultaneous nonlinear equations called collinearity (Azuma & Ward, 1991) to estimate the pose of the sensor fixture shown in figure 3 (bottom). There was one equation for each measurement, expressing the constraint that a ray from the front principal point of the sensor lens to the LED must be collinear with a ray from the rear principal point to the intersection with the sensor. Each estimate made use of a group of measurements (typically twenty or more) that together overconstrained the solution. Welch 2001 at Section 5.3. *See also* Defendants' Invalidity Contentions for further discussion.

Exhibit D-6

CLAIM 1	Welch 2001
[1.b] accepting configuration data from the sensor subsystem;	At least under Plaintiffs' apparent infringement theory, Welch 2001 discloses, either expressly or inherently, accepting configuration data from the sensor subsystem. In the alternative, this element would be obvious over Welch 2001 in light of the other references disclosed in Defendants' Invalidity Contentions and/or the knowledge of one of ordinary skill in the art. *See, e.g.*: To determine the mapping between sensor image-plane coordinates and three-space rays, we use a single LED mounted at a fixed location in the laboratory such that it is centered in the view directly out of the top lens of the HiBall. This ray defines the z or up axis for the HiBall coordinate system. We sample other rays by rotating the goniometer motors under computer control. We sample each view with rays spaced about every six minutes of arc throughout the field of view. We repeat each measurement 100 times to reduce the effects of noise on the individual measurements and to estimate the standard deviation of the measurements. Welch 2001 at Section 5.1. Given the tables of approximately 2,500 measurements for each of the 26 views, we first determine a 3 X 4 view matrix using standard linear least-squares techniques. Then, we determine the deviation of each measured point from that predicted by the ideal linear model. These deviations are resampled into a 25 X 25 grid indexed by sensor-plane coordinates using a simple scan-conversion procedure and averaging. Given a measurement from a sensor at runtime (section 5.2), we convert it to an "ideal" measurement by subtracting a deviation bilinearly interpolated from the nearest four entries in the table. Welch 2001 at Section 5.1. **The online measurements (section 5.2) are used to estimate the pose of the HiBall during operation. The 1991 system collected a group of diverse measurements for a variety of LEDs and sensors, and then used a method of simultaneous nonlinear equations called collinearity (Azuma & Ward, 1991) to estimate the pose of the sensor fixture shown in figure 3 (bottom).** Welch 2001 at Section 5.3. In contrast, **the approach we use with the new HiBall system produces tracker reports as each new measurement is made, rather than waiting to form a complete collection of observations.** Because single measurements underconstrain the mathematical solution, we refer to the approach as single-constraint-at-a-time (SCAAT) tracking (Welch, 1996; Welch & Bishop, 1997). **The key is that the single measurements provide some information about the HiBall's state, and thus can be used to incrementally improve a previous**

Exhibit D-6

CLAIM 1	Welch 2001
	estimate. We intentionally fuse each individual "insufficient" measurement immediately as it is obtained. With this approach, we are able to generate estimates more frequently, with less latency, and with improved accuracy, and we are able to estimate the LED positions online concurrently while tracking the HiBall (section 5.4). Welch 2001 at Section 5.3. **We use a Kalman filter (Kalman, 1960) to fuse the measurements into an estimate of the HiBall state x (the pose of the HiBall). We use the Kalman filter—a minimum-variance stochastic estimator—both because the sensor measurement noise and the typical user-motion dynamics can be modeled as normally distributed random processes, and because we want an efficient online method of estimation.** Welch 2001 at Section 5.3. The Kalman filter has been used previously to address similar or related problems. . . . A relevant example of a Kalman filter used for sensor fusion in a wide-area tracking system is given in Foxlin et al. (1998), which describes a hybrid inertial-acoustic system that is commercially available today (Intersense, 2000). Welch 2001 at Section 5.3. [O]ne key benefit warrants discussion here. There is a direct relationship between the complexity of the estimation algorithm, the corresponding speed (execution time per estimation cycle), and the change in HiBall pose between estimation cycles (figure 12). As the algorithmic complexity increases, the execution time increases, which allows for significant nonlinear HiBall motion between estimation cycles, which in turn implies the need for a more complex estimation algorithm. Welch 2001 at Section 5.3.

Exhibit D-6

CLAIM 1	Welch 2001
	 Figure 12. The SCAAT approach, on the other hand, is an attempt to reverse this cycle. Because we intentionally use a single constraint per estimate, the algorithmic complexity is drastically reduced, which reduces the execution time, and hence the amount of motion between estimation cycles. Because the amount of motion is limited, we are able to use a simple dynamic (process) model in the Kalman filter, which further simplifies the computations. In short, the simplicity of the approach means that it can run very fast, which means it can pro- duce estimates very rapidly, with low noise. Welch 2001 at Section 5.3. The Kalman filter requires both a model of the process dynamics and a model of the relationship between the process state and the available measurements. In part due to the simplicity of the SCAAT approach, we are able to use a simple position-velocity (PV) process model (Brown & Hwang, 1992). . . . We model the continuous change in the HiBall state with the simple differential equation

Exhibit D-6

CLAIM 1	Welch 2001

$$\frac{d}{dt}\bar{x}(t) = \begin{bmatrix} 0 & 1 \\ 0 & 0 \end{bmatrix}\begin{bmatrix} x_p(t) \\ x_v(t) \end{bmatrix} + \begin{bmatrix} 0 \\ \mu \end{bmatrix} u(t), \qquad (1)$$

where $u(t)$ is a normally distributed white (in the frequency spectrum) scalar noise process, and the scalar μ represents the magnitude or spectral density of the noise. We use a similar model with a distinct noise process for each of the six pose elements. We determine the individual noise magnitudes using an offline simulation of the system and a nonlinear optimization strategy that seeks to minimize the variance between the estimated pose and a known motion path. (See section 6.2.2.).

Welch 2001 at Section 5.3.

The differential equation (1) represents a continuous integrated random walk, or an integrated Wiener or Brownian-motion process. Specifically, we model each component of the linear and angular HiBall velocities as a random walk, and then use these (assuming constant intermeasurement velocity) to estimate the HiBall pose at time $t + \delta t$ as follows:

Exhibit D-6

CLAIM 1	Welch 2001

$$\bar{x}(t+\delta t) = \begin{bmatrix} 1 & \delta t \\ 0 & 1 \end{bmatrix} \bar{x}(t) \qquad (2)$$

for each of the six pose elements. In addition to a relatively simple process model, the HiBall measurement model is relatively simple. For any ceiling LED (section 4.2) and HiBall view (section 4.1), the 2-D sensor measurement can be modeled as

$$\begin{bmatrix} u \\ v \end{bmatrix} = \begin{bmatrix} c_x/c_z \\ c_y/c_z \end{bmatrix} \qquad (3)$$

where

$$\begin{bmatrix} c_x \\ c_y \\ c_z \end{bmatrix} = VR^T(\bar{l}_{xyz} - \bar{x}_{xyz}), \qquad (4)$$

V is the camera viewing matrix from section 5.1, $\bar{l}_{xyz}$ is the position of the LED in the world, $\bar{x}_{xyz}$ is the position of the HiBall in the world, and R is a rotation matrix corresponding to the orientation of the HiBall in the world. In practice, we maintain the orientation of the HiBall as a combination of a global (external to the state) quaternion and a set of incremental angles as described by Welch (1996) and Welch and Bishop (1997).

Welch 2001 at Section 5.3.

Exhibit D-6

CLAIM 1	Welch 2001
	Because the measurement model (3) and (4) is non-linear, we use an extended Kalman filter, making use of the Jacobian of the nonlinear HiBall measurement model to transform the covariance of the Kalman filter. Welch 2001 at Section 5.3. Along with the benefit of simplicity and speed, the SCAAT approach offers the additional capability of being able to estimate the 3-D positions of the LEDs in the world concurrently with the pose of the HiBall, online, in real time. This capability is a tremendous benefit in terms of the accuracy and noise characteristics of the estimates. The method we now use for autocalibration involves defining a distinct SCAAT Kalman filter for each LED. Specifically, for each LED, we maintain a state $\bar{l}$ (estimate of the 3-D position) and a 3×3 Kalman filter covariance. At the beginning of each estimation cycle, we form an augmented state vector $\hat{x}$ using the appropriate LED state and the current HiBall state: $\hat{x} = [\bar{x}^T, \bar{l}^T]^T$. Similarly, we augment the Kalman filter error covariance matrix with that of the LED filter. We then follow the normal steps outlined in section 5.3, with the result being that the LED portion of the filter state and covariance is updated in accordance with the measurement residual. At the end of the cycle, we extract the LED portions of the state and covariance from the augmented filter, and save them externally. The effect is that, as the system is being used, it continually refines its estimates of the LED positions, thereby continually improving its estimates of the HiBall pose. Again, for additional information, see Welch (1996) and Welch and Bishop (1997).

Exhibit D-6

CLAIM 1	Welch 2001
	Welch 2001 at Section 5.4. The recursive nature of the Kalman filter (section 5.3) **requires that the filter be initialized with a known state and corresponding covariance before steady-state operation can begin.** Such an initialization (or acquisition) must take place prior to any tracking session, but also upon the (rare) occasion when the filter diverges and "loses lock" as a result of blocked sensor views, for example. Welch 2001 at Section 5.5. The acquisition process is complicated by the fact that each LEPD sees a number of different widely separated views (section 4.1). Therefore, detecting an LED provides at best an ambiguous set of potential LED directions in HiBall coordinates. Moreover, before acquisition, no assumptions can be made to limit the search space of visible LEDs. As such, a relatively slow brute-force algorithm is used to acquire lock. Welch 2001 at Section 5.5. As a result of a mechanical design tradeoff, each sensor field of view is less than six degrees. The focal length is set by the size of the sensor housing, which is set by the diameter of the sensors themselves. Energetics is also a factor, limiting how small the lenses can be while maintaining sufficient light-collecting area. As a result of these design tradeoffs, even a momentary small error in the HiBall pose estimate can cause the recursive estimates to diverge and the system to lose lock after only a few LED sightings. And yet the system is quite robust. In practice, users can jump around, crawl on the floor, lean over, even wave their hands in front of the sensors, and the system does not lose lock. During one session, we were using the HiBall as a 3-D digitization probe, a Hi-Ball on the end of a pencil-shaped fiberglass wand (figure 14, left). We laid the probe down on a table at one point, and were amazed to later notice that it was still tracking, even though it was observing only three or four LEDs near the edge of the ceiling. We picked up the probe and continued using it, without it ever losing lock.   **Figure 13.**

Exhibit D-6

CLAIM 1	Welch 2001
	  Figure 14. Welch 2001 at Section 6.1. To make measurements of the noise when the HiBall is in motion, we rely on the assumption that almost all of the signal resulting from normal human motion is at frequencies below 2 Hz. We use a high-pass filter (Welch, 1967) on the pose estimates, and assume the output is noise. The resulting statistics are comparable to those made with the HiBall stationary, except at poses for which there are very few LEDs visible in only one or two views. In these poses, near the edge of the ceiling, the geometry of the constraints results in amplification of errors. For nearly all of the working volume of the tracker, the standard deviation of the noise on measurements while the HiBall is still or moving is about 0.2 mm and 0.03 deg. Welch 2001 at Section 6.1. During the design of the HiBall system, we made substantial use of simulation, in some domains to a very detailed level. For example, Zemax (Focus Software, 1995) was used extensively in the design and optimization of the optical design, including the design of the filter glass lenses, and geometry of the optical-component layout. Welch 2001 at Section 6.2. To produce realistic data for developing and tuning our algorithms, we collected several motion paths (sequences of pose estimates) from our first-generation electro-optical tracker (figure 3) at its 70 Hz maximum report rate. These paths were recorded from both naive users visiting our monthly “demo days” and from experienced users in our labs. . . . we filtered the raw path data with a noncausal zero-phase-shift, low-pass filter to eliminate energy above 2 Hz. The output of the low-pass filtering was then resampled at whatever rate we wanted to run the

Exhibit D-6

CLAIM 1	Welch 2001
	simulated tracker, usually 1,000 Hz. Welch 2001 at Section 6.2. **The simulator reads camera models describing the 26 views, the sensor noise parameters, the LED positions and their expected error, and the motion path described above.** Before beginning the simulation, the LED positions are perturbed from their ideal positions by adding normally distributed error to each axis. Then, for each simulated cycle of operation, the "true" poses are up- dated using the input motion path. Next, a view is chosen and a visible LED within that view is selected, and the image-plane coordinates of the LED on the chosen sensor are computed using the camera model for the view and the LED as described in section 5.3. These sensor coordinates are then perturbed based on the sensor noise model (section 6.2.1) using the distance and angle to the LED. These noise-corrupted sensor readings are then fed to the SCAAT filter to produce an up- dated position estimate. The position estimate is com- pared to the true position to produce a scalar error metric that is described next. Welch 2001 at Section 6.2. The error metric we used combines the error in pose in a way that relates to the effects of tracker error on a head-worn display user. **We define a set of points arrayed around the user in a fixed configuration. We compute two sets of coordinates for these points: the true position using the true pose and their estimated position using the estimated pose.** The error metric is then the sum of the distances between the true and estimated positions of these points. By adjusting the distance of the points from the user, we can control the relative importance of the orientation and the position error in the combined error metric. If the distance is small, then the position error is weighted most heavily; if the distance is large, then the orientation error is weighted most heavily. Our two error metrics for the entire run are the square root of the sum of the squares of all the distances, and the peak distance. Welch 2001 at Section 6.2. *See also* Defendants' Invalidity Contentions for further discussion.
[1.c] configuring the estimation system according to the accepted configuration data;	At least under Plaintiffs' apparent infringement theory, Welch 2001 discloses, either expressly or inherently, configuring the estimation system according to the accepted configuration data. In the alternative, this element would be obvious over Welch 2001 in light of the other references disclosed in Defendants' Invalidity Contentions and/or the knowledge of one of ordinary skill in the art.

Exhibit D-6

CLAIM 1	Welch 2001
	See, e.g.: **[T]here are fewer mechanical considerations when mounting sensors in the environment for an outside-looking-in configuration.** Because landmarks can be relatively simple, small, and cheap, they can often be located in numerous places on the user, and communication from the user to the rest of the system can be relatively simple or even unnecessary. This is particularly attractive for full-body motion capture. Welch 2001 at Section 2. However, there are some significant advantages to the inside-looking-out approach for head tracking. By operating with sensors on the user rather than in the environment, the system can be scaled indefinitely. . . . The inside-looking-out configuration is also motivated by a desire to maximize sensitivity to changes in user pose. Welch 2001 at Section 2. **The HiBall Tracking System consists of three main components (figure 6). An outward-looking sensing unit we call the HiBall is fixed to each user to be tracked. The HiBall unit observes a subsystem of fixed-location infrared LEDs we call the Ceiling. Communication and synchronization between the host computer and these subsystems is coordinated by the Ceiling-HiBall Interface Board (CIB).** Welch 2001 at Section 3.

Exhibit D-6

CLAIM 1	Welch 2001

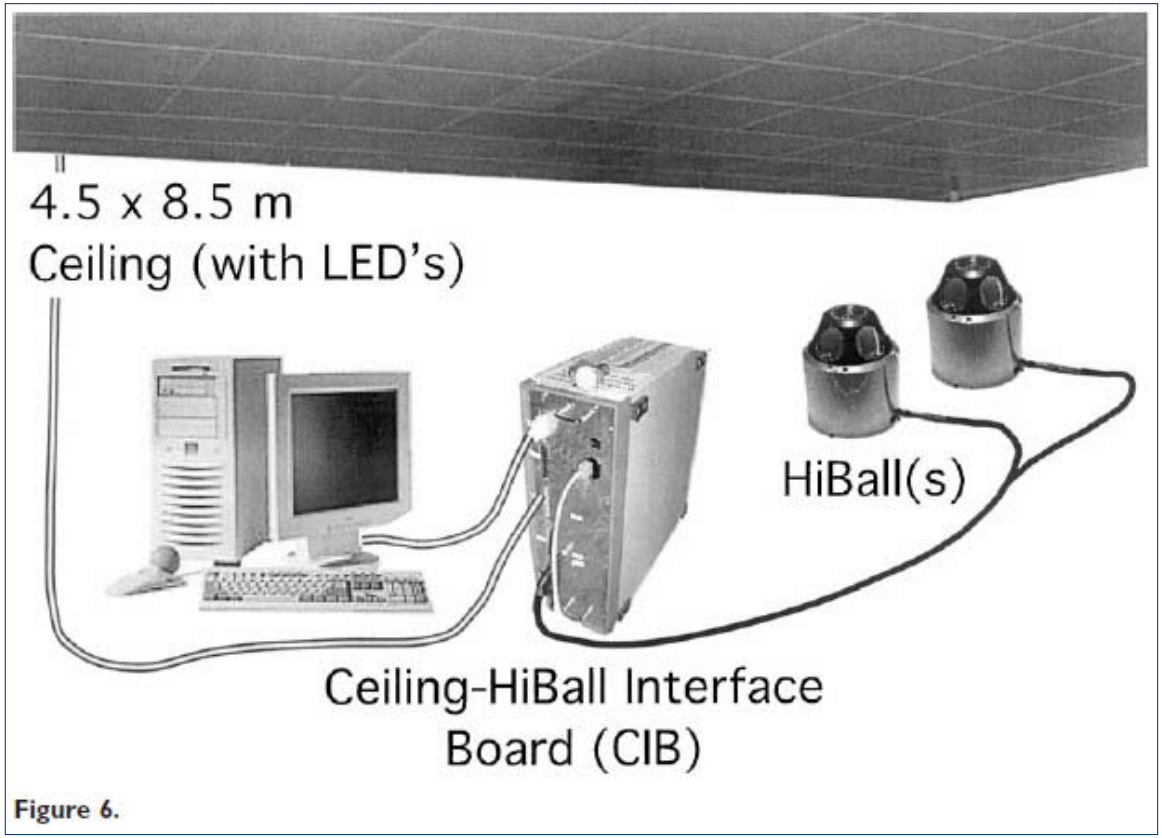

Figure 6.

To determine the mapping between sensor image-plane coordinates and three-space rays, we use a single LED mounted at a fixed location in the laboratory such that it is centered in the view directly out of the top lens of the HiBall. This ray defines the z or up axis for the HiBall coordinate system. We sample other rays by rotating the goniometer motors under computer control. We sample each view with rays spaced about every six minutes of arc throughout the field of view. We repeat each measurement 100 times to reduce the effects of noise on the individual measurements and to estimate the standard deviation of the measurements.
Welch 2001 at Section 5.1.

Given the tables of approximately 2,500 measurements for each of the 26 views, we first determine a 3 X 4 view matrix using standard linear least-squares techniques. Then, we determine the deviation of each

Exhibit D-6

CLAIM 1	Welch 2001
	measured point from that predicted by the ideal linear model. These deviations are resampled into a 25 X 25 grid indexed by sensor-plane coordinates using a simple scan-conversion procedure and averaging. Given a measurement from a sensor at runtime (section 5.2), we convert it to an "ideal" measurement by subtracting a deviation bilinearly interpolated from the nearest four entries in the table. Welch 2001 at Section 5.1. The online measurements (section 5.2) are used to estimate the pose of the HiBall during operation. The 1991 system collected a group of diverse measurements for a variety of LEDs and sensors, and then used a method of simultaneous nonlinear equations called collinearity (Azuma & Ward, 1991) to estimate the pose of the sensor fixture shown in figure 3 (bottom). Welch 2001 at Section 5.3. In contrast, the approach we use with the new HiBall system produces tracker reports as each new measurement is made, rather than waiting to form a complete collection of observations. Because single measurements underconstrain the mathematical solution, we refer to the approach as single-constraint-at-a-time (SCAAT) tracking (Welch, 1996; Welch & Bishop, 1997). The key is that the single measurements provide some information about the HiBall's state, and thus can be used to incrementally improve a previous estimate. We intentionally fuse each individual "insufficient" measurement immediately as it is obtained. With this approach, we are able to generate estimates more frequently, with less latency, and with improved accuracy, and we are able to estimate the LED positions online concurrently while tracking the HiBall (section 5.4). Welch 2001 at Section 5.3. **We use a Kalman filter (Kalman, 1960) to fuse the measurements into an estimate of the HiBall state x (the pose of the HiBall). We use the Kalman filter—a minimum-variance stochastic estimator—both because the sensor measurement noise and the typical user-motion dynamics can be modeled as normally distributed random processes, and because we want an efficient online method of estimation.** Welch 2001 at Section 5.3. The Kalman filter has been used previously to address similar or related problems. . . . A relevant example of a Kalman filter used for sensor fusion in a wide-area tracking system is given in Foxlin et al. (1998), which describes a hybrid inertial-acoustic system that is commercially available today (Intersense, 2000). Welch 2001 at Section 5.3.

Exhibit D-6

CLAIM 1	Welch 2001
	[O]ne key benefit warrants discussion here. There is a direct relationship between the complexity of the estimation algorithm, the corresponding speed (execution time per estimation cycle), and the change in HiBall pose between estimation cycles (figure 12). As the algorithmic complexity increases, the execution time increases, which allows for significant nonlinear HiBall motion between estimation cycles, which in turn implies the need for a more complex estimation algorithm. Welch 2001 at Section 5.3.  Figure 12. The SCAAT approach, on the other hand, is an attempt to reverse this cycle. Because we intentionally use a single constraint per estimate, the algorithmic complexity is drastically reduced, which reduces the execution time, and hence the amount of motion between estimation cycles. Because the amount of motion is limited, we are able to use a simple dynamic (process) model in the Kalman filter, which further simplifies the computations. In short, the simplicity of the approach means that it can run very fast, which means it can pro- duce estimates very rapidly,

Exhibit D-6

CLAIM 1	Welch 2001
	with low noise. Welch 2001 at Section 5.3. **The Kalman filter requires both a model of the process dynamics and a model of the relationship between the process state and the available measurements.** In part due to the simplicity of the SCAAT approach, we are able to use a simple position-velocity (PV) process model (Brown & Hwang, 1992). . . . We model the continuous change in the HiBall state with the simple differential equation $$\frac{d}{dt}\bar{x}(t) = \begin{bmatrix} 0 & 1 \\ 0 & 0 \end{bmatrix}\begin{bmatrix} x_p(t) \\ x_v(t) \end{bmatrix} + \begin{bmatrix} 0 \\ \mu \end{bmatrix} u(t), \qquad (1)$$ where $u(t)$ is a normally distributed white (in the frequency spectrum) scalar noise process, and the scalar μ represents the magnitude or spectral density of the noise. We use a similar model with a distinct noise process for each of the six pose elements. We determine the individual noise magnitudes using an offline simulation of the system and a nonlinear optimization strategy that seeks to minimize the variance between the estimated pose and a known motion path. (See section 6.2.2.). Welch 2001 at Section 5.3. The differential equation (1) represents a continuous integrated random walk, or an integrated Wiener or Brownian-motion process. Specifically, we model each component of the linear and angular HiBall velocities as a random walk, and then use these (assuming constant intermeasurement velocity) to estimate the HiBall pose at time $t + \delta t$ as follows:

Exhibit D-6

CLAIM 1	Welch 2001

$$\bar{x}(t+\delta t) = \begin{bmatrix} 1 & \delta t \\ 0 & 1 \end{bmatrix} \bar{x}(t) \qquad (2)$$

for each of the six pose elements. In addition to a relatively simple process model, the HiBall measurement model is relatively simple. For any ceiling LED (section 4.2) and HiBall view (section 4.1), the 2-D sensor measurement can be modeled as

$$\begin{bmatrix} u \\ v \end{bmatrix} = \begin{bmatrix} c_x/c_z \\ c_y/c_z \end{bmatrix} \qquad (3)$$

where

$$\begin{bmatrix} c_x \\ c_y \\ c_z \end{bmatrix} = VR^T(\bar{l}_{xyz} - \bar{x}_{xyz}), \qquad (4)$$

V is the camera viewing matrix from section 5.1, $\bar{l}_{xyz}$ is the position of the LED in the world, $\bar{x}_{xyz}$ is the position of the HiBall in the world, and R is a rotation matrix corresponding to the orientation of the HiBall in the world. In practice, we maintain the orientation of the HiBall as a combination of a global (external to the state) quaternion and a set of incremental angles as described by Welch (1996) and Welch and Bishop (1997).

Welch 2001 at Section 5.3.

Exhibit D-6

CLAIM 1	Welch 2001
	Because the measurement model (3) and (4) is non-linear, we use an extended Kalman filter, making use of the Jacobian of the nonlinear HiBall measurement model to transform the covariance of the Kalman filter. Welch 2001 at Section 5.3. Along with the benefit of simplicity and speed, the SCAAT approach offers the additional capability of being able to estimate the 3-D positions of the LEDs in the world concurrently with the pose of the HiBall, online, in real time. This capability is a tremendous benefit in terms of the accuracy and noise characteristics of the estimates. The method we now use for autocalibration involves defining a distinct SCAAT Kalman filter for each LED. Specifically, for each LED, we maintain a state $\bar{l}$ (estimate of the 3-D position) and a 3×3 Kalman filter covariance. At the beginning of each estimation cycle, we form an augmented state vector $\hat{x}$ using the appropriate LED state and the current HiBall state: $\hat{x} = [\bar{x}^T, \bar{l}^T]^T$. Similarly, we augment the Kalman filter error covariance matrix with that of the LED filter. We then follow the normal steps outlined in section 5.3, with the result being that the LED portion of the filter state and covariance is updated in accordance with the measurement residual. At the end of the cycle, we extract the LED portions of the state and covariance from the augmented filter, and save them externally. The effect is that, as the system is being used, it continually refines its estimates of the LED positions, thereby continually improving its estimates of the HiBall pose. Again, for additional information, see Welch (1996) and Welch and Bishop (1997).

Exhibit D-6

CLAIM 1	Welch 2001
	Welch 2001 at Section 5.4. **The recursive nature of the Kalman filter (section 5.3) requires that the filter be initialized with a known state and corresponding covariance before steady-state operation can begin. Such an initialization (or acquisition) must take place prior to any tracking session, but also upon the (rare) occasion when the filter diverges and "loses lock" as a result of blocked sensor views, for example.** Welch 2001 at Section 5.5. The acquisition process is complicated by the fact that each LEPD sees a number of different widely separated views (section 4.1). Therefore, detecting an LED provides at best an ambiguous set of potential LED directions in HiBall coordinates. Moreover, before acquisition, no assumptions can be made to limit the search space of visible LEDs. As such, a relatively slow brute-force algorithm is used to acquire lock. Welch 2001 at Section 5.5. As a result of a mechanical design tradeoff, each sensor field of view is less than six degrees. The focal length is set by the size of the sensor housing, which is set by the diameter of the sensors themselves. Energetics is also a factor, limiting how small the lenses can be while maintaining sufficient light-collecting area. As a result of these design tradeoffs, even a momentary small error in the HiBall pose estimate can cause the recursive estimates to diverge and the system to lose lock after only a few LED sightings. And yet the system is quite robust. In practice, users can jump around, crawl on the floor, lean over, even wave their hands in front of the sensors, and the system does not lose lock. During one session, we were using the HiBall as a 3-D digitization probe, a Hi-Ball on the end of a pencil-shaped fiberglass wand (figure 14, left). We laid the probe down on a table at one point, and were amazed to later notice that it was still tracking, even though it was observing only three or four LEDs near the edge of the ceiling. We picked up the probe and continued using it, without it ever losing lock.   Figure 13.

Exhibit D-6

CLAIM 1	Welch 2001
	  Figure 14. Welch 2001 at Section 6.1. To make measurements of the noise when the HiBall is in motion, we rely on the assumption that almost all of the signal resulting from normal human motion is at frequencies below 2 Hz. We use a high-pass filter (Welch, 1967) on the pose estimates, and assume the output is noise. The resulting statistics are comparable to those made with the HiBall stationary, except at poses for which there are very few LEDs visible in only one or two views. In these poses, near the edge of the ceiling, the geometry of the constraints results in amplification of errors. For nearly all of the working volume of the tracker, the standard deviation of the noise on measurements while the HiBall is still or moving is about 0.2 mm and 0.03 deg. Welch 2001 at Section 6.1. During the design of the HiBall system, we made substantial use of simulation, in some domains to a very detailed level. For example, Zemax (Focus Software, 1995) was used extensively in the design and optimization of the optical design, including the design of the filter glass lenses, and geometry of the optical-component layout. Welch 2001 at Section 6.2. To produce realistic data for developing and tuning our algorithms, we collected several motion paths (sequences of pose estimates) from our first-generation electro-optical tracker (figure 3) at its 70 Hz maximum report rate. These paths were recorded from both naive users visiting our monthly “demo days” and from experienced users in our labs. . . . we filtered the raw path data with a noncausal zero-phase-shift, low-pass filter to eliminate energy above 2 Hz. The output of the low-pass filtering was then resampled at whatever rate we wanted to run the

Exhibit D-6

CLAIM 1	Welch 2001
	simulated tracker, usually 1,000 Hz. Welch 2001 at Section 6.2. The simulator reads camera models describing the 26 views, the sensor noise parameters, the LED positions and their expected error, and the motion path described above. Before beginning the simulation, the LED positions are perturbed from their ideal positions by adding normally distributed error to each axis. Then, for each simulated cycle of operation, the "true" poses are up- dated using the input motion path. Next, a view is chosen and a visible LED within that view is selected, and the image-plane coordinates of the LED on the chosen sensor are computed using the camera model for the view and the LED as described in section 5.3. These sensor coordinates are then perturbed based on the sensor noise model (section 6.2.1) using the distance and angle to the LED. These noise-corrupted sensor readings are then fed to the SCAAT filter to produce an up- dated position estimate. The position estimate is com- pared to the true position to produce a scalar error metric that is described next. Welch 2001 at Section 6.2. The error metric we used combines the error in pose in a way that relates to the effects of tracker error on a head-worn display user. We define a set of points arrayed around the user in a fixed configuration. We compute two sets of coordinates for these points: the true position using the true pose and their estimated position using the estimated pose. The error metric is then the sum of the distances between the true and estimated positions of these points. By adjusting the distance of the points from the user, we can control the relative importance of the orientation and the position error in the combined error metric. If the distance is small, then the position error is weighted most heavily; if the distance is large, then the orientation error is weighted most heavily. Our two error metrics for the entire run are the square root of the sum of the squares of all the distances, and the peak distance. Welch 2001 at Section 6.2. *See also* Defendants' Invalidity Contentions for further discussion.
[1.d] repeatedly updating a state estimate, including accepting measurement information from the sensor subsystem, and updating the state	At least under Plaintiffs' apparent infringement theory, Welch 2001 discloses, either expressly or inherently, repeatedly updating a state estimate, including accepting measurement information from the sensor subsystem, and updating the state estimate according to the accepted configuration data and the accepted measurement data. In the alternative, this element would be obvious over Welch 2001 in light of the other references disclosed in Defendants' Invalidity Contentions and/or the knowledge of one of ordinary skill in the art.

Exhibit D-6

CLAIM 1	Welch 2001
estimate according to the accepted configuration data and the accepted measurement data.	*See, e.g.*: To determine the mapping between sensor image-plane coordinates and three-space rays, we use a single LED mounted at a fixed location in the laboratory such that it is centered in the view directly out of the top lens of the HiBall. This ray defines the z or up axis for the HiBall coordinate system. We sample other rays by rotating the goniometer motors under computer control. We sample each view with rays spaced about every six minutes of arc throughout the field of view. We repeat each measurement 100 times to reduce the effects of noise on the individual measurements and to estimate the standard deviation of the measurements. Welch 2001 at Section 5.1. Given the tables of approximately 2,500 measurements for each of the 26 views, we first determine a 3 X 4 view matrix using standard linear least-squares techniques. Then, we determine the deviation of each measured point from that predicted by the ideal linear model. These deviations are resampled into a 25 X 25 grid indexed by sensor-plane coordinates using a simple scan-conversion procedure and averaging. Given a measurement from a sensor at runtime (section 5.2), we convert it to an "ideal" measurement by subtracting a deviation bilinearly interpolated from the nearest four entries in the table. Welch 2001 at Section 5.1. The online measurements (section 5.2) are used to estimate the pose of the HiBall during operation. The 1991 system collected a group of diverse measurements for a variety of LEDs and sensors, and then used a method of simultaneous nonlinear equations called collinearity (Azuma & Ward, 1991) to estimate the pose of the sensor fixture shown in figure 3 (bottom). Welch 2001 at Section 5.3. In contrast, the approach we use with the new HiBall system produces tracker reports as each new measurement is made, rather than waiting to form a complete collection of observations. **Because single measurements underconstrain the mathematical solution, we refer to the approach as single-constraint-at-a-time (SCAAT) tracking (Welch, 1996; Welch & Bishop, 1997). The key is that the single measurements provide some information about the HiBall's state, and thus can be used to incrementally improve a previous estimate.** We intentionally fuse each individual "insufficient" measurement immediately as it is obtained. With this approach, we are able to generate estimates more frequently, with less latency, and with improved accuracy, and we are able to estimate the LED positions online concurrently while tracking the HiBall (section 5.4). Welch 2001 at Section 5.3.

Exhibit D-6

CLAIM 1	Welch 2001
	We use a Kalman filter (Kalman, 1960) to fuse the measurements into an estimate of the HiBall state x (the pose of the HiBall). We use the Kalman filter—a minimum-variance stochastic estimator—both because the sensor measurement noise and the typical user-motion dynamics can be modeled as normally distributed random processes, and because we want an efficient online method of estimation. Welch 2001 at Section 5.3. The Kalman filter has been used previously to address similar or related problems. . . . A relevant example of a Kalman filter used for sensor fusion in a wide-area tracking system is given in Foxlin et al. (1998), which describes a hybrid inertial-acoustic system that is commercially available today (Intersense, 2000). Welch 2001 at Section 5.3. [O]ne key benefit warrants discussion here. There is a direct relationship between the complexity of the estimation algorithm, the corresponding speed (execution time per estimation cycle), and the change in HiBall pose between estimation cycles (figure 12). As the algorithmic complexity increases, the execution time increases, which allows for significant nonlinear HiBall motion between estimation cycles, which in turn implies the need for a more complex estimation algorithm. Welch 2001 at Section 5.3.

Exhibit D-6

CLAIM 1	Welch 2001

Figure 12.

The SCAAT approach, on the other hand, is an attempt to reverse this cycle. Because we intentionally use a single constraint per estimate, the algorithmic complexity is drastically reduced, which reduces the execution time, and hence the amount of motion between estimation cycles. Because the amount of motion is limited, we are able to use a simple dynamic (process) model in the Kalman filter, which further simplifies the computations. **In short, the simplicity of the approach means that it can run very fast, which means it can pro- duce estimates very rapidly, with low noise.**
Welch 2001 at Section 5.3.

The Kalman filter requires both a model of the process dynamics and a model of the relationship between the process state and the available measurements. In part due to the simplicity of the SCAAT approach, we are able to use a simple position-velocity (PV) process model (Brown & Hwang, 1992). . . . We model the continuous change in the HiBall state with the simple differential equation

Exhibit D-6

CLAIM 1	Welch 2001

$$\frac{d}{dt}\bar{x}(t) = \begin{bmatrix} 0 & 1 \\ 0 & 0 \end{bmatrix}\begin{bmatrix} x_p(t) \\ x_v(t) \end{bmatrix} + \begin{bmatrix} 0 \\ \mu \end{bmatrix} u(t), \qquad (1)$$

where $u(t)$ is a normally distributed white (in the frequency spectrum) scalar noise process, and the scalar μ represents the magnitude or spectral density of the noise. We use a similar model with a distinct noise process for each of the six pose elements. We determine the individual noise magnitudes using an offline simulation of the system and a nonlinear optimization strategy that seeks to minimize the variance between the estimated pose and a known motion path. (See section 6.2.2.).

Welch 2001 at Section 5.3.

The differential equation (1) represents a continuous integrated random walk, or an integrated Wiener or Brownian-motion process. **Specifically, we model each component of the linear and angular HiBall velocities as a random walk, and then use these (assuming constant intermeasurement velocity) to estimate the HiBall pose at time t + δt as follows:**

Exhibit D-6

CLAIM 1	Welch 2001

$$\bar{x}(t+\delta t) = \begin{bmatrix} 1 & \delta t \\ 0 & 1 \end{bmatrix} \bar{x}(t) \qquad (2)$$

for each of the six pose elements. In addition to a relatively simple process model, the HiBall measurement model is relatively simple. For any ceiling LED (section 4.2) and HiBall view (section 4.1), the 2-D sensor measurement can be modeled as

$$\begin{bmatrix} u \\ v \end{bmatrix} = \begin{bmatrix} c_x/c_z \\ c_y/c_z \end{bmatrix} \qquad (3)$$

where

$$\begin{bmatrix} c_x \\ c_y \\ c_z \end{bmatrix} = VR^T(\bar{l}_{xyz} - \bar{x}_{xyz}), \qquad (4)$$

V is the camera viewing matrix from section 5.1, $\bar{l}_{xyz}$ is the position of the LED in the world, $\bar{x}_{xyz}$ is the position of the HiBall in the world, and R is a rotation matrix corresponding to the orientation of the HiBall in the world. In practice, we maintain the orientation of the HiBall as a combination of a global (external to the state) quaternion and a set of incremental angles as described by Welch (1996) and Welch and Bishop (1997).

Welch 2001 at Section 5.3.

Exhibit D-6

CLAIM 1	Welch 2001
	Because the measurement model (3) and (4) is non-linear, we use an extended Kalman filter, making use of the Jacobian of the nonlinear HiBall measurement model to transform the covariance of the Kalman filter. Welch 2001 at Section 5.3. **Along with the benefit of simplicity and speed, the SCAAT approach offers the additional capability of being able to estimate the 3-D positions of the LEDs in the world concurrently with the pose of the HiBall, online, in real time.** This capability is a tremendous benefit in terms of the accuracy and noise characteristics of the estimates.

Exhibit D-6

CLAIM 1	Welch 2001

> The method we now use for autocalibration involves defining a distinct SCAAT Kalman filter for each LED. Specifically, for each LED, we maintain a state $\bar{l}$ (estimate of the 3-D position) and a 3×3 Kalman filter covariance. At the beginning of each estimation cycle, we form an augmented state vector $\hat{x}$ using the appropriate LED state and the current HiBall state: $\hat{x} = [\bar{x}^T, \bar{l}^T]^T$. Similarly, we augment the Kalman filter error covariance matrix with that of the LED filter. We then follow the normal steps outlined in section 5.3, with the result being that the LED portion of the filter state and covariance is updated in accordance with the measurement residual. At the end of the cycle, we extract the LED portions of the state and covariance from the augmented filter, and save them externally. The effect is that, as the system is being used, it continually refines its estimates of the LED positions, thereby continually improving its estimates of the HiBall pose. Again, for additional information, see Welch (1996) and Welch and Bishop (1997).

Welch 2001 at Section 5.4.

The recursive nature of the Kalman filter (section 5.3) requires that the filter be initialized with a known state and corresponding covariance before steady-state operation can begin. Such an initialization (or acquisition) must take place prior to any tracking session, but also upon the (rare) occasion when the filter diverges and "loses lock" as a result of blocked sensor views, for example.
Welch 2001 at Section 5.5.

Exhibit D-6

CLAIM 1	Welch 2001
	The acquisition process is complicated by the fact that each LEPD sees a number of different widely separated views (section 4.1). Therefore, detecting an LED provides at best an ambiguous set of potential LED directions in HiBall coordinates. Moreover, before acquisition, no assumptions can be made to limit the search space of visible LEDs. As such, a relatively slow brute-force algorithm is used to acquire lock. Welch 2001 at Section 5.5. As a result of a mechanical design tradeoff, each sensor field of view is less than six degrees. The focal length is set by the size of the sensor housing, which is set by the diameter of the sensors themselves. Energetics is also a factor, limiting how small the lenses can be while maintaining sufficient light-collecting area. As a result of these design tradeoffs, even a momentary small error in the HiBall pose estimate can cause the recursive estimates to diverge and the system to lose lock after only a few LED sightings. And yet the system is quite robust. In practice, users can jump around, crawl on the floor, lean over, even wave their hands in front of the sensors, and the system does not lose lock. During one session, we were using the HiBall as a 3-D digitization probe, a Hi-Ball on the end of a pencil-shaped fiberglass wand (figure 14, left). We laid the probe down on a table at one point, and were amazed to later notice that it was still tracking, even though it was observing only three or four LEDs near the edge of the ceiling. We picked up the probe and continued using it, without it ever losing lock.  Figure 13.

Exhibit D-6

CLAIM 1	Welch 2001
	  Figure 14. Welch 2001 at Section 6.1. To make measurements of the noise when the HiBall is in motion, we rely on the assumption that almost all of the signal resulting from normal human motion is at frequencies below 2 Hz. We use a high-pass filter (Welch, 1967) on the pose estimates, and assume the output is noise. The resulting statistics are comparable to those made with the HiBall stationary, except at poses for which there are very few LEDs visible in only one or two views. In these poses, near the edge of the ceiling, the geometry of the constraints results in amplification of errors. For nearly all of the working volume of the tracker, the standard deviation of the noise on measurements while the HiBall is still or moving is about 0.2 mm and 0.03 deg. Welch 2001 at Section 6.1. During the design of the HiBall system, we made substantial use of simulation, in some domains to a very detailed level. For example, Zemax (Focus Software, 1995) was used extensively in the design and optimization of the optical design, including the design of the filter glass lenses, and geometry of the optical-component layout. Welch 2001 at Section 6.2. To produce realistic data for developing and tuning our algorithms, we collected several motion paths (sequences of pose estimates) from our first-generation electro-optical tracker (figure 3) at its 70 Hz maximum report rate. These paths were recorded from both naive users visiting our monthly “demo days” and from experienced users in our labs. . . . we filtered the raw path data with a noncausal zero-phase-shift, low-pass filter to eliminate energy above 2 Hz. The output of the low-pass filtering was then resampled at whatever rate we wanted to run the

CLAIM 1	Welch 2001
	simulated tracker, usually 1,000 Hz. Welch 2001 at Section 6.2. The simulator reads camera models describing the 26 views, the sensor noise parameters, the LED positions and their expected error, and the motion path described above. **Before beginning the simulation, the LED positions are perturbed from their ideal positions by adding normally distributed error to each axis. Then, for each simulated cycle of operation, the "true" poses are up- dated using the input motion path. Next, a view is chosen and a visible LED within that view is selected, and the image-plane coordinates of the LED on the chosen sensor are computed using the camera model for the view and the LED as described in section 5.3. These sensor coordinates are then perturbed based on the sensor noise model (section 6.2.1) using the distance and angle to the LED. These noise-corrupted sensor readings are then fed to the SCAAT filter to produce an up- dated position estimate.** The position estimate is com- pared to the true position to produce a scalar error metric that is described next. Welch 2001 at Section 6.2. The error metric we used combines the error in pose in a way that relates to the effects of tracker error on a head-worn display user. We define a set of points arrayed around the user in a fixed configuration. We compute two sets of coordinates for these points: the true position using the true pose and their estimated position using the estimated pose. The error metric is then the sum of the distances between the true and estimated positions of these points. By adjusting the distance of the points from the user, we can control the relative importance of the orientation and the position error in the combined error metric. If the distance is small, then the position error is weighted most heavily; if the distance is large, then the orientation error is weighted most heavily. Our two error metrics for the entire run are the square root of the sum of the squares of all the distances, and the peak distance. Welch 2001 at Section 6.2. *See also* Defendants' Invalidity Contentions for further discussion.

B. DEPENDENT CLAIM 2

CLAIM 2	Welch 2001
[2] The method of claim 1 wherein coupling the	At least under Plaintiffs' apparent infringement theory, Welch 2001 discloses, either expressly or inherently, the method of claim 1 wherein coupling the sensor subsystem to the estimation subsystem includes coupling software

Exhibit D-6

CLAIM 2	Welch 2001
sensor subsystem to the estimation subsystem includes coupling software modules each associated with one or more of the sensing elements.	modules each associated with one or more of the sensing elements. In the alternative, this element would be obvious over Welch 2001 in light of the other references disclosed in Defendants' Invalidity Contentions and/or the knowledge of one of ordinary skill in the art. *See, e.g.*: Thanks to significant improvements in hardware and software, this HiBall system offers unprecedented speed, resolution, accuracy, robustness, and flexibility. The bulky and heavy sensors and backpack of the previous system have been replaced by a small HiBall unit (figure 4, bottom). In addition, the precisely machined LED ceiling panels of the previous system have been replaced by looser-tolerance panels that are relatively inexpensive to make and simple to install (figure 4, top; figure 10). **Finally, we are using an unusual Kalman-filter-based algorithm that generates very accurate pose estimates at a high rate with low latency, and that simultaneously self-calibrates the system.** Welch 2001 at Section 1.3.

Exhibit D-6

CLAIM 2	Welch 2001

Figure 4.

In contrast, the approach we use with the new HiBall system produces tracker reports as each new measurement is made, rather than waiting to form a complete collection of observations. **Because single measurements underconstrain the mathematical solution, we refer to the approach as single-constraint-at-a-time (SCAAT) tracking (Welch, 1996; Welch & Bishop, 1997). The key is that the single measurements provide some information about the HiBall's state, and thus can be used to incrementally improve a previous estimate.** We intentionally fuse each individual "insufficient" measurement immediately as it is obtained. With this approach, we are able to generate estimates more frequently, with less latency, and with improved accuracy,

Exhibit D-6

CLAIM 2	Welch 2001
	and we are able to estimate the LED positions online concurrently while tracking the HiBall (section 5.4). Welch 2001 at Section 5.3. **We use a Kalman filter (Kalman, 1960) to fuse the measurements into an estimate of the HiBall state x (the pose of the HiBall). We use the Kalman filter—a minimum-variance stochastic estimator—both because the sensor measurement noise and the typical user-motion dynamics can be modeled as normally distributed random processes, and because we want an efficient online method of estimation.** Welch 2001 at Section 5.3. The Kalman filter has been used previously to address similar or related problems. . . . A relevant example of a Kalman filter used for sensor fusion in a wide-area tracking system is given in Foxlin et al. (1998), which describes a hybrid inertial-acoustic system that is commercially available today (Intersense, 2000). Welch 2001 at Section 5.3. [O]ne key benefit warrants discussion here. There is a direct relationship between the complexity of the estimation algorithm, the corresponding speed (execution time per estimation cycle), and the change in HiBall pose between estimation cycles (figure 12). As the algorithmic complexity increases, the execution time increases, which allows for significant nonlinear HiBall motion between estimation cycles, which in turn implies the need for a more complex estimation algorithm. Welch 2001 at Section 5.3.

Exhibit D-6

CLAIM 2	Welch 2001
	 Figure 12. The SCAAT approach, on the other hand, is an attempt to reverse this cycle. Because we intentionally use a single constraint per estimate, the algorithmic complexity is drastically reduced, which reduces the execution time, and hence the amount of motion between estimation cycles. Because the amount of motion is limited, we are able to use a simple dynamic (process) model in the Kalman filter, which further simplifies the computations. **In short, the simplicity of the approach means that it can run very fast, which means it can pro- duce estimates very rapidly, with low noise.** Welch 2001 at Section 5.3. The Kalman filter requires both a model of the process dynamics and a model of the relationship between the process state and the available measurements. In part due to the simplicity of the SCAAT approach, we are able to use a simple position-velocity (PV) process model (Brown & Hwang, 1992). . . . We model the continuous change in the HiBall state with the simple differential equation

Exhibit D-6

CLAIM 2	Welch 2001

$$\frac{d}{dt}\bar{x}(t) = \begin{bmatrix} 0 & 1 \\ 0 & 0 \end{bmatrix}\begin{bmatrix} x_p(t) \\ x_v(t) \end{bmatrix} + \begin{bmatrix} 0 \\ \mu \end{bmatrix} u(t), \qquad (1)$$

where $u(t)$ is a normally distributed white (in the frequency spectrum) scalar noise process, and the scalar μ represents the magnitude or spectral density of the noise. We use a similar model with a distinct noise process for each of the six pose elements. We determine the individual noise magnitudes using an offline simulation of the system and a nonlinear optimization strategy that seeks to minimize the variance between the estimated pose and a known motion path. (See section 6.2.2.).

Welch 2001 at Section 5.3.

The differential equation (1) represents a continuous integrated random walk, or an integrated Wiener or Brownian-motion process. **Specifically, we model each component of the linear and angular HiBall velocities as a random walk, and then use these (assuming constant intermeasurement velocity) to estimate the HiBall pose at time t + δt as follows:**

Exhibit D-6

CLAIM 2	Welch 2001

$$\bar{x}(t+\delta t) = \begin{bmatrix} 1 & \delta t \\ 0 & 1 \end{bmatrix} \bar{x}(t) \qquad (2)$$

for each of the six pose elements. In addition to a relatively simple process model, the HiBall measurement model is relatively simple. For any ceiling LED (section 4.2) and HiBall view (section 4.1), the 2-D sensor measurement can be modeled as

$$\begin{bmatrix} u \\ v \end{bmatrix} = \begin{bmatrix} c_x/c_z \\ c_y/c_z \end{bmatrix} \qquad (3)$$

where

$$\begin{bmatrix} c_x \\ c_y \\ c_z \end{bmatrix} = VR^T(\bar{l}_{xyz} - \bar{x}_{xyz}), \qquad (4)$$

V is the camera viewing matrix from section 5.1, $\bar{l}_{xyz}$ is the position of the LED in the world, $\bar{x}_{xyz}$ is the position of the HiBall in the world, and R is a rotation matrix corresponding to the orientation of the HiBall in the world. In practice, we maintain the orientation of the HiBall as a combination of a global (external to the state) quaternion and a set of incremental angles as described by Welch (1996) and Welch and Bishop (1997).

Welch 2001 at Section 5.3.

Exhibit D-6

CLAIM 2	Welch 2001
	Because the measurement model (3) and (4) is non-linear, we use an extended Kalman filter, making use of the Jacobian of the nonlinear HiBall measurement model to transform the covariance of the Kalman filter. Welch 2001 at Section 5.3. **Along with the benefit of simplicity and speed, the SCAAT approach offers the additional capability of being able to estimate the 3-D positions of the LEDs in the world concurrently with the pose of the HiBall, online, in real time.** This capability is a tremendous benefit in terms of the accuracy and noise characteristics of the estimates.

Exhibit D-6

CLAIM 2	Welch 2001
	The method we now use for autocalibration involves defining a distinct SCAAT Kalman filter for each LED. Specifically, for each LED, we maintain a state $\bar{l}$ (estimate of the 3-D position) and a 3×3 Kalman filter covariance. At the beginning of each estimation cycle, we form an augmented state vector $\hat{x}$ using the appropriate LED state and the current HiBall state: $\hat{x} = [\bar{x}^T, \bar{l}^T]^T$. Similarly, we augment the Kalman filter error covariance matrix with that of the LED filter. We then follow the normal steps outlined in section 5.3, with the result being that the LED portion of the filter state and covariance is updated in accordance with the measurement residual. At the end of the cycle, we extract the LED portions of the state and covariance from the augmented filter, and save them externally. The effect is that, as the system is being used, it continually refines its estimates of the LED positions, thereby continually improving its estimates of the HiBall pose. Again, for additional information, see Welch (1996) and Welch and Bishop (1997). Welch 2001 at Section 5.4. **The recursive nature of the Kalman filter** (section 5.3) requires that the filter be initialized with a known state and corresponding covariance before steady-state operation can begin. Such an initialization (or acquisition) must take place prior to any tracking session, but also upon the (rare) occasion when the filter diverges and "loses lock" as a result of blocked sensor views, for example. Welch 2001 at Section 5.5.

CLAIM 2	Welch 2001
	The acquisition process is complicated by the fact that each LEPD sees a number of different widely separated views (section 4.1). Therefore, detecting an LED provides at best an ambiguous set of potential LED directions in HiBall coordinates. Moreover, before acquisition, no assumptions can be made to limit the search space of visible LEDs. As such, a relatively slow brute-force algorithm is used to acquire lock. Welch 2001 at Section 5.5. During the design of the HiBall system, we made substantial use of simulation, in some domains to a very detailed level. For example, Zemax (Focus Software, 1995) was used extensively in the design and optimization of the optical design, including the design of the filter glass lenses, and geometry of the optical-component layout. Welch 2001 at Section 6.2. **The method we now use for autocalibration involves defining a distinct SCAAT Kalman filter for each LED. Specifically, for each LED, we maintain a state #l (estimate of the 3-D position) and a 3 x 3 Kalman filter covariance.** At the beginning of each estimation cycle, we form an augmented state vector xÜ using the appropriate LED state and the current HiBall state: xÜ 5 [x# T, l#T]T. Similarly, we augment the Kalman filter error covariance matrix with that of the LED filter. We then follow the normal steps outlined in section 5.3, with the result being that the LED portion of the filter state and covariance is updated in accordance with the measurement residual. At the end of the cycle, we extract the LED portions of the state and covariance from the augmented filter, and save them externally. The effect is that, as the system is being used, it continually refines its estimates of the LED positions, thereby continually improving its estimates of the HiBall pose. Again, for additional information, see Welch (1996) and Welch and Bishop (1997). Welch 2001 at Section 5.4 *See* Disclosures with respect to Claim 1, *supra*; *see also* Defendants' Invalidity Contentions for further discussion.

C. DEPENDENT CLAIM 5

CLAIM 5	Welch 2001
[5] The method of claim 1 wherein the state	At least under Plaintiffs' apparent infringement theory, Welch 2001 discloses, either expressly or inherently, the method of claim 1 wherein the state estimate characterizes an estimate of a location of the object. In the alternative,

Exhibit D-6

CLAIM 5	Welch 2001
estimate characterizes an estimate of a location of the object.	this element would be obvious over Welch 2001 in light of the other references disclosed in Defendants' Invalidity Contentions and/or the knowledge of one of ordinary skill in the art. *See, e.g.*: As part of his 1984 dissertation on Self-Tracker, Bishop put forward the idea of outward-looking tracking systems based on user-mounted sensors that estimate user pose by observing landmarks in the environment (Bishop, 1984). He described two kinds of landmarks: high signal-to-noise-ratio beacons such as light-emitting diodes (LEDs) and low signal-to-noise- ratio landmarks such as naturally occurring features. Bishop designed and demonstrated custom VLSI chips (figure 2) that combined image sensing and processing on a single chip (Bishop & Fuchs, 1984). The idea was to combine multiple instances of these chips into an outward-looking cluster that estimated cluster motion by observing natural features in the unmodified environment. Integrating the resulting motion to estimate pose is prone to accumulating error, so further development required a complementary system based on easily detectable landmarks (LEDs) at known locations. Welch 2001 at Section 1.2. As a result of these improvements, the HiBall Tracking System can generate more than 2,000 pose estimates per second, with less than 1 ms of latency, better than 0.5 mm and 0.03 deg. of absolute error and noise, everywhere in a 4.5 m x 8.5 m room (with more than two meters of height variation). The area can be expanded by adding more panels, or by using checker-board configurations that spread panels over a larger area. The weight of the user-worn HiBall is approximately 300 grams, making it lighter than one optical sensor in the 1991 system. Multiple HiBall units can be daisy-chained together for head or hand tracking, pose-aware input devices, or precise 3-D point digitization throughout the entire working volume. Welch 2001 at Section 1.3.

CLAIM 5	Welch 2001
	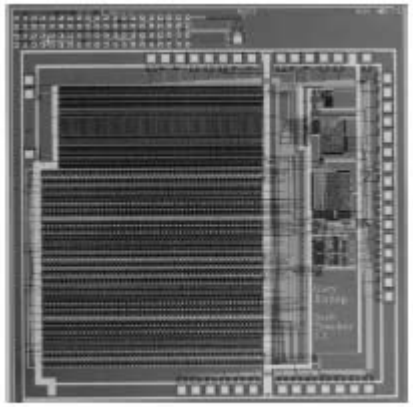 Figure 2. To determine the mapping between sensor image-plane coordinates and three-space rays, we use a single LED mounted at a fixed location in the laboratory such that it is centered in the view directly out of the top lens of the HiBall. This ray defines the z or up axis for the HiBall coordinate system. We sample other rays by rotating the goniometer motors under computer control. We sample each view with rays spaced about every six minutes of arc throughout the field of view. We repeat each measurement 100 times to reduce the effects of noise on the individual measurements and to estimate the standard deviation of the measurements. Welch 2001 at Section 5.1. Each HiBall observes LEDs through multiple sensor-lens views that are distributed over a large solid angle. LEDs are sequentially flashed (one at a time) such that they are seen via a diverse set of views for each HiBall. Initial acquisition is performed using a brute-force search through LED space, but, once initial lock is made, the selection of LEDs to flash is tailored to the views of the active HiBall units. **Pose estimates are maintained using a Kalman-filter-based prediction-correction approach known as single-constraint-at-a-time (SCAAT) tracking.** This technique has been extended to provide self-calibration of the ceiling, concurrent with HiBall tracking. Welch 2001 at Section 3. The design results in a ceiling with a rectangular LED pattern with periods of 7.6 cm and 15.2 cm. This spacing is used for the initial estimates of the LED positions in the lab; then, during normal operation, the SCAAT algorithm continually refines the LED position estimates (section 5.4). The SCAAT autocalibration not only

CLAIM 5	Welch 2001
	relaxes design and installation constraints, but provides greater precision in the face of initial and ongoing uncertainty in the ceiling structure. Welch 2001 at Section 4.2. **The online measurements (section 5.2) are used to estimate the pose of the HiBall during operation.** The 1991 system collected a group of diverse measurements for a variety of LEDs and sensors, and then used a method of simultaneous nonlinear equations called collinearity (Azuma & Ward, 1991) to estimate the pose of the sensor fixture shown in figure 3 (bottom). Welch 2001 at Section 5.3. In contrast, the approach we use with the new HiBall system produces tracker reports as each new measurement is made, rather than waiting to form a complete collection of observations. Because single measurements underconstrain the mathematical solution, we refer to the approach as single-constraint-at-a-time (SCAAT) tracking (Welch, 1996; Welch & Bishop, 1997). The key is that the single measurements provide some information about the HiBall's state, and thus can be used to incrementally improve a previous estimate. We intentionally fuse each individual "insufficient" measurement immediately as it is obtained. **With this approach, we are able to generate estimates more frequently, with less latency, and with improved accuracy, and we are able to estimate the LED positions online concurrently while tracking the HiBall (section 5.4).** Welch 2001 at Section 5.3. We use a Kalman filter (Kalman, 1960) to fuse the measurements into an estimate of the HiBall state x (the pose of the HiBall). We use the Kalman filter—a minimum-variance stochastic estimator—both because the sensor measurement noise and the typical user-motion dynamics can be modeled as normally distributed random processes, and because we want an efficient online method of estimation. Welch 2001 at Section 5.3. The Kalman filter has been used previously to address similar or related problems. . . . A relevant example of a Kalman filter used for sensor fusion in a wide-area tracking system is given in Foxlin et al. (1998), which describes a hybrid inertial-acoustic system that is commercially available today (Intersense, 2000). Welch 2001 at Section 5.3. [O]ne key benefit warrants discussion here. There is a direct relationship between the complexity of the estimation algorithm, the corresponding speed (execution time per estimation cycle), and the change in HiBall pose between estimation cycles (figure 12). As the algorithmic complexity increases, the execution time

Exhibit D-6

CLAIM 5	Welch 2001
	increases, which allows for significant nonlinear HiBall motion between estimation cycles, which in turn implies the need for a more complex estimation algorithm. Welch 2001 at Section 5.3.  Figure 12. The SCAAT approach, on the other hand, is an attempt to reverse this cycle. Because we intentionally use a single constraint per estimate, the algorithmic complexity is drastically reduced, which reduces the execution time, and hence the amount of motion between estimation cycles. Because the amount of motion is limited, we are able to use a simple dynamic (process) model in the Kalman filter, which further simplifies the computations. In short, the simplicity of the approach means that it can run very fast, which means it can pro- duce estimates very rapidly, with low noise. Welch 2001 at Section 5.3.

CLAIM 5	Welch 2001
	In this article, we describe a new and vastly improved version of the 1991 system. We call the new system the HiBall Tracking System. Thanks to significant improvements in hardware and software, this HiBall system offers unprecedented speed, resolution, accuracy, robustness, and flexibility. The bulky and heavy sensors and backpack of the previous system have been replaced by a small HiBall unit (figure 4, bottom). In addition, the precisely machined LED ceiling panels of the previous system have been replaced by looser-tolerance panels that are relatively inexpensive to make and simple to install (figure 4, top; figure 10). **Finally, we are using an unusual Kalman-filter-based algorithm that generates very accurate pose estimates at a high rate with low latency, and that simultaneously self-calibrates the system.** Welch 2001 at Section 1.3 *See* Disclosures with respect to Claim 1, *supra*; *see also* Defendants' Invalidity Contentions for further discussion.

D. DEPENDENT CLAIM 6

CLAIM 6	Welch 2001
[6] The method of claim 1 wherein the state estimate characterizes configuration information for one or more sensing elements fixed to the object.	At least under Plaintiffs' apparent infringement theory, Welch 2001 discloses, either expressly or inherently, the method of claim 1 wherein the state estimate characterizes configuration information for one or more sensing elements fixed to the object. In the alternative, this element would be obvious over Welch 2001 in light of the other references disclosed in Defendants' Invalidity Contentions and/or the knowledge of one of ordinary skill in the art. *See, e.g.*: As part of his 1984 dissertation on Self-Tracker, Bishop put forward the idea of outward-looking tracking systems based on user-mounted sensors that estimate user pose by observing landmarks in the environment (Bishop, 1984). He described two kinds of landmarks: high signal-to-noise-ratio beacons such as light-emitting diodes (LEDs) and low signal-to-noise- ratio landmarks such as naturally occurring features. Bishop designed and demonstrated custom VLSI chips (figure 2) that combined image sensing and processing on a single chip (Bishop & Fuchs, 1984). The idea was to combine multiple instances of these chips into an outward-looking cluster that estimated cluster motion by observing natural features in the unmodified environment. Integrating the resulting motion to estimate pose is prone to accumulating error, so further development required a

CLAIM 6	Welch 2001
	complementary system based on easily detectable landmarks (LEDs) at known locations. Welch 2001 at Section 1.2. 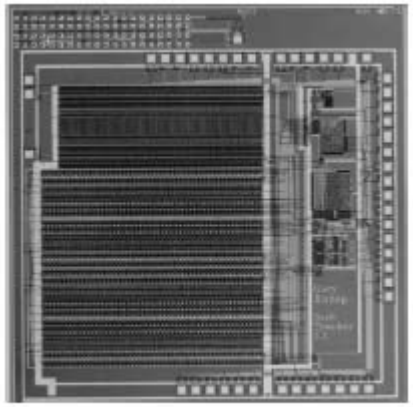 Figure 2. To determine the mapping between sensor image-plane coordinates and three-space rays, we use a single LED mounted at a fixed location in the laboratory such that it is centered in the view directly out of the top lens of the HiBall. This ray defines the z or up axis for the HiBall coordinate system. We sample other rays by rotating the goniometer motors under computer control. We sample each view with rays spaced about every six minutes of arc throughout the field of view. We repeat each measurement 100 times to reduce the effects of noise on the individual measurements and to estimate the standard deviation of the measurements. Welch 2001 at Section 5.1. Each HiBall observes LEDs through multiple sensor-lens views that are distributed over a large solid angle. **LEDs are sequentially flashed (one at a time) such that they are seen via a diverse set of views for each HiBall. Initial acquisition is performed using a brute-force search through LED space, but, once initial lock is made, the selection of LEDs to flash is tailored to the views of the active HiBall units.** Pose estimates are maintained using a Kalman-filter-based prediction-correction approach known as single-constraint-at-a-time (SCAAT) tracking. This technique has been extended to provide self-calibration of the ceiling, concurrent with HiBall tracking. Welch 2001 at Section 3.

Exhibit D-6

CLAIM 6	Welch 2001
	The design results in a ceiling with a rectangular LED pattern with periods of 7.6 cm and 15.2 cm. This spacing is used for the initial estimates of the LED positions in the lab; then, during normal operation, the SCAAT algorithm continually refines the LED position estimates (section 5.4). The SCAAT autocalibration not only relaxes design and installation constraints, but provides greater precision in the face of initial and ongoing uncertainty in the ceiling structure. Welch 2001 at Section 4.2. The online measurements (section 5.2) are used to estimate the pose of the HiBall during operation. The 1991 system collected a group of diverse measurements for a variety of LEDs and sensors, and then used a method of simultaneous nonlinear equations called collinearity (Azuma & Ward, 1991) to estimate the pose of the sensor fixture shown in figure 3 (bottom). Welch 2001 at Section 5.3. In contrast, the approach we use with the new HiBall system produces tracker reports as each new measurement is made, rather than waiting to form a complete collection of observations. Because single measurements underconstrain the mathematical solution, we refer to the approach as single-constraint-at-a-time (SCAAT) tracking (Welch, 1996; Welch & Bishop, 1997). The key is that the single measurements provide some information about the HiBall's state, and thus can be used to incrementally improve a previous estimate. We intentionally fuse each individual "insufficient" measurement immediately as it is obtained. With this approach, we are able to generate estimates more frequently, with less latency, and with improved accuracy, and we are able to estimate the LED positions online concurrently while tracking the HiBall (section 5.4). Welch 2001 at Section 5.3. We use a Kalman filter (Kalman, 1960) to fuse the measurements into an estimate of the HiBall state x (the pose of the HiBall). We use the Kalman filter—a minimum-variance stochastic estimator—both because the sensor measurement noise and the typical user-motion dynamics can be modeled as normally distributed random processes, and because we want an efficient online method of estimation. Welch 2001 at Section 5.3. The Kalman filter has been used previously to address similar or related problems. . . . A relevant example of a Kalman filter used for sensor fusion in a wide-area tracking system is given in Foxlin et al. (1998), which describes a hybrid inertial-acoustic system that is commercially available today (Intersense, 2000). Welch 2001 at Section 5.3.

Exhibit D-6

CLAIM 6	Welch 2001
	[O]ne key benefit warrants discussion here. There is a direct relationship between the complexity of the estimation algorithm, the corresponding speed (execution time per estimation cycle), and the change in HiBall pose between estimation cycles (figure 12). As the algorithmic complexity increases, the execution time increases, which allows for significant nonlinear HiBall motion between estimation cycles, which in turn implies the need for a more complex estimation algorithm. Welch 2001 at Section 5.3.  Figure 12. The SCAAT approach, on the other hand, is an attempt to reverse this cycle. Because we intentionally use a single constraint per estimate, the algorithmic complexity is drastically reduced, which reduces the execution time, and hence the amount of motion between estimation cycles. Because the amount of motion is limited, we are able to use a simple dynamic (process) model in the Kalman filter, which further simplifies the computations. In short, the simplicity of the approach means that it can run very fast, which means it can pro- duce estimates

CLAIM 6	Welch 2001
	very rapidly, with low noise. Welch 2001 at Section 5.3. In all of the optical systems we have developed (see section 1.2), we have chosen what we call an insidelooking-out configuration, in which the optical sensors are on the (moving) user and the landmarks (for instance, the LEDs) are fixed in the laboratory. The corresponding outside-looking-in alternative would be to place the landmarks on the user and to fix the optical sensors in the laboratory. (One can think about similar outside-in and inside-out distinctions for acoustic and magnetic technologies.) The two configurations are depicted in figure 5. Welch 2001 at Section 2 **The method we now use for autocalibration involves defining a distinct SCAAT Kalman filter for each LED. Specifically, for each LED, we maintain a state #l (estimate of the 3-D position) and a 3 x 3 Kalman filter covariance. At the beginning of each estimation cycle, we form an augmented state vector xÜ using the appropriate LED state and the current HiBall state: xÜ 5 [x# T, l#T]T. Similarly, we augment the Kalman filter error covariance matrix with that of the LED filter. We then follow the normal steps outlined in section 5.3, with the result being that the LED portion of the filter state and covariance is updated in accordance with the measurement residual. At the end of the cycle, we extract the LED portions of the state and covariance from the augmented filter, and save them externally. The effect is that, as the system is being used, it continually refines its estimates of the LED positions, thereby continually improving its estimates of the HiBall pose. Again, for additional information, see Welch (1996) and Welch and Bishop (1997).** Welch 2001 at Section 5.4 *See* Disclosures with respect to Claim 1, *supra*; *see also* Defendants' Invalidity Contentions for further discussion.

E. DEPENDENT CLAIM 7

CLAIM 7	Welch 2001
[7] The method of claim 6 wherein the configuration information for the one	At least under Plaintiffs' apparent infringement theory, Welch 2001 discloses, either expressly or inherently, the method of claim 6 wherein the configuration information for the one or more sensing elements fixed to the object includes information related to position or orientation of said sensing elements relative to the object. In the

Exhibit D-6

CLAIM 7	Welch 2001
or more sensing elements fixed to the object includes information related to position or orientation of said sensing elements relative to the object.	alternative, this element would be obvious over Welch 2001 in light of the other references disclosed in Defendants' Invalidity Contentions and/or the knowledge of one of ordinary skill in the art. *See, e.g.*: In 1991, we demonstrated a working, scalable, electro-optical head-tracking system in the Tomorrow's Realities gallery at that year's ACM SIGGRAPH conference (Wang et al., 1990; Wang, Chi, & Fuchs, 1990; Ward et al., 1992). **The system (figure 3) used four, head-worn, lateral-effect photodiodes that looked up- ward at a regular array of infrared LEDs installed in precisely machined ceiling panels. A user-worn backpack contained electronics that digitized and communicated the photo-coordinates of the sighted LEDs.** Photo-grammetric techniques were used to compute a user's head pose using the known LED positions and the corresponding measured photo-coordinates from each LEPD sensor (Azuma & Ward, 1991). Welch 2001 at Section 1.2.

Exhibit D-6

CLAIM 7	Welch 2001
	

Exhibit D-6

CLAIM 7	Welch 2001
	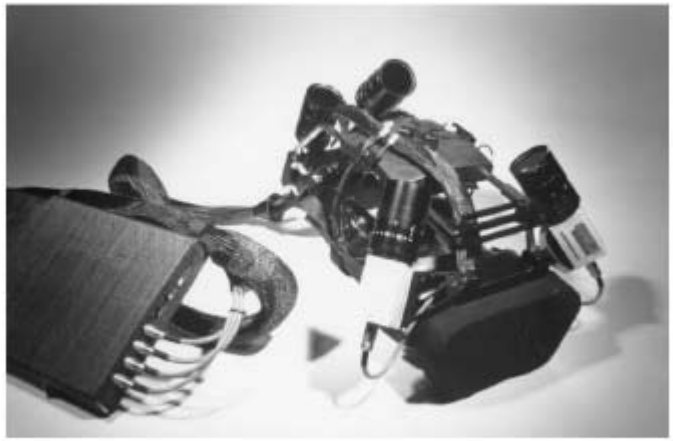 Figure 3. Thanks to significant improvements in hardware and software, this HiBall system offers unprecedented speed, resolution, accuracy, robustness, and flexibility. The bulky and heavy sensors and backpack of the previous system have been replaced by a small HiBall unit (figure 4, bottom). In addition, the precisely machined LED ceiling panels of the previous system have been replaced by looser-tolerance panels that are relatively inexpensive to make and simple to install (figure 4, top; figure 10). Finally, we are using an unusual Kalman-filter-based algorithm that generates very accurate pose estimates at a high rate with low latency, and that simultaneously self-calibrates the system. Welch 2001 at Section 1.3.

Exhibit D-6

CLAIM 7	Welch 2001
	  Figure 4. In all of the optical systems we have developed (see section 1.2), we have chosen what we call an inside-looking-out configuration, in which the optical sensors are on the (moving) user and the landmarks (for instance, the LEDs) are fixed in the laboratory. **The corresponding outside-looking-in alternative would be to place the landmarks on the user and to fix the optical sensors in the laboratory. (**One can think about similar outside-in and inside-out distinctions for acoustic and magnetic technologies.) The two configurations are depicted in figure 5. Welch 2001 at Section 2.

Exhibit D-6

CLAIM 7	Welch 2001
	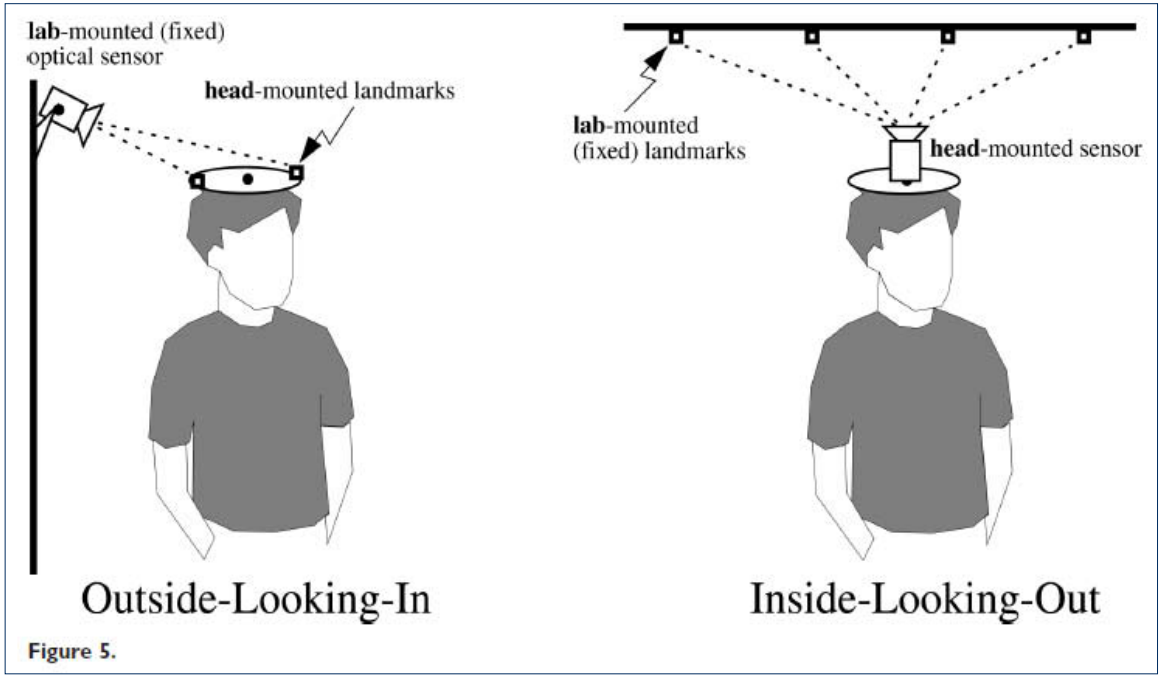 Figure 5. *See* Disclosures with respect to Claim 6, *supra*; *see also* Defendants' Invalidity Contentions for further discussion.

F. DEPENDENT CLAIM 8

CLAIM 8	Welch 2001
[8] The method of claim 6 wherein the configuration information for the one or more sensing elements fixed to the object includes operational	At least under Plaintiffs' apparent infringement theory, Welch 2001 discloses, either expressly or inherently, the method of claim 6 wherein the configuration information for the one or more sensing elements fixed to the object includes operational parameters for the one or more sensing elements. In the alternative, this element would be obvious over Welch 2001 in light of the other references disclosed in Defendants' Invalidity Contentions and/or the knowledge of one of ordinary skill in the art. *See, e.g.*:

Exhibit D-6

CLAIM 8	Welch 2001
parameters for the one or more sensing elements.	In all of the optical systems we have developed (see section 1.2), we have chosen what we call an inside-looking-out configuration, in which the optical sensors are on the (moving) user and the landmarks (for instance, the LEDs) are fixed in the laboratory. **The corresponding outside-looking-in alternative would be to place the landmarks on the user and to fix the optical sensors in the laboratory. (**One can think about similar outside-in and inside-out distinctions for acoustic and magnetic technologies.) The two configurations are depicted in figure 5. Welch 2001 at Section 2. Along with the benefit of simplicity and speed, the SCAAT approach offers the additional capability of being able to estimate the 3-D positions of the LEDs in the world concurrently with the pose of the HiBall, online, in real time. This capability is a tremendous benefit in terms of the accuracy and noise characteristics of the estimates.

Exhibit D-6

CLAIM 8	Welch 2001
	The method we now use for autocalibration involves defining a distinct SCAAT Kalman filter for each LED. Specifically, for each LED, we maintain a state $\bar{l}$ (estimate of the 3-D position) and a 3×3 Kalman filter covariance. At the beginning of each estimation cycle, we form an augmented state vector $\hat{x}$ using the appropriate LED state and the current HiBall state: $\hat{x} = [\bar{x}^T, \bar{l}^T]^T$. Similarly, we augment the Kalman filter error covariance matrix with that of the LED filter. We then follow the normal steps outlined in section 5.3, with the result being that the LED portion of the filter state and covariance is updated in accordance with the measurement residual. At the end of the cycle, we extract the LED portions of the state and covariance from the augmented filter, and save them externally. The effect is that, as the system is being used, it continually refines its estimates of the LED positions, thereby continually improving its estimates of the HiBall pose. Again, for additional information, see Welch (1996) and Welch and Bishop (1997). Welch 2001 at Section 5.4. **The recursive nature of the Kalman filter (section 5.3) requires that the filter be initialized with a known state and corresponding covariance before steady-state operation can begin. Such an initialization (or acquisition) must take place prior to any tracking session, but also upon the (rare) occasion when the filter diverges and "loses lock" as a result of blocked sensor views, for example.** Welch 2001 at Section 5.5.

Exhibit D-6

CLAIM 8	Welch 2001
	The acquisition process is complicated by the fact that each LEPD sees a number of different widely separated views (section 4.1). Therefore, detecting an LED provides at best an ambiguous set of potential LED directions in HiBall coordinates. Moreover, before acquisition, no assumptions can be made to limit the search space of visible LEDs. As such, a relatively slow brute-force algorithm is used to acquire lock. Welch 2001 at Section 5.5. As a result of a mechanical design tradeoff, each sensor field of view is less than six degrees. The focal length is set by the size of the sensor housing, which is set by the diameter of the sensors themselves. Energetics is also a factor, limiting how small the lenses can be while maintaining sufficient light-collecting area. As a result of these design tradeoffs, even a momentary small error in the HiBall pose estimate can cause the recursive estimates to diverge and the system to lose lock after only a few LED sightings. And yet the system is quite robust. In practice, users can jump around, crawl on the floor, lean over, even wave their hands in front of the sensors, and the system does not lose lock. During one session, we were using the HiBall as a 3-D digitization probe, a Hi-Ball on the end of a pencil-shaped fiberglass wand (figure 14, left). We laid the probe down on a table at one point, and were amazed to later notice that it was still tracking, even though it was observing only three or four LEDs near the edge of the ceiling. We picked up the probe and continued using it, without it ever losing lock.   Figure 13.

Exhibit D-6

CLAIM 8	Welch 2001

Figure 14.

Welch 2001 at Section 6.1.

To make measurements of the noise when the HiBall is in motion, we rely on the assumption that almost all of the signal resulting from normal human motion is at frequencies below 2 Hz. **We use a high-pass filter (Welch, 1967) on the pose estimates, and assume the output is noise.** The resulting statistics are comparable to those made with the HiBall stationary, except at poses for which there are very few LEDs visible in only one or two views. In these poses, near the edge of the ceiling, the geometry of the constraints results in amplification of errors. For nearly all of the working volume of the tracker, the standard deviation of the noise on measurements while the HiBall is still or moving is about 0.2 mm and 0.03 deg.
Welch 2001 at Section 6.1.

During the design of the HiBall system, we made substantial use of simulation, in some domains to a very detailed level. For example, Zemax (Focus Software, 1995) was used extensively in the design and optimization of the optical design, including the design of the filter glass lenses, and geometry of the optical-component layout.
Welch 2001 at Section 6.2.

To produce realistic data for developing and tuning our algorithms, we collected several motion paths (sequences of pose estimates) from our first-generation electro-optical tracker (figure 3) at its 70 Hz maximum report rate. These paths were recorded from both naive users visiting our monthly “demo days” and from experienced users in our labs. . . . we filtered the raw path data with a noncausal zero-phase-shift, low-pass filter to eliminate energy

CLAIM 8	Welch 2001
	above 2 Hz. The output of the low-pass filtering was then resampled at whatever rate we wanted to run the simulated tracker, usually 1,000 Hz. Welch 2001 at Section 6.2. The simulator reads camera models describing the 26 views, the sensor noise parameters, the LED positions and their expected error, and the motion path described above. Before beginning the simulation, the LED positions are perturbed from their ideal positions by adding normally distributed error to each axis. Then, for each simulated cycle of operation, the "true" poses are up- dated using the input motion path. Next, a view is chosen and a visible LED within that view is selected, and the image-plane coordinates of the LED on the chosen sensor are computed using the camera model for the view and the LED as described in section 5.3. These sensor coordinates are then perturbed based on the sensor noise model (section 6.2.1) using the distance and angle to the LED. These noise-corrupted sensor readings are then fed to the SCAAT filter to produce an up- dated position estimate. The position estimate is com- pared to the true position to produce a scalar error metric that is described next. Welch 2001 at Section 6.2. The error metric we used combines the error in pose in a way that relates to the effects of tracker error on a head-worn display user. **We define a set of points arrayed around the user in a fixed configuration. We compute two sets of coordinates for these points: the true position using the true pose and their estimated position using the estimated pose. The error metric is then the sum of the distances between the true and estimated positions of these points. By adjusting the distance of the points from the user, we can control the relative importance of the orientation and the position error in the combined error metric.** If the distance is small, then the position error is weighted most heavily; if the distance is large, then the orientation error is weighted most heavily. Our two error metrics for the entire run are the square root of the sum of the squares of all the distances, and the peak distance. Welch 2001 at Section 6.2. *See* Disclosures with respect to Claim 6, *supra*; *see also* Defendants' Invalidity Contentions for further discussion.

G. DEPENDENT CLAIM 24

CLAIM 24	Welch 2001
[24] The method of claim 1 wherein updating the state estimate includes applying a Kalman Filter approach.	At least under Plaintiffs' apparent infringement theory, Welch 2001 discloses, either expressly or inherently, the method of claim 1 wherein updating the state estimate includes applying a Kalman Filter approach. In the alternative, this element would be obvious over Welch 2001 in light of the other references disclosed in Defendants' Invalidity Contentions and/or the knowledge of one of ordinary skill in the art. *See, e.g.*: Thanks to significant improvements in hardware and software, this HiBall system offers unprecedented speed, resolution, accuracy, robustness, and flexibility. The bulky and heavy sensors and backpack of the previous system have been replaced by a small HiBall unit (figure 4, bottom). In addition, the precisely machined LED ceiling panels of the previous system have been replaced by looser-tolerance panels that are relatively inexpensive to make and simple to install (figure 4, top; figure 10). **Finally, we are using an unusual Kalman-filter-based algorithm that generates very accurate pose estimates at a high rate with low latency, and that simultaneously self-calibrates the system.** Welch 2001 at Section 1.3.

Exhibit D-6

CLAIM 24	Welch 2001

Figure 4.

Each HiBall observes LEDs through multiple sensor-lens views that are distributed over a large solid angle. LEDs are sequentially flashed (one at a time) such that they are seen via a diverse set of views for each HiBall. Initial acquisition is performed using a brute-force search through LED space, but, once initial lock is made, the selection of LEDs to flash is tailored to the views of the active HiBall units. **Pose estimates are maintained using a Kalman-filter-based prediction-correction approach known as single-constraint-at-a-time (SCAAT) tracking. This technique has been extended to provide self-calibration of the ceiling, concurrent**

Exhibit D-6

CLAIM 24	Welch 2001
	with HiBall tracking. **Welch 2001 at Section 3.** **We use a Kalman filter (Kalman, 1960) to fuse the measurements into an estimate of the HiBall state x (the pose of the HiBall). We use the Kalman filter—a minimum-variance stochastic estimator—both because the sensor measurement noise and the typical user-motion dynamics can be modeled as normally distributed random processes, and because we want an efficient online method of estimation.** Welch 2001 at Section 5.3. **The Kalman filter has been used previously to address similar or related problems. . . .** A relevant example of a Kalman filter used for sensor fusion in a wide-area tracking system is given in Foxlin et al. (1998), which describes a hybrid inertial-acoustic system that is commercially available today (Intersense, 2000). Welch 2001 at Section 5.3. The SCAAT approach, on the other hand, is an attempt to reverse this cycle. Because we intentionally use a single constraint per estimate, the algorithmic complexity is drastically reduced, which reduces the execution time, and hence the amount of motion between estimation cycles. **Because the amount of motion is limited, we are able to use a simple dynamic (process) model in the Kalman filter, which further simplifies the computations.** In short, the simplicity of the approach means that it can run very fast, which means it can produce estimates very rapidly, with low noise. Welch 2001 at Section 5.3. **The Kalman filter requires both a model of the process dynamics and a model of the relationship between the process state and the available measurements. In part due to the simplicity of the SCAAT approach, we are able to use a simple position-velocity (PV) process model** (Brown & Hwang, 1992). . . . We model the continuous change in the HiBall state with the simple differential equation

CLAIM 24	Welch 2001
	$$\frac{d}{dt}\bar{x}(t) = \begin{bmatrix} 0 & 1 \\ 0 & 0 \end{bmatrix}\begin{bmatrix} x_p(t) \\ x_v(t) \end{bmatrix} + \begin{bmatrix} 0 \\ \mu \end{bmatrix} u(t), \qquad (1)$$ where $u(t)$ is a normally distributed white (in the frequency spectrum) scalar noise process, and the scalar μ represents the magnitude or spectral density of the noise. We use a similar model with a distinct noise process for each of the six pose elements. We determine the individual noise magnitudes using an offline simulation of the system and a nonlinear optimization strategy that seeks to minimize the variance between the estimated pose and a known motion path. (See section 6.2.2.). Welch 2001 at Section 5.3. **The recursive nature of the Kalman filter (section 5.3) requires that the filter be initialized with a known state and corresponding covariance before steady-state operation can begin.** Such an initialization (or acquisition) must take place prior to any tracking session, but also upon the (rare) occasion when the filter diverges and "loses lock" as a result of blocked sensor views, for example. Welch 2001 at Section 5.5. *See* Disclosures with respect to Claim 1, *supra*; *see also* Defendants' Invalidity Contentions for further discussion.

H. DEPENDENT CLAIM 25

CLAIM 25	Welch 2001
[25] The method of claim 1 wherein each of said sensing elements	At least under Plaintiffs' apparent infringement theory, Welch 2001 discloses, either expressly or inherently, the method of claim 1 wherein each of said sensing elements comprises at least one of a sensor and a target. In the

Exhibit D-6

CLAIM 25	Welch 2001
comprises at least one of a sensor and a target.	alternative, this element would be obvious over Welch 2001 in light of the other references disclosed in Defendants' Invalidity Contentions and/or the knowledge of one of ordinary skill in the art. *See, e.g.*: 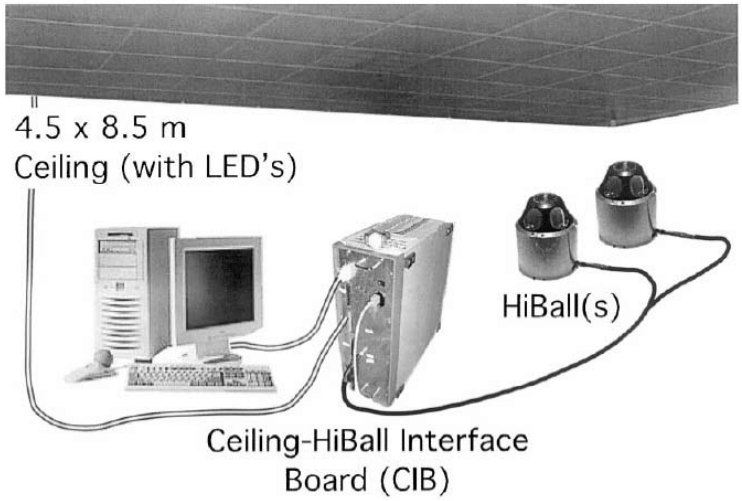 Figure 6. Welch 2001 at Fig. 3 **In all of the optical systems we have developed (see section 1.2), we have chosen what we call an inside-looking-out configuration, in which the optical sensors are on the (moving) user and the landmarks (for instance, the LEDs) are fixed in the laboratory.** The corresponding outside-looking-in alternative would be to place the landmarks on the user and to fix the optical sensors in the laboratory. (One can think about similar outside-in and inside-out distinctions for acoustic and magnetic technologies.) The two configurations are depicted in figure 5. Welch 2001 at Section 2. **As a result of a mechanical design tradeoff, each sensor field of view is less than six degrees. The focal length is set by the size of the sensor housing, which is set by the diameter of the sensors themselves. Energetics is**

Exhibit D-6

CLAIM 25	Welch 2001
	also a factor, limiting how small the lenses can be while maintaining sufficient light-collecting area. As a result of these design tradeoffs, even a momentary small error in the HiBall pose estimate can cause the recursive estimates to diverge and the system to lose lock after only a few LED sightings. And yet the system is quite robust. In practice, users can jump around, crawl on the floor, lean over, even wave their hands in front of the sensors, and the system does not lose lock. During one session, we were using the HiBall as a 3-D digitization probe, a Hi-Ball on the end of a pencil-shaped fiberglass wand (figure 14, left). We laid the probe down on a table at one point, and were amazed to later notice that it was still tracking, even though it was observing only three or four LEDs near the edge of the ceiling. We picked up the probe and continued using it, without it ever losing lock.   Figure 13.   Figure 14. Welch 2001 at Section 6.1.

Exhibit D-6

CLAIM 25	Welch 2001
	See Disclosures with respect to Claim 1, *supra*; *see also* Defendants' Invalidity Contentions for further discussion.

I. DEPENDENT CLAIM 28

CLAIM 28	Welch 2001
[28] The method of claim 1 wherein the object is selected from a group consisting of a vehicle, a robot, a person, a part of a person, a flying object, a floating object, an underwater moving object, an animal, a camera, a sensing apparatus, a helmet, a tool, a piece of sports equipment, a shoe, a boot, an article of clothing, a personal protective equipment, a rigid object having a dimension between 1 nanometer to 109 meters.	At least under Plaintiffs' apparent infringement theory, Welch 2001 discloses, either expressly or inherently, the method of claim 1 wherein the object is selected from a group consisting of a vehicle, a robot, a person, a part of a person, a flying object, a floating object, an underwater moving object, an animal, a camera, a sensing apparatus, a helmet, a tool, a piece of sports equipment, a shoe, a boot, an article of clothing, a personal protective equipment, a rigid object having a dimension between 1 nanometer to 109 meters. In the alternative, this element would be obvious over Welch 2001 in light of the other references disclosed in Defendants' Invalidity Contentions and/or the knowledge of one of ordinary skill in the art. *See, e.g.*: In 1991, we demonstrated a working, scalable, electro-optical head-tracking system in the Tomorrow's Realities gallery at that year's ACM SIGGRAPH conference (Wang et al., 1990; Wang, Chi, & Fuchs, 1990; Ward et al., 1992). The system (figure 3) used four, head-worn, lateral-effect photodiodes that looked up- ward at a regular array of infrared LEDs installed in precisely machined ceiling panels. **A user-worn backpack contained electronics that digitized and communicated the photo-coordinates of the sighted LEDs. Photo-grammetric techniques were used to compute a user's head pose using the known LED positions and the corresponding measured photo-coordinates from each LEPD sensor (Azuma & Ward, 1991).** Welch 2001 at Section 1.2.

Exhibit D-6

CLAIM 28	Welch 2001
	

Exhibit D-6

CLAIM 28	Welch 2001
	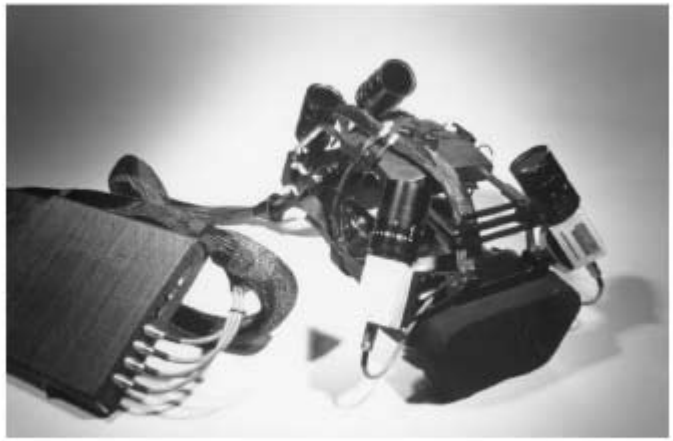 Figure 3. Thanks to significant improvements in hardware and software, this HiBall system offers unprecedented speed, resolution, accuracy, robustness, and flexibility. The bulky and heavy sensors and backpack of the previous system have been replaced by a small HiBall unit (figure 4, bottom). In addition, the precisely machined LED ceiling panels of the previous system have been replaced by looser-tolerance panels that are relatively inexpensive to make and simple to install (figure 4, top; figure 10). Finally, we are using an unusual Kalman-filter-based algorithm that generates very accurate pose estimates at a high rate with low latency, and that simultaneously self-calibrates the system. Welch 2001 at Section 1.3.

Exhibit D-6

CLAIM 28	Welch 2001
	  Figure 4.

CLAIM 28	Welch 2001
	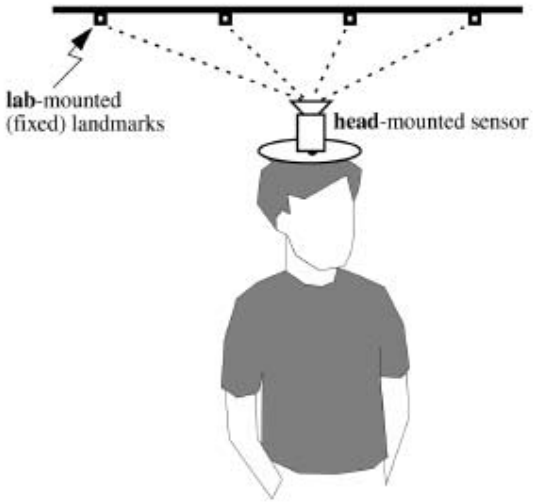 Inside-Looking-Out *See* Disclosures with respect to Claim 1, *supra*; *see also* Defendants' Invalidity Contentions for further discussion.

J. DEPENDENT CLAIM 29

CLAIM 29	Welch 2001
[29] The method of claim 1 wherein the state estimate comprises information related to a position or an orientation of the object relative to a reference coordinate frame.	At least under Plaintiffs' apparent infringement theory, Welch 2001 discloses, either expressly or inherently, the method of claim 1 wherein the state estimate comprises information related to a position or an orientation of the object relative to a reference coordinate frame. In the alternative, this element would be obvious over Welch 2001 in light of the other references disclosed in Defendants' Invalidity Contentions and/or the knowledge of one of ordinary skill in the art. *See, e.g.*:

Exhibit D-6

CLAIM 29	Welch 2001
	As part of his 1984 dissertation on Self-Tracker, Bishop put forward the idea of outward-looking tracking systems based on user-mounted sensors that estimate user pose by observing landmarks in the environment (Bishop, 1984). He described two kinds of landmarks: high signal-to-noise-ratio beacons such as light-emitting diodes (LEDs) and low signal-to-noise- ratio landmarks such as naturally occurring features. Bishop designed and demonstrated custom VLSI chips (figure 2) that combined image sensing and processing on a single chip (Bishop & Fuchs, 1984). The idea was to combine multiple instances of these chips into an outward-looking cluster that estimated cluster motion by observing natural features in the unmodified environment. Integrating the resulting motion to estimate pose is prone to accumulating error, so further development required a complementary system based on easily detectable landmarks (LEDs) at known locations. Welch 2001 at Section 1.2. 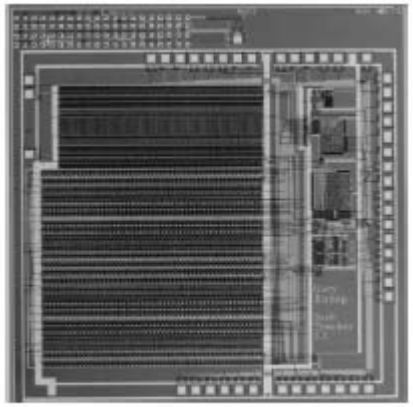 Figure 2. In 1991, we demonstrated a working, scalable, electro-optical head-tracking system in the Tomorrow's Realities gallery at that year's ACM SIGGRAPH conference (Wang et al., 1990; Wang, Chi, & Fuchs, 1990; Ward et al., 1992). The system (figure 3) used four, head-worn, lateral-effect photodiodes that looked up- ward at a regular array of infrared LEDs installed in precisely machined ceiling panels. A user-worn backpack contained electronics that digitized and communicated the photo-coordinates of the sighted LEDs. **Photo-grammetric techniques were used to compute a user's head pose using the known LED positions and the corresponding**

Exhibit D-6

CLAIM 29	Welch 2001
	measured photo-coordinates from each LEPD sensor (Azuma & Ward, 1991). Welch 2001 at Section 1.2. 

Exhibit D-6

CLAIM 29	Welch 2001
	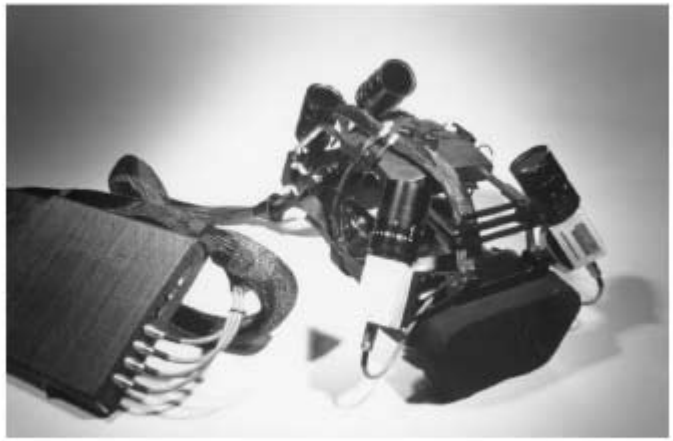 Figure 3. Thanks to significant improvements in hardware and software, this HiBall system offers unprecedented speed, resolution, accuracy, robustness, and flexibility. The bulky and heavy sensors and backpack of the previous system have been replaced by a small HiBall unit (figure 4, bottom). In addition, the precisely machined LED ceiling panels of the previous system have been replaced by looser-tolerance panels that are relatively inexpensive to make and simple to install (figure 4, top; figure 10). Finally, we are using an unusual Kalman-filter-based algorithm that generates very accurate pose estimates at a high rate with low latency, and that simultaneously self-calibrates the system. Welch 2001 at Section 1.3.

Exhibit D-6

CLAIM 29	Welch 2001
	  Figure 4. *See* Disclosures with respect to Claim 1, *supra*; *see also* Defendants' Invalidity Contentions for further discussion.

K. INDEPENDENT CLAIM 47

CLAIM 47	Welch 2001
[47.pre] A method of using multiple sensors in a tracking system comprising:	At least under Plaintiffs' apparent infringement theory, Welch 2001 discloses, either expressly or inherently, a method of using multiple sensors in a tracking system. No party has yet asserted that the preamble is limiting, nor has the Court construed the preamble as limiting. However, to the extent that the preamble is limiting, it is disclosed by Welch 2001. In the alternative, this element would be obvious over Welch 2001 in light of the other references disclosed in Defendants' Invalidity Contentions and/or the knowledge of one of ordinary skill in the art. *See, e.g.*: We present results and a complete description of our most recent **electro-optical system, the HiBall Tracking System.** In particular, we discuss motivation for the geometric configuration and describe the novel optical, mechanical, electronic, and algorithmic aspects that enable unprecedented speed, resolution, accuracy, robustness, and flexibility. Welch 2001 at Abstract. **Systems for head tracking for interactive computer graphics** have been explored for more than thirty years. Welch 2001 at Section 1. As part of his 1984 dissertation on Self-Tracker, Bishop put forward the idea of **outward-looking tracking systems based on user-mounted sensors** that estimate user pose by observing landmarks in the environment (Bishop, 1984). He described two kinds of landmarks: high signal-to-noise-ratio beacons such as light-emitting diodes (LEDs) and low signal-to-noise- ratio landmarks such as naturally occurring features. Bishop designed and demonstrated custom VLSI chips (figure 2) that combined **image sensing and processing on a single chip** (Bishop & Fuchs, 1984). **The idea was to combine multiple instances of these chips into an outward-looking cluster that estimated cluster motion by observing natural features in the unmodified environment.** Integrating the resulting motion to estimate pose is prone to accumulating error, so further development required a complementary system based on easily detectable landmarks (LEDs) at known locations. Welch 2001 at Section 1.2.

Exhibit D-6

CLAIM 47	Welch 2001
	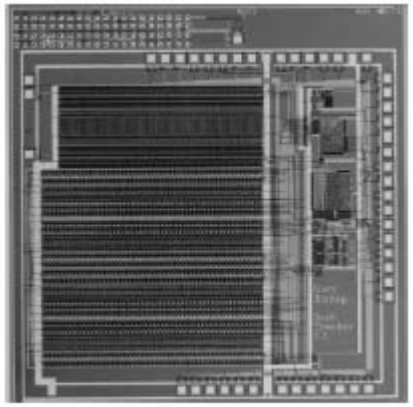 Figure 2. In 1991, we demonstrated a working, scalable, electro-optical head-tracking system in the Tomorrow's Realities gallery at that year's ACM SIGGRAPH conference (Wang et al., 1990; Wang, Chi, & Fuchs, 1990; Ward et al., 1992). **The system (figure 3) used four, head-worn, lateral-effect photodiodes that looked up- ward at a regular array of infrared LEDs installed in precisely machined ceiling panels.** A user-worn backpack contained electronics that digitized and communicated the photo-coordinates of the sighted LEDs. Photo-grammetric techniques were used to compute a user's head pose using the known LED positions and the corresponding measured photo-coordinates from each LEPD sensor (Azuma & Ward, 1991). Welch 2001 at Section 1.2.

Exhibit D-6

CLAIM 47	Welch 2001
	

Exhibit D-6

CLAIM 47	Welch 2001
	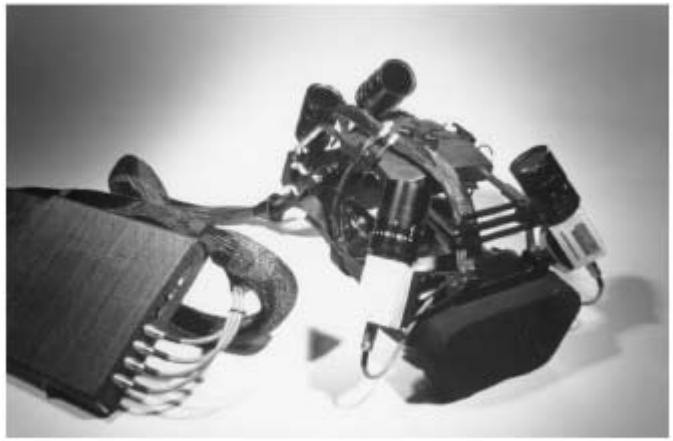 Figure 3. As part of his 1984 dissertation on Self-Tracker, Bishop put forward the idea of outward-looking tracking systems based on user-mounted sensors that estimate user pose by observing landmarks in the environment (Bishop, 1984). He described two kinds of landmarks: high signal-to-noise-ratio beacons such as light-emitting diodes (LEDs) and low signal-to-noise- ratio landmarks such as naturally occurring features. Bishop designed and demonstrated custom VLSI chips (figure 2) that combined image sensing and processing on a single chip (Bishop & Fuchs, 1984). The idea was to combine multiple instances of these chips into an outward-looking cluster that estimated cluster motion by observing natural features in the unmodified environment. Integrating the resulting motion to estimate pose is prone to accumulating error, so further development required a complementary system based on easily detectable landmarks (LEDs) at known locations. Welch 2001 at Section 1.2.

Exhibit D-6

CLAIM 47	Welch 2001

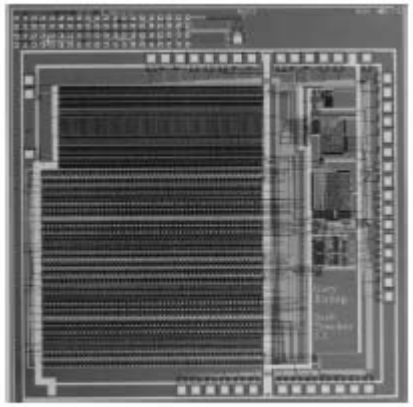

Figure 2.

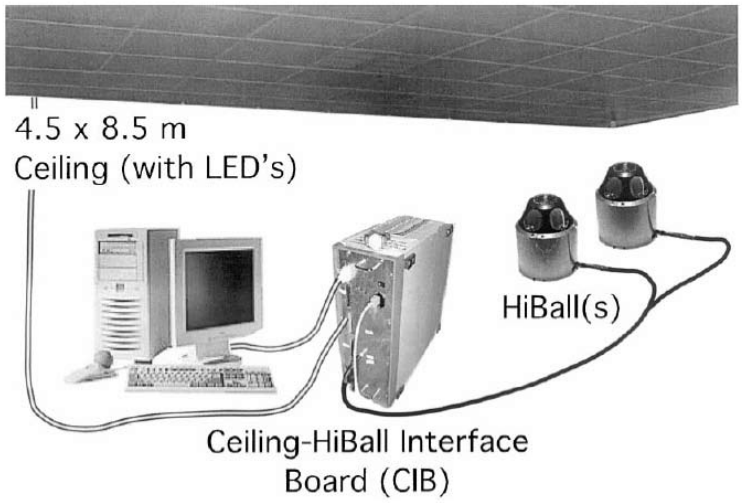

Figure 6.

HiBall sensor unit was designed as a single, rigid, hollow ball having dodecahedral symmetry, with lenses in the upper six faces and LEPDs on the insides of the opposing six lower faces (figure 7). This immediately

Exhibit D-6

CLAIM 47	Welch 2001
	gives six primary "camera" views uniformly spaced by 57 deg. The views efficiently share the same internal air space and are rigid with respect to each other. In addition, light entering any lens sufficiently off-axis can be seen by a neigh- boring LEPD, giving rise to five secondary views through the top or central lens, and three secondary views through the five other lenses. Overall, this provides 26 fields of view that are used to sense widely separated groups of LEDs in the environment. Welch 2001 at Section 4.1. The Ceiling-HiBall Interface Board (CIB) (figure 11) provides communication and synchronization between a host personal computer, the HiBall (section 4.1), and the ceiling (section 4.2). The CIB has four ceiling ports allowing interleaving of ceiling panels for up to four simultaneous LED flashes and/or higher ceiling bandwidth. (The ceiling bandwidth is inherently limited by LED power restrictions as described in section 4.2, but this can be increased by spatially multiplexing the ceiling panels.) The CIB has two tether interfaces that can communicate with up to four daisy-chained HiBall units. The full-duplex communication with the HiBall units uses a modulation scheme (BPSK) allowing future wireless operation. The interface from the CIB to the host PC is the stable IEEE1284C extended parallel port (EPP) standard. The CIB comprises analog drive and receive components as well as digital logic components. The digital components implement store and forward in both directions and synchronize the timing of the LED "on" interval within the HiBall darklight-dark intervals (section 5.2). The protocol supports full-duplex flow control. The data are arranged into packets that incorporate error detection. Welch 2001 at Section 4.3. *See also* Defendants' Invalidity Contentions for further discussion.
[47.a] providing an estimation module;	At least under Plaintiffs' apparent infringement theory, Welch 2001 discloses, either expressly or inherently, providing an estimation module. In the alternative, this element would be obvious over Welch 2001 in light of the other references disclosed in Defendants' Invalidity Contentions and/or the knowledge of one of ordinary skill in the art. *See, e.g.*: The HiBall Tracking System consists of three main components (figure 6). An outward-looking sensing unit we call the HiBall is fixed to each user to be tracked. The HiBall unit observes a subsystem of fixed-location infrared LEDs we call the Ceiling. **Communication and synchronization between the host computer and these**

Exhibit D-6

CLAIM 47	Welch 2001
	subsystems is coordinated by the Ceiling-HiBall Interface Board (CIB). Welch 2001 at Section 3. 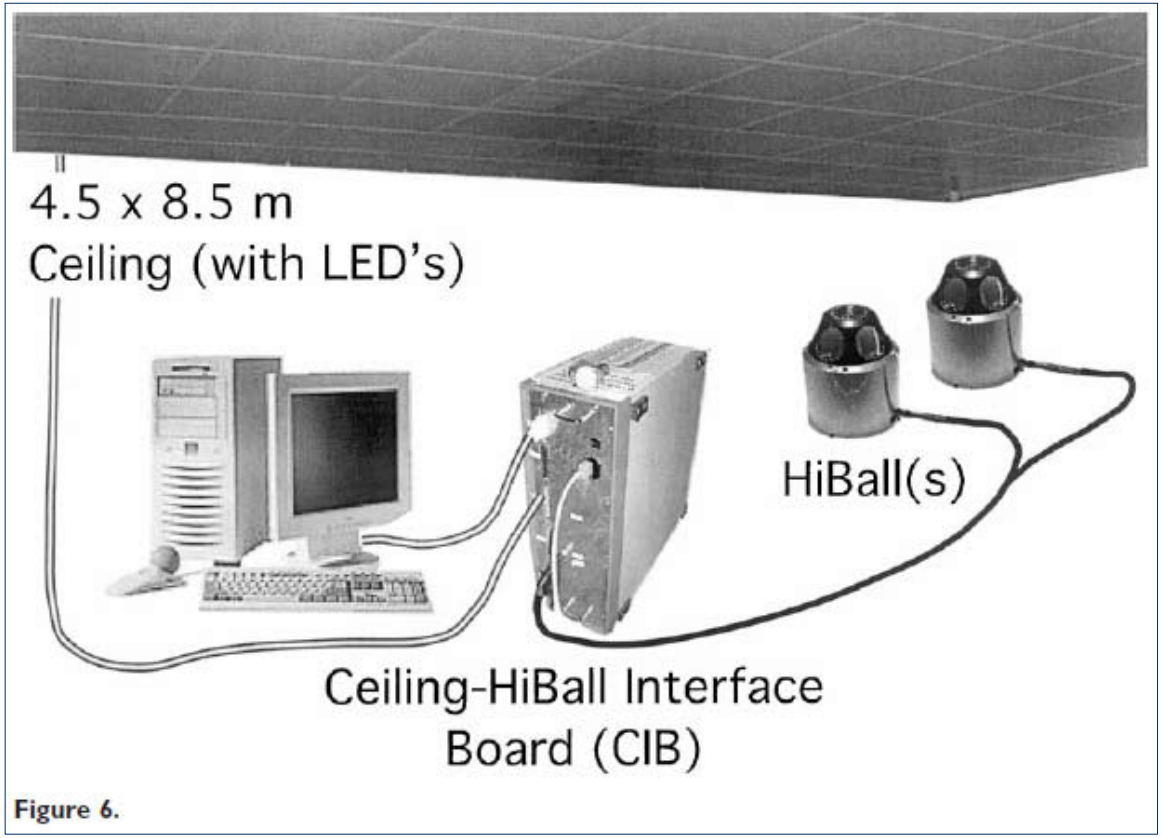 Figure 6. Each HiBall observes LEDs through multiple sensor-lens views that are distributed over a large solid angle. LEDs are sequentially flashed (one at a time) such that they are seen via a diverse set of views for each HiBall. Initial acquisition is performed using a brute-force search through LED space, but, once initial lock is made, the selection of LEDs to flash is tailored to the views of the active HiBall units. **Pose estimates are maintained using a Kalman-filter-based prediction-correction approach known as single-constraint-at-a-time**

Exhibit D-6

CLAIM 47	Welch 2001
	(SCAAT) tracking. This technique has been extended to provide self-calibration of the ceiling, concurrent with HiBall tracking. Welch 2001 at Section 3. HiBall sensor unit was designed as a single, rigid, hollow ball having dodecahedral symmetry, with lenses in the upper six faces and LEPDs on the insides of the opposing six lower faces (figure 7). This immediately gives six primary "camera" views uniformly spaced by 57 deg. The views efficiently share the same internal air space and are rigid with respect to each other. In addition, light entering any lens sufficiently off-axis can be seen by a neigh- boring LEPD, giving rise to five secondary views through the top or central lens, and three secondary views through the five other lenses. Overall, this provides 26 fields of view that are used to sense widely separated groups of LEDs in the environment. Welch 2001 at Section 4.1.

Exhibit D-6

CLAIM 47	Welch 2001
	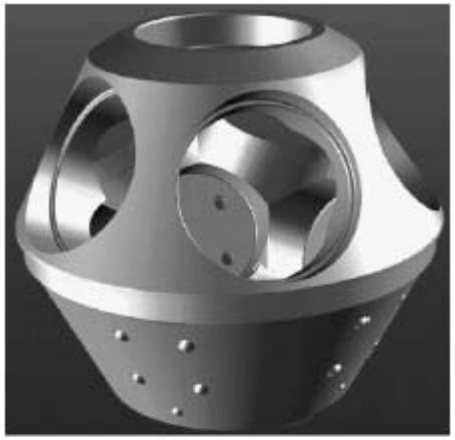  Figure 7. The LEPDs themselves are not imaging devices; rather, they detect the centroid of the luminous flux incident on the detector. The x-position of the centroid determines the ratio of two output y-position determines the ratio of two other output currents. The total output current of each pair are commensurate and are proportional to the total incident flux. Consequently, focus is not an issue, so the simple fixed-focus lenses work well over a range of LED distances from about half a meter to infinity. The LEPDs and associated electronic components are mounted on a custom rigid-flex printed circuitboard (figure 8). This arrangement makes efficient use of the internal HiBall volume while maintaining isolation between analog and digital circuitry, and increasing reliability by alleviating

CLAIM 47	Welch 2001
	the need for intercomponent mechanical connectors. Welch 2001 at Section 4.1. 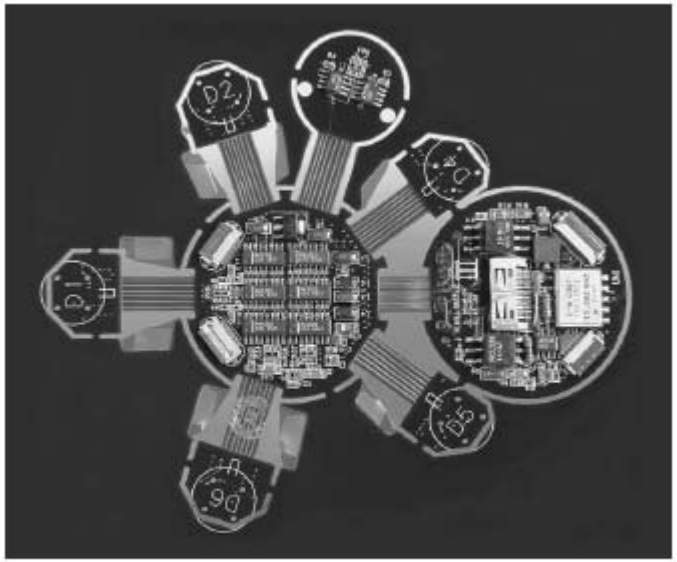 Figure 8. Figure 9 shows the physical arrangement of the folded electronics in the HiBall. Each LEPD has four transimpedance amplifiers (shown together as one "Amp" in figure 9), the analog outputs of which are multiplexed with those of the other LEPDs, then sampled, held, and converted by four 16-bit Delta-Sigma analog-to-digital (A/D) converters. **Multiple samples are integrated via an accumulator. The digitized LEPD data are organized into packets for communication back to the CIB.** The packets also contain information to assist in error detection. The communication protocol is simple, and, while presently implemented by wire, the modulation scheme is amenable to a wireless implementation. Welch 2001 at Section 4.1.

Exhibit D-6

CLAIM 47	Welch 2001

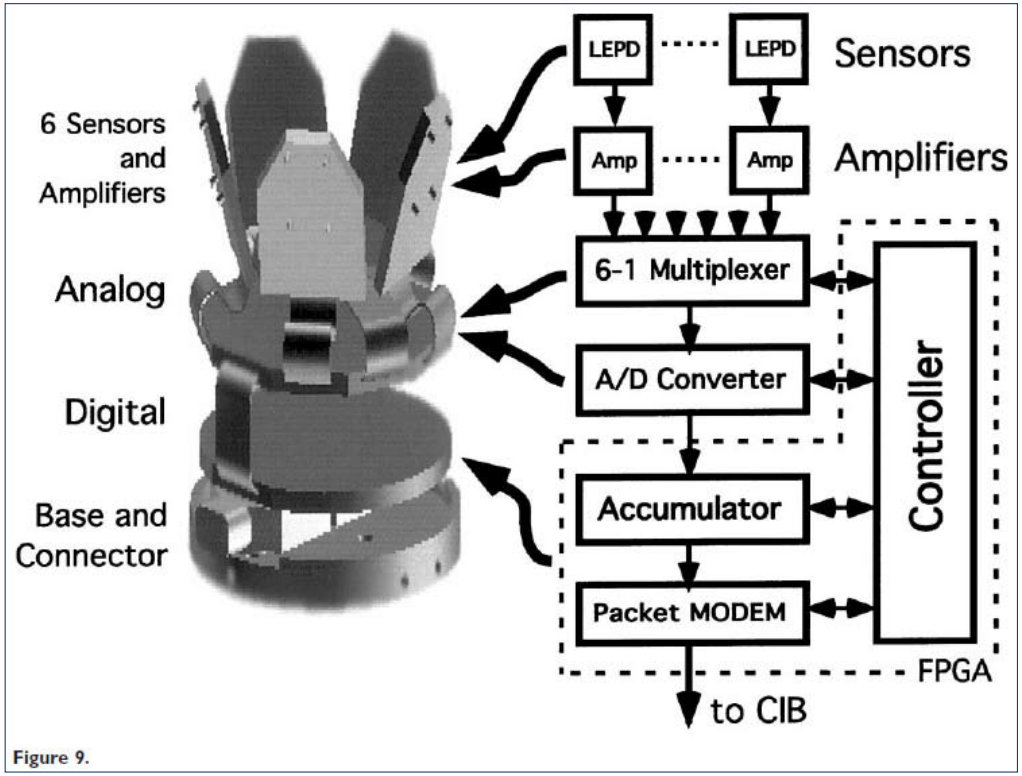

Figure 9.

The design results in a ceiling with a rectangular LED pattern with periods of 7.6 cm and 15.2 cm. **This spacing is used for the initial estimates of the LED positions in the lab; then, during normal operation, the SCAAT algorithm continually refines the LED position estimates (section 5.4). The SCAAT autocalibration not only relaxes design and installation constraints, but provides greater precision in the face of initial and ongoing uncertainty in the ceiling structure.**
Welch 2001 at Section 4.2.

The CIB comprises analog drive and receive components as well as digital logic components. The digital components implement store and forward in both directions and synchronize the timing of the LED "on" interval within the HiBall dark-light-dark intervals (section 5.2). The protocol supports full-duplex flow

Exhibit D-6

CLAIM 47	Welch 2001
	control. The data are arranged into packets that incorporate error detection. Welch 2001 at Section 4.3. *See also* Defendants' Invalidity Contentions for further discussion.
[47.b] coupling one or more sensor modules to the estimation module, each associated with a different set of one or more sensors;	At least under Plaintiffs' apparent infringement theory, Welch 2001 discloses, either expressly or inherently, coupling one or more sensor modules to the estimation module, each associated with a different set of one or more sensors. In the alternative, this element would be obvious over Welch 2001 in light of the other references disclosed in Defendants' Invalidity Contentions and/or the knowledge of one of ordinary skill in the art. *See, e.g.*: The HiBall Tracking System consists of three main components (figure 6). **An outward-looking sensing unit we call the HiBall is fixed to each user to be tracked. The HiBall unit observes a subsystem of fixed-location infrared LEDs we call the Ceiling. Communication and synchronization between the host computer and these subsystems is coordinated by the Ceiling-HiBall Interface Board (CIB)**. Welch 2001 at Section 3.

Exhibit D-6

CLAIM 47	Welch 2001

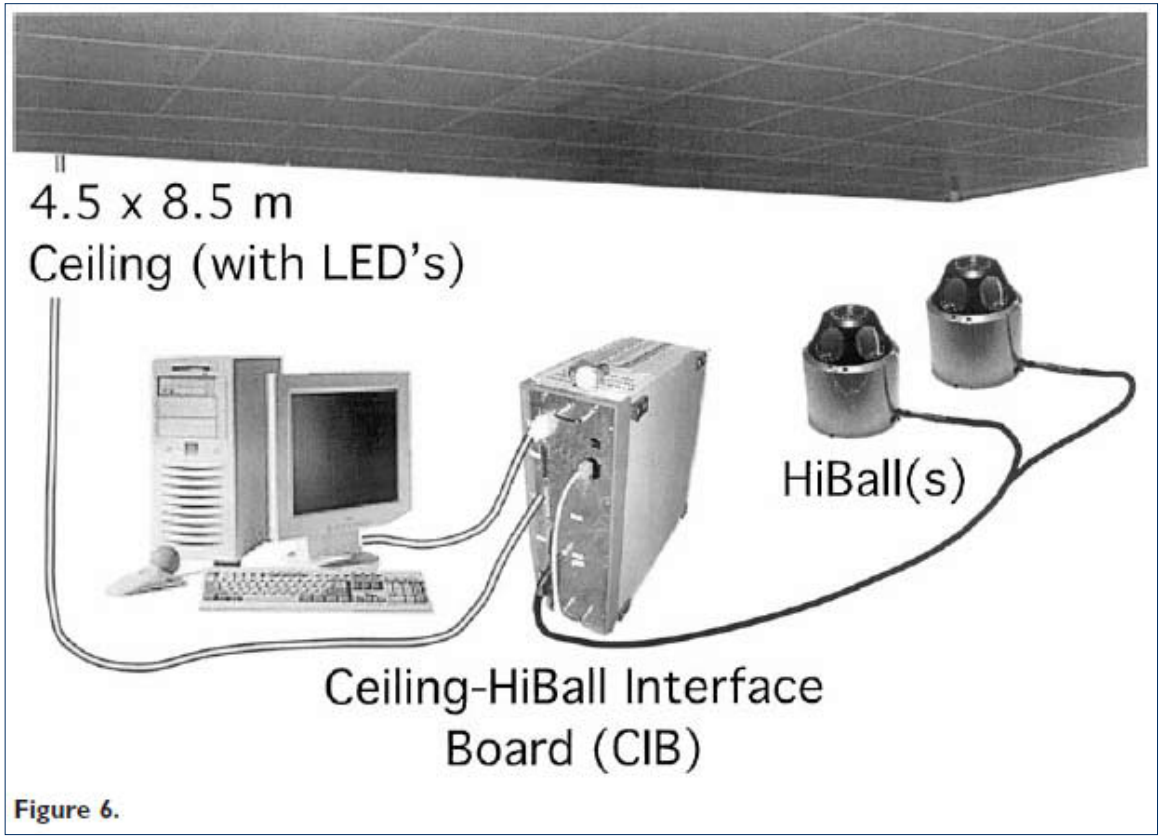

Figure 6.

Each HiBall observes LEDs through **multiple sensor-lens views that are distributed over a large solid angle. LEDs are sequentially flashed (one at a time) such that they are seen via a diverse set of views for each HiBall.** Initial acquisition is performed using a brute-force search through LED space, but, once initial lock is made, the selection of LEDs to flash is tailored to the views of the active HiBall units. Pose estimates are maintained using a Kalman-filter-based prediction-correction approach known as single-constraint-at-a-time (SCAAT) tracking. This technique has been extended to provide self-calibration of the ceiling, concurrent with HiBall tracking. Welch 2001 at Section 3.

HiBall sensor unit was designed as a single, rigid, hollow ball having dodecahedral symmetry, with lenses in the upper six faces and LEPDs on the insides of the opposing six lower faces (figure 7). This immediately gives six

Exhibit D-6

CLAIM 47	Welch 2001
	primary "camera" views uniformly spaced by 57 deg. The views efficiently share the same internal air space and are rigid with respect to each other. In addition, light entering any lens sufficiently off-axis can be seen by a neigh- boring LEPD, giving rise to five secondary views through the top or central lens, and three secondary views through the five other lenses. Overall, this provides 26 fields of view that are used to sense widely separated groups of LEDs in the environment. Welch 2001 at Section 4.1. 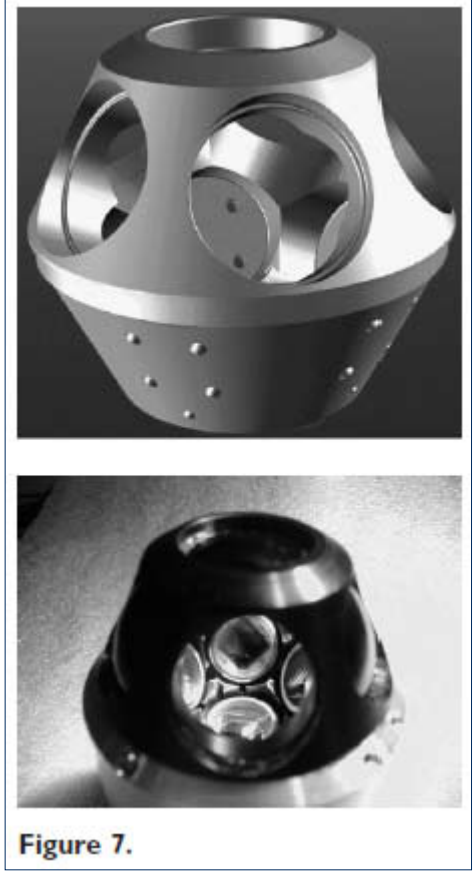 Figure 7.

Exhibit D-6

CLAIM 47	Welch 2001
	The LEPDs themselves are not imaging devices; rather, they detect the centroid of the luminous flux incident on the detector. The x-position of the centroid determines the ratio of two output y-position determines the ratio of two other output currents. The total output current of each pair are commensurate and are proportional to the total incident flux. Consequently, focus is not an issue, so the simple fixed-focus lenses work well over a range of LED distances from about half a meter to infinity. The LEPDs and associated electronic components are mounted on a custom rigid-flex printed circuitboard (figure 8). This arrangement makes efficient use of the internal HiBall volume while maintaining isolation between analog and digital circuitry, and increasing reliability by alleviating the need for intercomponent mechanical connectors. Welch 2001 at Section 4.1. 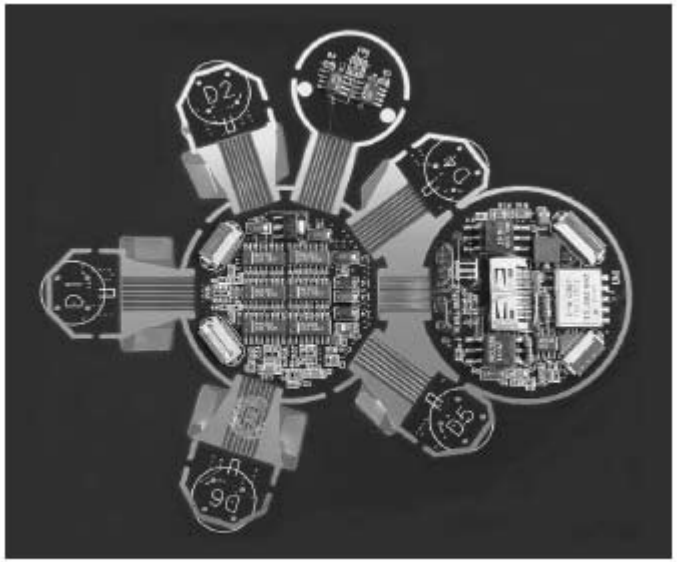 Figure 8. Figure 9 shows the physical arrangement of the folded electronics in the HiBall. Each LEPD has four transimpedance amplifiers (shown together as one "Amp" in figure 9), the analog outputs of which are multiplexed with those of the other LEPDs, then sampled, held, and converted by four 16-bit Delta-Sigma analog-to-digital (A/D) converters. Multiple samples are integrated via an accumulator. The digitized LEPD data are organized into packets for communication back to the CIB. The packets also contain information to assist in

CLAIM 47	Welch 2001
	error detection. The communication protocol is simple, and, while presently implemented by wire, the modulation scheme is amenable to a wireless implementation. Welch 2001 at Section 4.1. 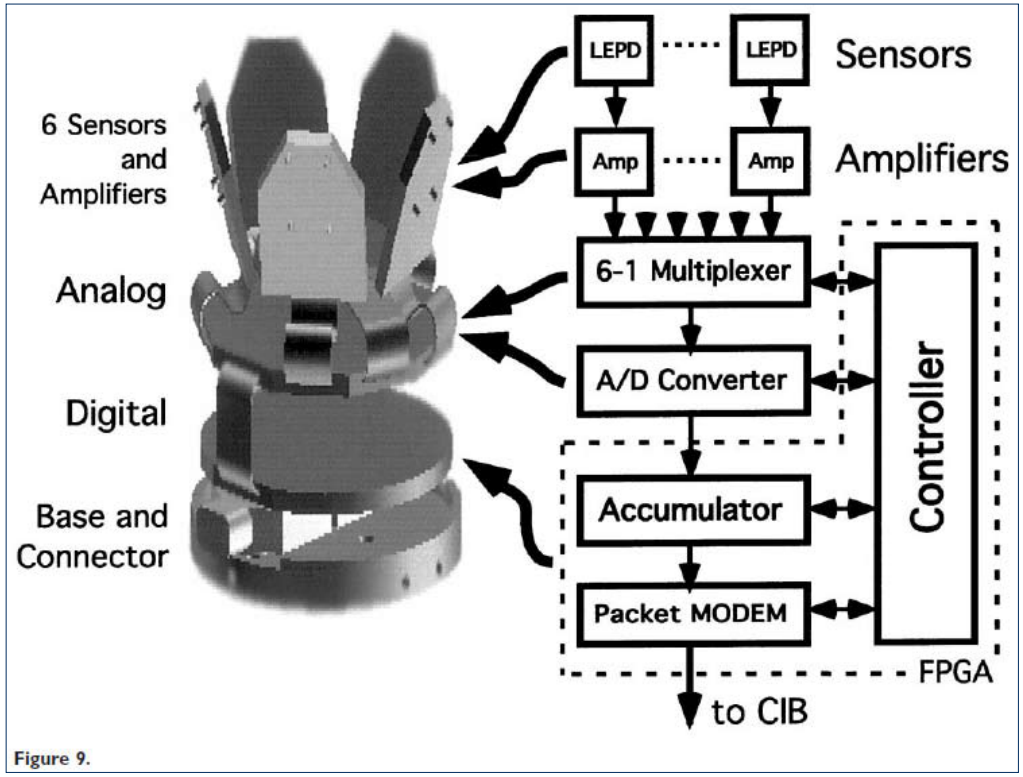 Figure 9. The design results in a ceiling with a rectangular LED pattern with periods of 7.6 cm and 15.2 cm. This spacing is used for the initial estimates of the LED positions in the lab; then, during normal operation, the SCAAT algorithm continually refines the LED position estimates (section 5.4). The SCAAT autocalibration not only relaxes design and installation constraints, but provides greater precision in the face of initial and ongoing uncertainty in the ceiling structure. Welch 2001 at Section 4.2.

Exhibit D-6

CLAIM 47	Welch 2001
	The CIB comprises analog drive and receive components as well as digital logic components. The digital components implement store and forward in both directions and synchronize the timing of the LED "on" interval within the HiBall dark-light-dark intervals (section 5.2). The protocol supports full-duplex flow control. The data are arranged into packets that incorporate error detection. Welch 2001 at Section 4.3. *See also* Defendants' Invalidity Contentions for further discussion.
[47.c] configuring the tracking system, including	At least under Plaintiffs' apparent infringement theory, Welch 2001 discloses, either expressly or inherently, configuring the tracking system. In the alternative, this element would be obvious over Welch 2001 in light of the other references disclosed in Defendants' Invalidity Contentions and/or the knowledge of one of ordinary skill in the art. *See, e.g.*: After each HiBall is assembled, we perform an offline calibration procedure to determine the correspondence between image-plane coordinates and rays in space. This involves more than just determining the view transform for each of the 26 views. Nonlinearities in the silicon sensor and distortions in the lens (such as spherical aberration) cause significant deviations from a simple pinhole camera model. We dealt with all of these issues through the use of a two-part camera model. The first part is a standard pinhole camera represented by a 3 x 4 matrix. The second part is a table mapping real image-plane coordinates to ideal image-plane coordinates. Welch 2001 at Section 5.1. Both parts of the camera model are determined using a **calibration procedure** that relies on a goniometer (an angular positioning system) of our own design. This device consists of two servo motors mounted together such that one motor provides rotation about the vertical axis while the second motor provides rotation about an axis orthogonal to vertical. An important characteristic of the goniometer is that the rotational axes of the two motors intersect at a point at the center of the HiBall optical sphere; this point is defined as the origin of the HiBall. . . . The rotational positioning motors were rated to provide twenty arc-second precision; we further calibrated them to six arc seconds using a laboratory grade theodolite—an angle measuring system. Welch 2001 at Section 5.1.

Exhibit D-6

CLAIM 47	Welch 2001
	To determine the **mapping between sensor image-plane coordinates and three-space rays,** we use a single LED mounted at a fixed location in the laboratory such that it is centered in the view directly out of the top lens of the HiBall. This ray defines the z or up axis for the HiBall coordinate system. We sample other rays by rotating the goniometer motors under computer control. We sample each view with rays spaced about every six minutes of arc throughout the field of view. We repeat each measurement 100 times to reduce the effects of noise on the individual measurements and to estimate the standard deviation of the measurements. Welch 2001 at Section 5.1. Given the tables of approximately 2,500 measurements for each of the 26 views, we first determine a 3 X 4 view matrix using standard linear least-squares techniques. Then, we determine the deviation of each measured point from that predicted by the ideal linear model. These deviations are resampled into a 25 X 25 grid indexed by sensor-plane coordinates using a simple scan-conversion procedure and averaging. **Given a measurement from a sensor at runtime (section 5.2), we convert it to an "ideal" measurement by subtracting a deviation bilinearly interpolated from the nearest four entries in the table.** Welch 2001 at Section 5.1. Upon receiving a command from the CIB (section 4.3), which is synchronized with a CIB command to the ceiling, the HiBall selects the specified LEPD and performs three measurements, one before the LED flashes, one during the LED flash, and one after the LED flash. **Known as "dark-light-dark," this technique is used to subtract out DC bias, low-frequency noise, and background light from the LED signal. We then convert the measured sensor coordinates to "ideal" coordinates using the calibration tables described in section 5.1.** In addition, during runtime we attempt to maximize the signal-to-noise ratio of the measurement with an **automatic gain-control scheme.** For each LED, **we store a target signal strength factor.** We compute the LED current and number of integrations (of successive accumulated A/D samples) by dividing this strength factor by the square of the distance to the LED, estimated from the current position estimate. After a reading, we look at the strength of the actual measurement. If it is larger than expected, we reduce the gain; if it is less than expected, we increase the gain. The increase and decrease are implemented as online averages with scaling such that the gain factor decreases rapidly (to avoid overflow) and increases slowly. **Finally, we use the measured signal strength to estimate the noise on the signal using (Chi, 1995), and then use this as the measurement noise estimate for the Kalman filter** (section 5.3).

Exhibit D-6

CLAIM 47	Welch 2001
	Welch 2001 at Section 5.2 The online measurements (section 5.2) are used to estimate the pose of the HiBall during operation. The 1991 system collected a group of diverse measurements for a variety of LEDs and sensors, and then used a method of simultaneous nonlinear equations called collinearity (Azuma & Ward, 1991) to estimate the pose of the sensor fixture shown in figure 3 (bottom). Welch 2001 at Section 5.3. In contrast, the approach we use with the new HiBall system produces tracker reports as each new measurement is made, rather than waiting to form a complete collection of observations. Because single measurements underconstrain the mathematical solution, we refer to the approach as single-constraint-at-a-time (SCAAT) tracking (Welch, 1996; Welch & Bishop, 1997). The key is that the single measurements provide some information about the HiBall's state, and thus can be used to incrementally improve a previous estimate. We intentionally fuse each individual "insufficient" measurement immediately as it is obtained. With this approach, we are able to generate estimates more frequently, with less latency, and with improved accuracy, and we are able to estimate the LED positions online concurrently while tracking the HiBall (section 5.4). Welch 2001 at Section 5.3. We use a Kalman filter (Kalman, 1960) to fuse the measurements into an estimate of the HiBall state x (the pose of the HiBall). We use the Kalman filter—a minimum-variance stochastic estimator—both because the sensor measurement noise and the typical user-motion dynamics can be modeled as normally distributed random processes, and because we want an efficient online method of estimation. Welch 2001 at Section 5.3. The Kalman filter has been used previously to address similar or related problems. . . . A relevant example of a Kalman filter used for sensor fusion in a wide-area tracking system is given in Foxlin et al. (1998), which describes a hybrid inertial-acoustic system that is commercially available today (Intersense, 2000). Welch 2001 at Section 5.3. [O]ne key benefit warrants discussion here. There is a direct relationship between the complexity of the estimation algorithm, the corresponding speed (execution time per estimation cycle), and the change in HiBall pose between estimation cycles (figure 12). As the algorithmic complexity increases, the execution time increases, which allows for significant nonlinear HiBall motion between estimation cycles, which in turn implies

CLAIM 47	Welch 2001
	the need for a more complex estimation algorithm. Welch 2001 at Section 5.3.  Figure 12. The SCAAT approach, on the other hand, is an attempt to reverse this cycle. Because we intentionally use a single constraint per estimate, the algorithmic complexity is drastically reduced, which reduces the execution time, and hence the amount of motion between estimation cycles. Because the amount of motion is limited, we are able to use a simple dynamic (process) model in the Kalman filter, which further simplifies the computations. In short, the simplicity of the approach means that it can run very fast, which means it can pro- duce estimates very rapidly, with low noise. Welch 2001 at Section 5.3. The Kalman filter requires both a model of the process dynamics and a model of the relationship between the process state and the available measurements. In part due to the simplicity of the SCAAT approach, we are able

Exhibit D-6

CLAIM 47	Welch 2001
	to use a simple position-velocity (PV) process model (Brown & Hwang, 1992). . . . We model the continuous change in the HiBall state with the simple differential equation $$\frac{d}{dt}\bar{x}(t) = \begin{bmatrix} 0 & 1 \\ 0 & 0 \end{bmatrix}\begin{bmatrix} x_p(t) \\ x_v(t) \end{bmatrix} + \begin{bmatrix} 0 \\ \mu \end{bmatrix} u(t), \qquad (1)$$ where $u(t)$ is a normally distributed white (in the frequency spectrum) scalar noise process, and the scalar μ represents the magnitude or spectral density of the noise. We use a similar model with a distinct noise process for each of the six pose elements. We determine the individual noise magnitudes using an offline simulation of the system and a nonlinear optimization strategy that seeks to minimize the variance between the estimated pose and a known motion path. (See section 6.2.2.). Welch 2001 at Section 5.3. The differential equation (1) represents a continuous integrated random walk, or an integrated Wiener or Brownian-motion process. Specifically, we model each component of the linear and angular HiBall velocities as a random walk, and then use these (assuming constant intermeasurement velocity) to estimate the HiBall pose at time $t + \delta t$ as follows:

Exhibit D-6

CLAIM 47	Welch 2001

$$\bar{x}(t+\delta t) = \begin{bmatrix} 1 & \delta t \\ 0 & 1 \end{bmatrix} \bar{x}(t) \qquad (2)$$

for each of the six pose elements. In addition to a relatively simple process model, the HiBall measurement model is relatively simple. For any ceiling LED (section 4.2) and HiBall view (section 4.1), the 2-D sensor measurement can be modeled as

$$\begin{bmatrix} u \\ v \end{bmatrix} = \begin{bmatrix} c_x/c_z \\ c_y/c_z \end{bmatrix} \qquad (3)$$

where

$$\begin{bmatrix} c_x \\ c_y \\ c_z \end{bmatrix} = VR^T(\bar{l}_{xyz} - \bar{x}_{xyz}), \qquad (4)$$

V is the camera viewing matrix from section 5.1, $\bar{l}_{xyz}$ is the position of the LED in the world, $\bar{x}_{xyz}$ is the position of the HiBall in the world, and R is a rotation matrix corresponding to the orientation of the HiBall in the world. In practice, we maintain the orientation of the HiBall as a combination of a global (external to the state) quaternion and a set of incremental angles as described by Welch (1996) and Welch and Bishop (1997).

Welch 2001 at Section 5.3.

Exhibit D-6

CLAIM 47	Welch 2001
	Because the measurement model (3) and (4) is non-linear, we use an extended Kalman filter, making use of the Jacobian of the nonlinear HiBall measurement model to transform the covariance of the Kalman filter. Welch 2001 at Section 5.3. Along with the benefit of simplicity and speed, the SCAAT approach offers the additional capability of being able to estimate the 3-D positions of the LEDs in the world concurrently with the pose of the HiBall, online, in real time. This capability is a tremendous benefit in terms of the accuracy and noise characteristics of the estimates. The method we now use for autocalibration involves defining a distinct SCAAT Kalman filter for each LED. Specifically, for each LED, we maintain a state $\bar{l}$ (estimate of the 3-D position) and a 3×3 Kalman filter covariance. At the beginning of each estimation cycle, we form an augmented state vector $\hat{x}$ using the appropriate LED state and the current HiBall state: $\hat{x} = [\bar{x}^T, \bar{l}^T]^T$. Similarly, we augment the Kalman filter error covariance matrix with that of the LED filter. We then follow the normal steps outlined in section 5.3, with the result being that the LED portion of the filter state and covariance is updated in accordance with the measurement residual. At the end of the cycle, we extract the LED portions of the state and covariance from the augmented filter, and save them externally. The effect is that, as the system is being used, it continually refines its estimates of the LED positions, thereby continually improving its estimates of the HiBall pose. Again, for additional information, see Welch (1996) and Welch and Bishop (1997).

CLAIM 47	Welch 2001
	Welch 2001 at Section 5.4. The recursive nature of the Kalman filter (section 5.3) requires that the filter **be initialized with a known state** and corresponding covariance before steady-state operation can begin. Such an initialization (or acquisition) must take place prior to any tracking session, but also upon the (rare) occasion when the filter diverges and "loses lock" as a result of blocked sensor views, for example. Welch 2001 at Section 5.5. The acquisition process is complicated by the fact that each LEPD sees a number of different widely separated views (section 4.1). Therefore, detecting an LED provides at best an ambiguous set of potential LED directions in HiBall coordinates. Moreover, before acquisition, no assumptions can be made to limit the search space of visible LEDs. As such, a relatively slow brute-force algorithm is used to acquire lock. Welch 2001 at Section 5.5. As a result of a mechanical design tradeoff, each sensor field of view is less than six degrees. The focal length is set by the size of the sensor housing, which is set by the diameter of the sensors themselves. Energetics is also a factor, limiting how small the lenses can be while maintaining sufficient light-collecting area. As a result of these design tradeoffs, even a momentary small error in the HiBall pose estimate can cause the recursive estimates to diverge and the system to lose lock after only a few LED sightings. And yet the system is quite robust. In practice, users can jump around, crawl on the floor, lean over, even wave their hands in front of the sensors, and the system does not lose lock. During one session, we were using the HiBall as a 3-D digitization probe, a Hi-Ball on the end of a pencil-shaped fiberglass wand (figure 14, left). We laid the probe down on a table at one point, and were amazed to later notice that it was still tracking, even though it was observing only three or four LEDs near the edge of the ceiling. We picked up the probe and continued using it, without it ever losing lock.   **Figure 13.**

Exhibit D-6

CLAIM 47	Welch 2001

Figure 14.

Welch 2001 at Section 6.1.

To make measurements of the noise when the HiBall is in motion, we rely on the assumption that almost all of the signal resulting from normal human motion is at frequencies below 2 Hz. **We use a high-pass filter (Welch, 1967) on the pose estimates, and assume the output is noise.** The resulting statistics are comparable to those made with the HiBall stationary, except at poses for which there are very few LEDs visible in only one or two views. In these poses, near the edge of the ceiling, the geometry of the constraints results in amplification of errors. For nearly all of the working volume of the tracker, the standard deviation of the noise on measurements while the HiBall is still or moving is about 0.2 mm and 0.03 deg.
Welch 2001 at Section 6.1.

During the design of the HiBall system, we made substantial use of simulation, in some domains to a very detailed level. For example, Zemax (Focus Software, 1995) was used extensively in the design and optimization of the optical design, including the design of the filter glass lenses, and geometry of the optical-component layout.
Welch 2001 at Section 6.2.

To produce realistic data for developing and tuning our algorithms, we collected several motion paths (sequences of pose estimates) from our first-generation electro-optical tracker (figure 3) at its 70 Hz maximum report rate. These paths were recorded from both naive users visiting our monthly “demo days” and from experienced users in our labs. . . . we filtered the raw path data with a noncausal zero-phase-shift, low-pass filter to eliminate energy

CLAIM 47	Welch 2001
	above 2 Hz. The output of the low-pass filtering was then resampled at whatever rate we wanted to run the simulated tracker, usually 1,000 Hz. Welch 2001 at Section 6.2. The simulator reads camera models describing the 26 views, the sensor noise parameters, the LED positions and their expected error, and the motion path described above. Before beginning the simulation, the LED positions are perturbed from their ideal positions by adding normally distributed error to each axis. Then, for each simulated cycle of operation, the "true" poses are up- dated using the input motion path. Next, a view is chosen and a visible LED within that view is selected, and the image-plane coordinates of the LED on the chosen sensor are computed using the camera model for the view and the LED as described in section 5.3. These sensor coordinates are then perturbed based on the sensor noise model (section 6.2.1) using the distance and angle to the LED. These noise-corrupted sensor readings are then fed to the SCAAT filter to produce an up- dated position estimate. The position estimate is com- pared to the true position to produce a scalar error metric that is described next. Welch 2001 at Section 6.2. The error metric we used combines the error in pose in a way that relates to the effects of tracker error on a head-worn display user. We define a set of points arrayed around the user in a fixed configuration. We compute two sets of coordinates for these points: the true position using the true pose and their estimated position using the estimated pose. The error metric is then the sum of the distances between the true and estimated positions of these points. By adjusting the distance of the points from the user, we can control the relative importance of the orientation and the position error in the combined error metric. If the distance is small, then the position error is weighted most heavily; if the distance is large, then the orientation error is weighted most heavily. Our two error metrics for the entire run are the square root of the sum of the squares of all the distances, and the peak distance. Welch 2001 at Section 6.2. *See also* Defendants' Invalidity Contentions for further discussion.
[47.d] providing configuration information from each of the sensor modules to the estimation module	At least under Plaintiffs' apparent infringement theory, Welch 2001 discloses, either expressly or inherently, providing configuration information from each of the sensor modules to the estimation module regarding the characteristics of the sensors associated with the sensor module. In the alternative, this element would be obvious

CLAIM 47	Welch 2001
regarding the characteristics of the sensors associated with the sensor module, and	over Welch 2001 in light of the other references disclosed in Defendants' Invalidity Contentions and/or the knowledge of one of ordinary skill in the art. *See, e.g.*: After each HiBall is assembled, we perform an offline calibration procedure to determine the correspondence between image-plane coordinates and rays in space. This involves more than just determining the view transform for each of the 26 views. Nonlinearities in the silicon sensor and distortions in the lens (such as spherical aberration) cause significant deviations from a simple pinhole camera model. We dealt with all of these issues through the use of a two-part camera model. The first part is a standard pinhole camera represented by a 3 x 4 matrix. The second part is a table mapping real image-plane coordinates to ideal image-plane coordinates. Welch 2001 at Section 5.1. Both parts of the camera model are determined using **a calibration procedure** that relies on a goniometer (an angular positioning system) of our own design. This device consists of two servo motors mounted together such that one motor provides rotation about the vertical axis while the second motor provides rotation about an axis orthogonal to vertical. An important characteristic of the goniometer is that the rotational axes of the two motors intersect at a point at the center of the HiBall optical sphere; this point is defined as the origin of the HiBall. . . . **The rotational positioning motors were rated to provide twenty arc-second precision; we further calibrated them to six arc seconds using a laboratory grade theodolite—an angle measuring system.** Welch 2001 at Section 5.1. To determine the mapping between sensor image-plane coordinates and three-space rays, we use a single LED mounted at a fixed location in the laboratory such that it is centered in the view directly out of the top lens of the HiBall. This ray defines the z or up axis for the HiBall coordinate system. We sample other rays by rotating the goniometer motors under computer control. **We sample each view with rays spaced about every six minutes of arc throughout the field of view. We repeat each measurement 100 times to reduce the effects of noise on the individual measurements and to estimate the standard deviation of the measurements.** Welch 2001 at Section 5.1. Given the tables of approximately 2,500 measurements for each of the 26 views, we first determine a 3 X 4 view matrix using standard linear least-squares techniques. Then, we determine the deviation of each measured point from that predicted by the ideal linear model. These deviations are resampled into a 25 X 25 grid indexed by sensor-plane coordinates using a simple scan-conversion procedure and averaging. **Given a measurement from**

CLAIM 47	Welch 2001
	a sensor at runtime (section 5.2), we convert it to an "ideal" measurement by subtracting a deviation bilinearly interpolated from the nearest four entries in the table. Welch 2001 at Section 5.1. The online measurements (section 5.2) are used to estimate the pose of the HiBall during operation. The 1991 system collected a group of diverse measurements for a variety of LEDs and sensors, and then used a method of simultaneous nonlinear equations called collinearity (Azuma & Ward, 1991) to estimate the pose of the sensor fixture shown in figure 3 (bottom). Welch 2001 at Section 5.3. In contrast, the approach we use with the new HiBall system produces tracker reports as each new measurement is made, rather than waiting to form a complete collection of observations. Because single measurements underconstrain the mathematical solution, we refer to the approach as single-constraint-at-a-time (SCAAT) tracking (Welch, 1996; Welch & Bishop, 1997). The key is that the single measurements provide some information about the HiBall's state, and thus can be used to incrementally improve a previous estimate. We intentionally fuse each individual "insufficient" measurement immediately as it is obtained. With this approach, we are able to generate estimates more frequently, with less latency, and with improved accuracy, and we are able to estimate the LED positions online concurrently while tracking the HiBall (section 5.4). Welch 2001 at Section 5.3. We use a Kalman filter (Kalman, 1960) to fuse the measurements into an estimate of the HiBall state x (the pose of the HiBall). We use the Kalman filter—a minimum-variance stochastic estimator—both because the sensor measurement noise and the typical user-motion dynamics can be modeled as normally distributed random processes, and because we want an efficient online method of estimation. Welch 2001 at Section 5.3. The Kalman filter has been used previously to address similar or related problems. . . . A relevant example of a Kalman filter used for sensor fusion in a wide-area tracking system is given in Foxlin et al. (1998), which describes a hybrid inertial-acoustic system that is commercially available today (Intersense, 2000). Welch 2001 at Section 5.3. [O]ne key benefit warrants discussion here. There is a direct relationship between the complexity of the estimation algorithm, the corresponding speed (execution time per estimation cycle), and the change in HiBall pose between estimation cycles (figure 12). As the algorithmic complexity increases, the execution time

Exhibit D-6

CLAIM 47	Welch 2001
	increases, which allows for significant nonlinear HiBall motion between estimation cycles, which in turn implies the need for a more complex estimation algorithm. Welch 2001 at Section 5.3.  Figure 12. The SCAAT approach, on the other hand, is an attempt to reverse this cycle. Because we intentionally use a single constraint per estimate, the algorithmic complexity is drastically reduced, which reduces the execution time, and hence the amount of motion between estimation cycles. Because the amount of motion is limited, we are able to use a simple dynamic (process) model in the Kalman filter, which further simplifies the computations. In short, the simplicity of the approach means that it can run very fast, which means it can pro- duce estimates very rapidly, with low noise. Welch 2001 at Section 5.3.

Exhibit D-6

CLAIM 47	Welch 2001
	The Kalman filter requires both a model of the process dynamics and a model of the relationship between the process state and the available measurements. In part due to the simplicity of the SCAAT approach, we are able to use a simple position-velocity (PV) process model (Brown & Hwang, 1992). . . . We model the continuous change in the HiBall state with the simple differential equation $$\frac{d}{dt}\bar{x}(t) = \begin{bmatrix} 0 & 1 \\ 0 & 0 \end{bmatrix}\begin{bmatrix} x_p(t) \\ x_v(t) \end{bmatrix} + \begin{bmatrix} 0 \\ \mu \end{bmatrix} u(t), \qquad (1)$$ where $u(t)$ is a normally distributed white (in the frequency spectrum) scalar noise process, and the scalar μ represents the magnitude or spectral density of the noise. We use a similar model with a distinct noise process for each of the six pose elements. We determine the individual noise magnitudes using an offline simulation of the system and a nonlinear optimization strategy that seeks to minimize the variance between the estimated pose and a known motion path. (See section 6.2.2.). Welch 2001 at Section 5.3. The differential equation (1) represents a continuous integrated random walk, or an integrated Wiener or Brownian-motion process. Specifically, we model each component of the linear and angular HiBall velocities as a random walk, and then use these (assuming constant intermeasurement velocity) to estimate the HiBall pose at time $t + \delta t$ as follows:

Exhibit D-6

CLAIM 47	Welch 2001

$$\bar{x}(t+\delta t) = \begin{bmatrix} 1 & \delta t \\ 0 & 1 \end{bmatrix} \bar{x}(t) \qquad (2)$$

for each of the six pose elements. In addition to a relatively simple process model, the HiBall measurement model is relatively simple. For any ceiling LED (section 4.2) and HiBall view (section 4.1), the 2-D sensor measurement can be modeled as

$$\begin{bmatrix} u \\ v \end{bmatrix} = \begin{bmatrix} c_x/c_z \\ c_y/c_z \end{bmatrix} \qquad (3)$$

where

$$\begin{bmatrix} c_x \\ c_y \\ c_z \end{bmatrix} = VR^T(\bar{l}_{xyz} - \bar{x}_{xyz}), \qquad (4)$$

V is the camera viewing matrix from section 5.1, $\bar{l}_{xyz}$ is the position of the LED in the world, $\bar{x}_{xyz}$ is the position of the HiBall in the world, and R is a rotation matrix corresponding to the orientation of the HiBall in the world. In practice, we maintain the orientation of the HiBall as a combination of a global (external to the state) quaternion and a set of incremental angles as described by Welch (1996) and Welch and Bishop (1997).

Welch 2001 at Section 5.3.

Exhibit D-6

CLAIM 47	Welch 2001
	Because the measurement model (3) and (4) is non-linear, we use an extended Kalman filter, making use of the Jacobian of the nonlinear HiBall measurement model to transform the covariance of the Kalman filter. Welch 2001 at Section 5.3. Along with the benefit of simplicity and speed, the SCAAT approach offers the additional capability of being able to estimate the 3-D positions of the LEDs in the world concurrently with the pose of the HiBall, online, in real time. This capability is a tremendous benefit in terms of the accuracy and noise characteristics of the estimates. The method we now use for autocalibration involves defining a distinct SCAAT Kalman filter for each LED. Specifically, for each LED, we maintain a state $\bar{l}$ (estimate of the 3-D position) and a 3×3 Kalman filter covariance. At the beginning of each estimation cycle, we form an augmented state vector $\hat{x}$ using the appropriate LED state and the current HiBall state: $\hat{x} = [\bar{x}^T, \bar{l}^T]^T$. Similarly, we augment the Kalman filter error covariance matrix with that of the LED filter. We then follow the normal steps outlined in section 5.3, with the result being that the LED portion of the filter state and covariance is updated in accordance with the measurement residual. At the end of the cycle, we extract the LED portions of the state and covariance from the augmented filter, and save them externally. The effect is that, as the system is being used, it continually refines its estimates of the LED positions, thereby continually improving its estimates of the HiBall pose. Again, for additional information, see Welch (1996) and Welch and Bishop (1997).

CLAIM 47	Welch 2001
	Welch 2001 at Section 5.4. The recursive nature of the Kalman filter (section 5.3) requires that the filter **be initialized with a known state** and corresponding covariance before steady-state operation can begin. Such an initialization (or acquisition) must take place prior to any tracking session, but also upon the (rare) occasion when the filter diverges and "loses lock" as a result of blocked sensor views, for example. Welch 2001 at Section 5.5. The acquisition process is complicated by the fact that each LEPD sees a number of different widely separated views (section 4.1). Therefore, detecting an LED provides at best an ambiguous set of potential LED directions in HiBall coordinates. Moreover, before acquisition, no assumptions can be made to limit the search space of visible LEDs. As such, a relatively slow brute-force algorithm is used to acquire lock. Welch 2001 at Section 5.5. As a result of a mechanical design tradeoff, each sensor field of view is less than six degrees. The focal length is set by the size of the sensor housing, which is set by the diameter of the sensors themselves. Energetics is also a factor, limiting how small the lenses can be while maintaining sufficient light-collecting area. As a result of these design tradeoffs, even a momentary small error in the HiBall pose estimate can cause the recursive estimates to diverge and the system to lose lock after only a few LED sightings. And yet the system is quite robust. In practice, users can jump around, crawl on the floor, lean over, even wave their hands in front of the sensors, and the system does not lose lock. During one session, we were using the HiBall as a 3-D digitization probe, a Hi-Ball on the end of a pencil-shaped fiberglass wand (figure 14, left). We laid the probe down on a table at one point, and were amazed to later notice that it was still tracking, even though it was observing only three or four LEDs near the edge of the ceiling. We picked up the probe and continued using it, without it ever losing lock.   Figure 13.

Exhibit D-6

CLAIM 47	Welch 2001

Figure 14.

Welch 2001 at Section 6.1.

To make measurements of the noise when the HiBall is in motion, **we rely on the assumption that almost all of the signal resulting from normal human motion is at frequencies below 2 Hz.** We use a high-pass filter (Welch, 1967) on the pose estimates, and assume the output is noise. The resulting statistics are comparable to those made with the HiBall stationary, except at poses for which there are very few LEDs visible in only one or two views. In these poses, near the edge of the ceiling, the geometry of the constraints results in amplification of errors. For nearly all of the working volume of the tracker, the standard deviation of the noise on measurements while the HiBall is still or moving is about 0.2 mm and 0.03 deg.
Welch 2001 at Section 6.1.

During the design of the HiBall system, we made substantial use of simulation, in some domains to a very detailed level. For example, Zemax (Focus Software, 1995) was used extensively in the design and optimization of the optical design, including the design of the filter glass lenses, and geometry of the optical-component layout.
Welch 2001 at Section 6.2.

To produce realistic data for developing and tuning our algorithms, we collected several motion paths (sequences of pose estimates) from our first-generation electro-optical tracker (figure 3) at its 70 Hz maximum report rate. These paths were recorded from both naive users visiting our monthly “demo days” and from experienced users in our labs. . . . we filtered the raw path data with a noncausal zero-phase-shift, low-pass filter to eliminate energy

CLAIM 47	Welch 2001
	above 2 Hz. The output of the low-pass filtering was then resampled at whatever rate we wanted to run the simulated tracker, usually 1,000 Hz. Welch 2001 at Section 6.2. The simulator reads camera models describing the 26 views, the sensor noise parameters, the LED positions and their expected error, and the motion path described above. Before beginning the simulation, the LED positions are perturbed from their ideal positions by adding normally distributed error to each axis. Then, for each simulated cycle of operation, the "true" poses are up- dated using the input motion path. Next, a view is chosen and a visible LED within that view is selected, and the image-plane coordinates of the LED on the chosen sensor are computed using the camera model for the view and the LED as described in section 5.3. **These sensor coordinates are then perturbed based on the sensor noise model (section 6.2.1) using the distance and angle to the LED. These noise-corrupted sensor readings are then fed to the SCAAT filter to produce an up- dated position estimate. The position estimate is com- pared to the true position to produce a scalar error metric that is described next.** Welch 2001 at Section 6.2. **The error metric we used combines the error in pose in a way that relates to the effects of tracker error on a head-worn display user. We define a set of points arrayed around the user in a fixed configuration. We compute two sets of coordinates for these points: the true position using the true pose and their estimated position using the estimated pose.** The error metric is then the sum of the distances between the true and estimated positions of these points. By adjusting the distance of the points from the user, we can control the relative importance of the orientation and the position error in the combined error metric. If the distance is small, then the position error is weighted most heavily; if the distance is large, then the orientation error is weighted most heavily. Our two error metrics for the entire run are the square root of the sum of the squares of all the distances, and the peak distance. Welch 2001 at Section 6.2. *See also* Defendants' Invalidity Contentions for further discussion.
[47.e] configuring the estimation module using the provided	At least under Plaintiffs' apparent infringement theory, Welch 2001 discloses, either expressly or inherently, configuring the estimation module using the provided configuration information. In the alternative, this element

CLAIM 47	Welch 2001
configuration information;	would be obvious over Welch 2001 in light of the other references disclosed in Defendants' Invalidity Contentions and/or the knowledge of one of ordinary skill in the art. *See, e.g.*: After each HiBall is assembled, we perform an offline calibration procedure to determine the correspondence between image-plane coordinates and rays in space. This involves more than just determining the view transform for each of the 26 views. Nonlinearities in the silicon sensor and distortions in the lens (such as spherical aberration) cause significant deviations from a simple pinhole camera model. We dealt with all of these issues through the use of a two-part camera model. The first part is a standard pinhole camera represented by a 3 x 4 matrix. The second part is a table mapping real image-plane coordinates to ideal image-plane coordinates. Welch 2001 at Section 5.1. Both parts of the camera model are determined using a **calibration procedure** that relies on a goniometer (an angular positioning system) of our own design. This device consists of two servo motors mounted together such that one motor provides rotation about the vertical axis while the second motor provides rotation about an axis orthogonal to vertical. An important characteristic of the goniometer is that the rotational axes of the two motors intersect at a point at the center of the HiBall optical sphere; this point is defined as the origin of the HiBall. . . . The rotational positioning motors were rated to provide twenty arc-second precision; we further calibrated them to six arc seconds using a laboratory grade theodolite—an angle measuring system. Welch 2001 at Section 5.1. To determine the mapping between sensor image-plane coordinates and three-space rays, we use a single LED mounted at a fixed location in the laboratory such that it is centered in the view directly out of the top lens of the HiBall. This ray defines the z or up axis for the HiBall coordinate system. We sample other rays by rotating the goniometer motors under computer control. We sample each view with rays spaced about every six minutes of arc throughout the field of view. We repeat each measurement 100 times to reduce the effects of noise on the individual measurements and to estimate the standard deviation of the measurements. Welch 2001 at Section 5.1. Given the tables of approximately 2,500 measurements for each of the 26 views, we first determine a 3 X 4 view matrix using standard linear least-squares techniques. Then, we determine the deviation of each measured point from that predicted by the ideal linear model. These deviations are resampled into a 25 X 25 grid indexed by sensor-plane coordinates using a simple scan-conversion procedure and averaging. Given a measurement from a

CLAIM 47	Welch 2001
	sensor at runtime (section 5.2), we convert it to an "ideal" measurement by subtracting a deviation bilinearly interpolated from the nearest four entries in the table. Welch 2001 at Section 5.1. **The online measurements (section 5.2) are used to estimate the pose of the HiBall during operation.** The 1991 system collected a group of diverse measurements for a variety of LEDs and sensors, and then used a method of simultaneous nonlinear equations called collinearity (Azuma & Ward, 1991) to estimate the pose of the sensor fixture shown in figure 3 (bottom). Welch 2001 at Section 5.3. In contrast, the approach we use with the new HiBall system produces tracker reports as each new measurement is made, rather than waiting to form a complete collection of observations. Because single measurements underconstrain the mathematical solution, we refer to the approach as single-constraint-at-a-time (SCAAT) tracking (Welch, 1996; Welch & Bishop, 1997). The key is that the single measurements provide some information about the HiBall's state, and thus can be used to incrementally improve a previous estimate. We intentionally fuse each individual "insufficient" measurement immediately as it is obtained. With this approach, we are able to generate estimates more frequently, with less latency, and with improved accuracy, and we are able to estimate the LED positions online concurrently while tracking the HiBall (section 5.4). Welch 2001 at Section 5.3. **We use a Kalman filter (Kalman, 1960) to fuse the measurements into an estimate of the HiBall state x (the pose of the HiBall). We use the Kalman filter—a minimum-variance stochastic estimator—both because the sensor measurement noise and the typical user-motion dynamics can be modeled as normally distributed random processes, and because we want an efficient online method of estimation.** Welch 2001 at Section 5.3. The Kalman filter has been used previously to address similar or related problems. . . . A relevant example of a Kalman filter used for sensor fusion in a wide-area tracking system is given in Foxlin et al. (1998), which describes a hybrid inertial-acoustic system that is commercially available today (Intersense, 2000). Welch 2001 at Section 5.3. [O]ne key benefit warrants discussion here. There is a direct relationship between the complexity of the estimation algorithm, the corresponding speed (execution time per estimation cycle), and the change in HiBall pose between estimation cycles (figure 12). As the algorithmic complexity increases, the execution time

Exhibit D-6

CLAIM 47	Welch 2001
	increases, which allows for significant nonlinear HiBall motion between estimation cycles, which in turn implies the need for a more complex estimation algorithm. Welch 2001 at Section 5.3.  Figure 12. The SCAAT approach, on the other hand, is an attempt to reverse this cycle. Because we intentionally use a single constraint per estimate, the algorithmic complexity is drastically reduced, which reduces the execution time, and hence the amount of motion between estimation cycles. Because the amount of motion is limited, we are able to use a simple dynamic (process) model in the Kalman filter, which further simplifies the computations. In short, the simplicity of the approach means that it can run very fast, which means it can pro- duce estimates very rapidly, with low noise. Welch 2001 at Section 5.3.

Exhibit D-6

CLAIM 47	Welch 2001
	The Kalman filter requires both a model of the process dynamics and a model of the relationship between the process state and the available measurements. In part due to the simplicity of the SCAAT approach, we are able to use a simple position-velocity (PV) process model (Brown & Hwang, 1992). . . . We model the continuous change in the HiBall state with the simple differential equation $$\frac{d}{dt}\bar{x}(t) = \begin{bmatrix} 0 & 1 \\ 0 & 0 \end{bmatrix}\begin{bmatrix} x_p(t) \\ x_v(t) \end{bmatrix} + \begin{bmatrix} 0 \\ \mu \end{bmatrix} u(t), \qquad (1)$$ where $u(t)$ is a normally distributed white (in the frequency spectrum) scalar noise process, and the scalar μ represents the magnitude or spectral density of the noise. We use a similar model with a distinct noise process for each of the six pose elements. We determine the individual noise magnitudes using an offline simulation of the system and a nonlinear optimization strategy that seeks to minimize the variance between the estimated pose and a known motion path. (See section 6.2.2.). Welch 2001 at Section 5.3. The differential equation (1) represents a continuous integrated random walk, or an integrated Wiener or Brownian-motion process. Specifically, we model each component of the linear and angular HiBall velocities as a random walk, and then use these (assuming constant intermeasurement velocity) to estimate the HiBall pose at time $t + \delta t$ as follows:

Exhibit D-6

CLAIM 47	Welch 2001

$$\bar{x}(t+\delta t) = \begin{bmatrix} 1 & \delta t \\ 0 & 1 \end{bmatrix} \bar{x}(t) \qquad (2)$$

for each of the six pose elements. In addition to a relatively simple process model, the HiBall measurement model is relatively simple. For any ceiling LED (section 4.2) and HiBall view (section 4.1), the 2-D sensor measurement can be modeled as

$$\begin{bmatrix} u \\ v \end{bmatrix} = \begin{bmatrix} c_x/c_z \\ c_y/c_z \end{bmatrix} \qquad (3)$$

where

$$\begin{bmatrix} c_x \\ c_y \\ c_z \end{bmatrix} = VR^T(\bar{l}_{xyz} - \bar{x}_{xyz}), \qquad (4)$$

V is the camera viewing matrix from section 5.1, $\bar{l}_{xyz}$ is the position of the LED in the world, $\bar{x}_{xyz}$ is the position of the HiBall in the world, and R is a rotation matrix corresponding to the orientation of the HiBall in the world. In practice, we maintain the orientation of the HiBall as a combination of a global (external to the state) quaternion and a set of incremental angles as described by Welch (1996) and Welch and Bishop (1997).

Welch 2001 at Section 5.3.

CLAIM 47	Welch 2001
	Because the measurement model (3) and (4) is non-linear, we use an extended Kalman filter, making use of the Jacobian of the nonlinear HiBall measurement model to transform the covariance of the Kalman filter. Welch 2001 at Section 5.3. **Along with the benefit of simplicity and speed, the SCAAT approach offers the additional capability of being able to estimate the 3-D positions of the LEDs in the world concurrently with the pose of the HiBall, online, in real time.** This capability is a tremendous benefit in terms of the accuracy and noise characteristics of the estimates.

Exhibit D-6

CLAIM 47	Welch 2001
	The method we now use for autocalibration involves defining a distinct SCAAT Kalman filter for each LED. Specifically, for each LED, we maintain a state $\bar{l}$ (estimate of the 3-D position) and a 3×3 Kalman filter covariance. At the beginning of each estimation cycle, we form an augmented state vector $\hat{x}$ using the appropriate LED state and the current HiBall state: $\hat{x} = [\bar{x}^T, \bar{l}^T]^T$. Similarly, we augment the Kalman filter error covariance matrix with that of the LED filter. We then follow the normal steps outlined in section 5.3, with the result being that the LED portion of the filter state and covariance is updated in accordance with the measurement residual. At the end of the cycle, we extract the LED portions of the state and covariance from the augmented filter, and save them externally. The effect is that, as the system is being used, it continually refines its estimates of the LED positions, thereby continually improving its estimates of the HiBall pose. Again, for additional information, see Welch (1996) and Welch and Bishop (1997). Welch 2001 at Section 5.4. The recursive nature of the Kalman filter (section 5.3) requires that the filter be initialized with a known state and corresponding covariance before steady-state operation can begin. Such an initialization (or acquisition) must take place prior to any tracking session, but also upon the (rare) occasion when the filter diverges and "loses lock" as a result of blocked sensor views, for example. Welch 2001 at Section 5.5.

Exhibit D-6

CLAIM 47	Welch 2001
	The acquisition process is complicated by the fact that each LEPD sees a number of different widely separated views (section 4.1). Therefore, detecting an LED provides at best an ambiguous set of potential LED directions in HiBall coordinates. Moreover, before acquisition, no assumptions can be made to limit the search space of visible LEDs. As such, a relatively slow brute-force algorithm is used to acquire lock. Welch 2001 at Section 5.5. As a result of a mechanical design tradeoff, each sensor field of view is less than six degrees. The focal length is set by the size of the sensor housing, which is set by the diameter of the sensors themselves. Energetics is also a factor, limiting how small the lenses can be while maintaining sufficient light-collecting area. As a result of these design tradeoffs, even a momentary small error in the HiBall pose estimate can cause the recursive estimates to diverge and the system to lose lock after only a few LED sightings. And yet the system is quite robust. In practice, users can jump around, crawl on the floor, lean over, even wave their hands in front of the sensors, and the system does not lose lock. During one session, we were using the HiBall as a 3-D digitization probe, a Hi-Ball on the end of a pencil-shaped fiberglass wand (figure 14, left). We laid the probe down on a table at one point, and were amazed to later notice that it was still tracking, even though it was observing only three or four LEDs near the edge of the ceiling. We picked up the probe and continued using it, without it ever losing lock.   Figure 13.

CLAIM 47	Welch 2001

Figure 14.

Welch 2001 at Section 6.1.

To make measurements of the noise when the HiBall is in motion, we rely on the assumption that almost all of the signal resulting from normal human motion is at frequencies below 2 Hz. We use a high-pass filter (Welch, 1967) on the pose estimates, and assume the output is noise. The resulting statistics are comparable to those made with the HiBall stationary, except at poses for which there are very few LEDs visible in only one or two views. In these poses, near the edge of the ceiling, the geometry of the constraints results in amplification of errors. For nearly all of the working volume of the tracker, the standard deviation of the noise on measurements while the HiBall is still or moving is about 0.2 mm and 0.03 deg.
Welch 2001 at Section 6.1.

During the design of the HiBall system, we made substantial use of simulation, in some domains to a very detailed level. For example, Zemax (Focus Software, 1995) was used extensively in the design and optimization of the optical design, including the design of the filter glass lenses, and geometry of the optical-component layout.
Welch 2001 at Section 6.2.

To produce realistic data for developing and tuning our algorithms, we collected several motion paths (sequences of pose estimates) from our first-generation electro-optical tracker (figure 3) at its 70 Hz maximum report rate. These paths were recorded from both naive users visiting our monthly “demo days” and from experienced users in our labs. . . . we filtered the raw path data with a noncausal zero-phase-shift, low-pass filter to eliminate energy

CLAIM 47	Welch 2001
	above 2 Hz. The output of the low-pass filtering was then resampled at whatever rate we wanted to run the simulated tracker, usually 1,000 Hz. Welch 2001 at Section 6.2. The simulator reads camera models describing the 26 views, the sensor noise parameters, the LED positions and their expected error, and the motion path described above. Before beginning the simulation, the LED positions are perturbed from their ideal positions by adding normally distributed error to each axis. Then, for each simulated cycle of operation, the "true" poses are up- dated using the input motion path. Next, a view is chosen and a visible LED within that view is selected, and the image-plane coordinates of the LED on the chosen sensor are computed using the camera model for the view and the LED as described in section 5.3. These sensor coordinates are then perturbed based on the sensor noise model (section 6.2.1) using the distance and angle to the LED. **These noise-corrupted sensor readings are then fed to the SCAAT filter to produce an up- dated position estimate.** The position estimate is com- pared to the true position to produce a scalar error metric that is described next. Welch 2001 at Section 6.2. The error metric we used combines the error in pose in a way that relates to the effects of tracker error on a head-worn display user. We define a set of points arrayed around the user in a fixed configuration. We compute two sets of coordinates for these points: the true position using the true pose and their estimated position using the estimated pose. The error metric is then the sum of the distances between the true and estimated positions of these points. By adjusting the distance of the points from the user, we can control the relative importance of the orientation and the position error in the combined error metric. If the distance is small, then the position error is weighted most heavily; if the distance is large, then the orientation error is weighted most heavily. Our two error metrics for the entire run are the square root of the sum of the squares of all the distances, and the peak distance. Welch 2001 at Section 6.2. *See also* Defendants' Invalidity Contentions for further discussion.
[47.f] maintaining estimates of tracking parameters in the	At least under Plaintiffs' apparent infringement theory, Welch 2001 discloses, either expressly or inherently, maintaining estimates of tracking parameters in the estimation module. In the alternative, this element would be obvious over Welch 2001 in light of the other references disclosed in Defendants' Invalidity Contentions and/or the knowledge of one of ordinary skill in the art.

CLAIM 47	Welch 2001
estimation module, including repeatedly	*See, e.g.*: Both parts of the camera model are determined using a calibration procedure that relies on a goniometer (an angular positioning system) of our own design. This device consists of two servo motors mounted together such that one motor provides rotation about the vertical axis while the second motor provides rotation about an axis orthogonal to vertical. An important characteristic of the goniometer is that the rotational axes of the two motors intersect at a point at the center of the HiBall optical sphere; this point is defined as the origin of the HiBall. . . . The rotational positioning motors were rated to provide twenty arc-second precision; we further calibrated them to six arc seconds using a laboratory grade theodolite—an angle measuring system. Welch 2001 at Section 5.1. To determine the mapping between sensor image-plane coordinates and three-space rays, we use a single LED mounted at a fixed location in the laboratory such that it is centered in the view directly out of the top lens of the HiBall. This ray defines the z or up axis for the HiBall coordinate system. We sample other rays by rotating the goniometer motors under computer control. We sample each view with rays spaced about every six minutes of arc throughout the field of view. We repeat each measurement 100 times to reduce the effects of noise on the individual measurements and to estimate the standard deviation of the measurements. Welch 2001 at Section 5.1. Given the tables of approximately 2,500 measurements for each of the 26 views, we first determine a 3 X 4 view matrix using standard linear least-squares techniques. Then, we determine the deviation of each measured point from that predicted by the ideal linear model. These deviations are resampled into a 25 X 25 grid indexed by sensor-plane coordinates using a simple scan-conversion procedure and averaging. Given a measurement from a sensor at runtime (section 5.2), we convert it to an "ideal" measurement by subtracting a deviation bilinearly interpolated from the nearest four entries in the table. Welch 2001 at Section 5.1. The online measurements (section 5.2) are used to estimate the pose of the HiBall during operation. **The 1991 system collected a group of diverse measurements for a variety of LEDs and sensors, and then used a method of simultaneous nonlinear equations called collinearity (Azuma & Ward, 1991) to estimate the pose of the sensor fixture shown in figure 3 (bottom).** Welch 2001 at Section 5.3.

Exhibit D-6

CLAIM 47	Welch 2001
	In contrast, the approach we use with the new HiBall system produces tracker reports as each new measurement is made, rather than waiting to form a complete collection of observations. Because single measurements underconstrain the mathematical solution, we refer to the approach as single-constraint-at-a-time (SCAAT) tracking (Welch, 1996; Welch & Bishop, 1997). The key is that the single measurements provide some information about the HiBall's state, and thus can be used to incrementally improve a previous estimate. We intentionally fuse each individual "insufficient" measurement immediately as it is obtained. With this approach, we are able to generate estimates more frequently, with less latency, and with improved accuracy, and we are able to estimate the LED positions online concurrently while tracking the HiBall (section 5.4). Welch 2001 at Section 5.3. **We use a Kalman filter (Kalman, 1960) to fuse the measurements into an estimate of the HiBall state x (the pose of the HiBall).** We use the Kalman filter—a minimum-variance stochastic estimator—both because the sensor measurement noise and the typical user-motion dynamics can be modeled as normally distributed random processes, and because we want an efficient online method of estimation. Welch 2001 at Section 5.3. The Kalman filter has been used previously to address similar or related problems. . . . A relevant example of a Kalman filter used for sensor fusion in a wide-area tracking system is given in Foxlin et al. (1998), which describes a hybrid inertial-acoustic system that is commercially available today (Intersense, 2000). Welch 2001 at Section 5.3. [O]ne key benefit warrants discussion here. There is a direct relationship between the complexity of the estimation algorithm, the corresponding speed (execution time per estimation cycle), and the change in HiBall pose between estimation cycles (figure 12). As the algorithmic complexity increases, the execution time increases, which allows for significant nonlinear HiBall motion between estimation cycles, which in turn implies the need for a more complex estimation algorithm. Welch 2001 at Section 5.3.

Exhibit D-6

CLAIM 47	Welch 2001
	 Figure 12. The SCAAT approach, on the other hand, is an attempt to reverse this cycle. Because we intentionally use a single constraint per estimate, the algorithmic complexity is drastically reduced, which reduces the execution time, and hence the amount of motion between estimation cycles. Because the amount of motion is limited, we are able to use a simple dynamic (process) model in the Kalman filter, which further simplifies the computations. In short, the simplicity of the approach means that it can run very fast, which means it can pro- duce estimates very rapidly, with low noise. Welch 2001 at Section 5.3. The Kalman filter requires both a model of the process dynamics and a model of the relationship between the process state and the available measurements. In part due to the simplicity of the SCAAT approach, we are able to use a simple position-velocity (PV) process model (Brown & Hwang, 1992). . . . We model the continuous change in the HiBall state with the simple differential equation

Exhibit D-6

CLAIM 47	Welch 2001

$$\frac{d}{dt}\bar{x}(t) = \begin{bmatrix} 0 & 1 \\ 0 & 0 \end{bmatrix}\begin{bmatrix} x_p(t) \\ x_v(t) \end{bmatrix} + \begin{bmatrix} 0 \\ \mu \end{bmatrix} u(t), \qquad (1)$$

where $u(t)$ is a normally distributed white (in the frequency spectrum) scalar noise process, and the scalar μ represents the magnitude or spectral density of the noise. We use a similar model with a distinct noise process for each of the six pose elements. We determine the individual noise magnitudes using an offline simulation of the system and a nonlinear optimization strategy that seeks to minimize the variance between the estimated pose and a known motion path. (See section 6.2.2.).

Welch 2001 at Section 5.3.

The differential equation (1) represents a continuous integrated random walk, or an integrated Wiener or Brownian-motion process. Specifically, we model each component of the linear and angular HiBall velocities as a random walk, and then use these (assuming constant intermeasurement velocity) to estimate the HiBall pose at time $t + \delta t$ as follows:

Exhibit D-6

CLAIM 47	Welch 2001

$$\bar{x}(t+\delta t) = \begin{bmatrix} 1 & \delta t \\ 0 & 1 \end{bmatrix} \bar{x}(t) \qquad (2)$$

for each of the six pose elements. In addition to a relatively simple process model, the HiBall measurement model is relatively simple. For any ceiling LED (section 4.2) and HiBall view (section 4.1), the 2-D sensor measurement can be modeled as

$$\begin{bmatrix} u \\ v \end{bmatrix} = \begin{bmatrix} c_x/c_z \\ c_y/c_z \end{bmatrix} \qquad (3)$$

where

$$\begin{bmatrix} c_x \\ c_y \\ c_z \end{bmatrix} = VR^T(\bar{l}_{xyz} - \bar{x}_{xyz}), \qquad (4)$$

V is the camera viewing matrix from section 5.1, $\bar{l}_{xyz}$ is the position of the LED in the world, $\bar{x}_{xyz}$ is the position of the HiBall in the world, and R is a rotation matrix corresponding to the orientation of the HiBall in the world. In practice, we maintain the orientation of the HiBall as a combination of a global (external to the state) quaternion and a set of incremental angles as described by Welch (1996) and Welch and Bishop (1997).

Welch 2001 at Section 5.3.

Exhibit D-6

CLAIM 47	Welch 2001
	Because the measurement model (3) and (4) is non-linear, we use an extended Kalman filter, making use of the Jacobian of the nonlinear HiBall measurement model to transform the covariance of the Kalman filter. Welch 2001 at Section 5.3. Along with the benefit of simplicity and speed, the SCAAT approach offers the additional capability of being able to estimate the 3-D positions of the LEDs in the world concurrently with the pose of the HiBall, online, in real time. This capability is a tremendous benefit in terms of the accuracy and noise characteristics of the estimates. The method we now use for autocalibration involves defining a distinct SCAAT Kalman filter for each LED. Specifically, for each LED, we maintain a state $\bar{l}$ (estimate of the 3-D position) and a 3×3 Kalman filter covariance. At the beginning of each estimation cycle, we form an augmented state vector $\hat{x}$ using the appropriate LED state and the current HiBall state: $\hat{x} = [\bar{x}^T, \bar{l}^T]^T$. Similarly, we augment the Kalman filter error covariance matrix with that of the LED filter. We then follow the normal steps outlined in section 5.3, with the result being that the LED portion of the filter state and covariance is updated in accordance with the measurement residual. At the end of the cycle, we extract the LED portions of the state and covariance from the augmented filter, and save them externally. The effect is that, as the system is being used, it continually refines its estimates of the LED positions, thereby continually improving its estimates of the HiBall pose. Again, for additional information, see Welch (1996) and Welch and Bishop (1997).

CLAIM 47	Welch 2001
	Welch 2001 at Section 5.4. The recursive nature of the Kalman filter (section 5.3) requires that the filter be initialized with a known state and corresponding covariance before steady-state operation can begin. Such an initialization (or acquisition) must take place prior to any tracking session, but also upon the (rare) occasion when the filter diverges and "loses lock" as a result of blocked sensor views, for example. Welch 2001 at Section 5.5. The acquisition process is complicated by the fact that each LEPD sees a number of different widely separated views (section 4.1). Therefore, detecting an LED provides at best an ambiguous set of potential LED directions in HiBall coordinates. Moreover, before acquisition, no assumptions can be made to limit the search space of visible LEDs. As such, a relatively slow brute-force algorithm is used to acquire lock. Welch 2001 at Section 5.5. As a result of a mechanical design tradeoff, each sensor field of view is less than six degrees. The focal length is set by the size of the sensor housing, which is set by the diameter of the sensors themselves. Energetics is also a factor, limiting how small the lenses can be while maintaining sufficient light-collecting area. As a result of these design tradeoffs, even a momentary small error in the HiBall pose estimate can cause the recursive estimates to diverge and the system to lose lock after only a few LED sightings. And yet the system is quite robust. In practice, users can jump around, crawl on the floor, lean over, even wave their hands in front of the sensors, and the system does not lose lock. During one session, we were using the HiBall as a 3-D digitization probe, a Hi-Ball on the end of a pencil-shaped fiberglass wand (figure 14, left). We laid the probe down on a table at one point, and were amazed to later notice that it was still tracking, even though it was observing only three or four LEDs near the edge of the ceiling. We picked up the probe and continued using it, without it ever losing lock.   Figure 13.

Exhibit D-6

CLAIM 47	Welch 2001

Figure 14.

Welch 2001 at Section 6.1.

To make measurements of the noise when the HiBall is in motion, we rely on the assumption that almost all of the signal resulting from normal human motion is at frequencies below 2 Hz. We use a high-pass filter (Welch, 1967) on the pose estimates, and assume the output is noise. The resulting statistics are comparable to those made with the HiBall stationary, except at poses for which there are very few LEDs visible in only one or two views. In these poses, near the edge of the ceiling, the geometry of the constraints results in amplification of errors. For nearly all of the working volume of the tracker, the standard deviation of the noise on measurements while the HiBall is still or moving is about 0.2 mm and 0.03 deg.
Welch 2001 at Section 6.1.

During the design of the HiBall system, we made substantial use of simulation, in some domains to a very detailed level. For example, Zemax (Focus Software, 1995) was used extensively in the design and optimization of the optical design, including the design of the filter glass lenses, and geometry of the optical-component layout.
Welch 2001 at Section 6.2.

To produce realistic data for developing and tuning our algorithms, we collected several motion paths (sequences of pose estimates) from our first-generation electro-optical tracker (figure 3) at its 70 Hz maximum report rate. These paths were recorded from both naive users visiting our monthly “demo days” and from experienced users in our labs. . . . we filtered the raw path data with a noncausal zero-phase-shift, low-pass filter to eliminate energy

CLAIM 47	Welch 2001
	above 2 Hz. The output of the low-pass filtering was then resampled at whatever rate we wanted to run the simulated tracker, usually 1,000 Hz. Welch 2001 at Section 6.2. The simulator reads camera models describing the 26 views, the sensor noise parameters, the LED positions and their expected error, and the motion path described above. Before beginning the simulation, the LED positions are perturbed from their ideal positions by adding normally distributed error to each axis. Then, for each simulated cycle of operation, the "true" poses are up- dated using the input motion path. Next, a view is chosen and a visible LED within that view is selected, and the image-plane coordinates of the LED on the chosen sensor are computed using the camera model for the view and the LED as described in section 5.3. These sensor coordinates are then perturbed based on the sensor noise model (section 6.2.1) using the distance and angle to the LED. These noise-corrupted sensor readings are then fed to the SCAAT filter to produce an up- dated position estimate. The position estimate is com- pared to the true position to produce a scalar error metric that is described next. Welch 2001 at Section 6.2. The error metric we used combines the error in pose in a way that relates to the effects of tracker error on a head-worn display user. We define a set of points arrayed around the user in a fixed configuration. We compute two sets of coordinates for these points: the true position using the true pose and their estimated position using the estimated pose. The error metric is then the sum of the distances between the true and estimated positions of these points. By adjusting the distance of the points from the user, we can control the relative importance of the orientation and the position error in the combined error metric. If the distance is small, then the position error is weighted most heavily; if the distance is large, then the orientation error is weighted most heavily. Our two error metrics for the entire run are the square root of the sum of the squares of all the distances, and the peak distance. Welch 2001 at Section 6.2. *See also* Defendants' Invalidity Contentions for further discussion.
[47.g] passing data based on the estimates of the tracking parameters from the estimation module to	At least under Plaintiffs' apparent infringement theory, Welch 2001 discloses, either expressly or inherently, passing data based on the estimates of the tracking parameters from the estimation module to one or more of the sensor modules. In the alternative, this element would be obvious over Welch 2001 in light of the other references disclosed in Defendants' Invalidity Contentions and/or the knowledge of one of ordinary skill in the art.

Exhibit D-6

CLAIM 47	Welch 2001
one or more of the sensor modules,	*See, e.g.*: Both parts of the camera model are determined using a calibration procedure that relies on a goniometer (an angular positioning system) of our own design. This device consists of two servo motors mounted together such that one motor provides rotation about the vertical axis while the second motor provides rotation about an axis orthogonal to vertical. An important characteristic of the goniometer is that the rotational axes of the two motors intersect at a point at the center of the HiBall optical sphere; this point is defined as the origin of the HiBall. . . . The rotational positioning motors were rated to provide twenty arc-second precision; we further calibrated them to six arc seconds using a laboratory grade theodolite—an angle measuring system. Welch 2001 at Section 5.1. To determine the mapping between sensor image-plane coordinates and three-space rays, we use a single LED mounted at a fixed location in the laboratory such that it is centered in the view directly out of the top lens of the HiBall. This ray defines the z or up axis for the HiBall coordinate system. We sample other rays by rotating the goniometer motors under computer control. We sample each view with rays spaced about every six minutes of arc throughout the field of view. We repeat each measurement 100 times to reduce the effects of noise on the individual measurements and to estimate the standard deviation of the measurements. Welch 2001 at Section 5.1. Given the tables of approximately 2,500 measurements for each of the 26 views, we first determine a 3 X 4 view matrix using standard linear least-squares techniques. Then, we determine the deviation of each measured point from that predicted by the ideal linear model. These deviations are resampled into a 25 X 25 grid indexed by sensor-plane coordinates using a simple scan-conversion procedure and averaging. Given a measurement from a sensor at runtime (section 5.2), we convert it to an “ideal” measurement by subtracting a deviation bilinearly interpolated from the nearest four entries in the table. Welch 2001 at Section 5.1. The online measurements (section 5.2) are used to estimate the pose of the HiBall during operation. The 1991 system collected a group of diverse measurements for a variety of LEDs and sensors, and then used a method of simultaneous nonlinear equations called collinearity (Azuma & Ward, 1991) to estimate the pose of the sensor fixture shown in figure 3 (bottom). Welch 2001 at Section 5.3.

Exhibit D-6

CLAIM 47	Welch 2001
	In contrast, the approach we use with **the new HiBall system produces tracker reports as each new measurement is made,** rather than waiting to form a complete collection of observations. Because single measurements underconstrain the mathematical solution, we refer to the approach as single-constraint-at-a-time (SCAAT) tracking (Welch, 1996; Welch & Bishop, 1997). **The key is that the single measurements provide some information about the HiBall's state, and thus can be used to incrementally improve a previous estimate. We intentionally fuse each individual "insufficient" measurement immediately as it is obtained.** With this approach, we are able to generate estimates more frequently, with less latency, and with improved accuracy, and we are able to estimate the LED positions online concurrently while tracking the HiBall (section 5.4). Welch 2001 at Section 5.3. **We use a Kalman filter (Kalman, 1960) to fuse the measurements into an estimate of the HiBall state x (the pose of the HiBall). We use the Kalman filter—a minimum-variance stochastic estimator—both because the sensor measurement noise and the typical user-motion dynamics can be modeled as normally distributed random processes, and because we want an efficient online method of estimation.** Welch 2001 at Section 5.3. The Kalman filter has been used previously to address similar or related problems. . . . A relevant example of a Kalman filter used for sensor fusion in a wide-area tracking system is given in Foxlin et al. (1998), which describes a hybrid inertial-acoustic system that is commercially available today (Intersense, 2000). Welch 2001 at Section 5.3. [O]ne key benefit warrants discussion here. There is a direct relationship between the complexity of the estimation algorithm, the corresponding speed (execution time per estimation cycle), and the change in HiBall pose between estimation cycles (figure 12). As the algorithmic complexity increases, the execution time increases, which allows for significant nonlinear HiBall motion between estimation cycles, which in turn implies the need for a more complex estimation algorithm. Welch 2001 at Section 5.3.

Exhibit D-6

CLAIM 47	Welch 2001
	 Figure 12. The SCAAT approach, on the other hand, is an attempt to reverse this cycle. Because we intentionally use a single constraint per estimate, the algorithmic complexity is drastically reduced, which reduces the execution time, and hence the amount of motion between estimation cycles. Because the amount of motion is limited, we are able to use a simple dynamic (process) model in the Kalman filter, which further simplifies the computations. In short, the simplicity of the approach means that it can run very fast, which means it can pro- duce estimates very rapidly, with low noise. Welch 2001 at Section 5.3. The Kalman filter requires both a model of the process dynamics and a model of the relationship between the process state and the available measurements. In part due to the simplicity of the SCAAT approach, we are able to use a simple position-velocity (PV) process model (Brown & Hwang, 1992). . . . We model the continuous change in the HiBall state with the simple differential equation

Exhibit D-6

CLAIM 47	Welch 2001

$$\frac{d}{dt}\bar{x}(t) = \begin{bmatrix} 0 & 1 \\ 0 & 0 \end{bmatrix}\begin{bmatrix} x_p(t) \\ x_v(t) \end{bmatrix} + \begin{bmatrix} 0 \\ \mu \end{bmatrix} u(t), \qquad (1)$$

where $u(t)$ is a normally distributed white (in the frequency spectrum) scalar noise process, and the scalar μ represents the magnitude or spectral density of the noise. We use a similar model with a distinct noise process for each of the six pose elements. We determine the individual noise magnitudes using an offline simulation of the system and a nonlinear optimization strategy that seeks to minimize the variance between the estimated pose and a known motion path. (See section 6.2.2.).

Welch 2001 at Section 5.3.

The differential equation (1) represents a continuous integrated random walk, or an integrated Wiener or Brownian-motion process. Specifically, we model each component of the linear and angular HiBall velocities as a random walk, and then use these (assuming constant intermeasurement velocity) to estimate the HiBall pose at time $t + \delta t$ as follows:

Exhibit D-6

CLAIM 47	Welch 2001

$$\bar{x}(t+\delta t) = \begin{bmatrix} 1 & \delta t \\ 0 & 1 \end{bmatrix} \bar{x}(t) \qquad (2)$$

for each of the six pose elements. In addition to a relatively simple process model, the HiBall measurement model is relatively simple. For any ceiling LED (section 4.2) and HiBall view (section 4.1), the 2-D sensor measurement can be modeled as

$$\begin{bmatrix} u \\ v \end{bmatrix} = \begin{bmatrix} c_x/c_z \\ c_y/c_z \end{bmatrix} \qquad (3)$$

where

$$\begin{bmatrix} c_x \\ c_y \\ c_z \end{bmatrix} = VR^T(\bar{l}_{xyz} - \bar{x}_{xyz}), \qquad (4)$$

V is the camera viewing matrix from section 5.1, $\bar{l}_{xyz}$ is the position of the LED in the world, $\bar{x}_{xyz}$ is the position of the HiBall in the world, and R is a rotation matrix corresponding to the orientation of the HiBall in the world. In practice, we maintain the orientation of the HiBall as a combination of a global (external to the state) quaternion and a set of incremental angles as described by Welch (1996) and Welch and Bishop (1997).

Welch 2001 at Section 5.3.

Exhibit D-6

CLAIM 47	Welch 2001
	Because the measurement model (3) and (4) is non-linear, we use an extended Kalman filter, making use of the Jacobian of the nonlinear HiBall measurement model to transform the covariance of the Kalman filter. Welch 2001 at Section 5.3. Along with the benefit of simplicity and speed, the SCAAT approach offers the additional capability of being able to estimate the 3-D positions of the LEDs in the world concurrently with the pose of the HiBall, online, in real time. This capability is a tremendous benefit in terms of the accuracy and noise characteristics of the estimates. The method we now use for autocalibration involves defining a distinct SCAAT Kalman filter for each LED. Specifically, for each LED, we maintain a state $\bar{l}$ (estimate of the 3-D position) and a 3×3 Kalman filter covariance. At the beginning of each estimation cycle, we form an augmented state vector $\hat{x}$ using the appropriate LED state and the current HiBall state: $\hat{x} = [\bar{x}^T, \bar{l}^T]^T$. Similarly, we augment the Kalman filter error covariance matrix with that of the LED filter. We then follow the normal steps outlined in section 5.3, with the result being that the LED portion of the filter state and covariance is updated in accordance with the measurement residual. At the end of the cycle, we extract the LED portions of the state and covariance from the augmented filter, and save them externally. The effect is that, as the system is being used, it continually refines its estimates of the LED positions, thereby continually improving its estimates of the HiBall pose. Again, for additional information, see Welch (1996) and Welch and Bishop (1997).

CLAIM 47	Welch 2001
	Welch 2001 at Section 5.4. The recursive nature of the Kalman filter (section 5.3) requires that the filter be initialized with a known state and corresponding covariance before steady-state operation can begin. Such an initialization (or acquisition) must take place prior to any tracking session, but also upon the (rare) occasion when the filter diverges and "loses lock" as a result of blocked sensor views, for example. Welch 2001 at Section 5.5. The acquisition process is complicated by the fact that each LEPD sees a number of different widely separated views (section 4.1). Therefore, detecting an LED provides at best an ambiguous set of potential LED directions in HiBall coordinates. Moreover, before acquisition, no assumptions can be made to limit the search space of visible LEDs. As such, a relatively slow brute-force algorithm is used to acquire lock. Welch 2001 at Section 5.5. As a result of a mechanical design tradeoff, each sensor field of view is less than six degrees. The focal length is set by the size of the sensor housing, which is set by the diameter of the sensors themselves. Energetics is also a factor, limiting how small the lenses can be while maintaining sufficient light-collecting area. As a result of these design tradeoffs, even a momentary small error in the HiBall pose estimate can cause the recursive estimates to diverge and the system to lose lock after only a few LED sightings. And yet the system is quite robust. In practice, users can jump around, crawl on the floor, lean over, even wave their hands in front of the sensors, and the system does not lose lock. During one session, we were using the HiBall as a 3-D digitization probe, a Hi-Ball on the end of a pencil-shaped fiberglass wand (figure 14, left). We laid the probe down on a table at one point, and were amazed to later notice that it was still tracking, even though it was observing only three or four LEDs near the edge of the ceiling. We picked up the probe and continued using it, without it ever losing lock.   Figure 13.

Exhibit D-6

CLAIM 47	Welch 2001

Figure 14.

Welch 2001 at Section 6.1.

To make measurements of the noise when the HiBall is in motion, we rely on the assumption that almost all of the signal resulting from normal human motion is at frequencies below 2 Hz. We use a high-pass filter (Welch, 1967) on the pose estimates, and assume the output is noise. The resulting statistics are comparable to those made with the HiBall stationary, except at poses for which there are very few LEDs visible in only one or two views. In these poses, near the edge of the ceiling, the geometry of the constraints results in amplification of errors. For nearly all of the working volume of the tracker, the standard deviation of the noise on measurements while the HiBall is still or moving is about 0.2 mm and 0.03 deg.
Welch 2001 at Section 6.1.

During the design of the HiBall system, we made substantial use of simulation, in some domains to a very detailed level. For example, Zemax (Focus Software, 1995) was used extensively in the design and optimization of the optical design, including the design of the filter glass lenses, and geometry of the optical-component layout.
Welch 2001 at Section 6.2.

To produce realistic data for developing and tuning our algorithms, we collected several motion paths (sequences of pose estimates) from our first-generation electro-optical tracker (figure 3) at its 70 Hz maximum report rate. **These paths were recorded from both naive users visiting our monthly "demo days" and from experienced users in our labs. . . . we filtered the raw path data with a noncausal zero-phase-shift, low-pass filter to**

CLAIM 47	Welch 2001
	eliminate energy above 2 Hz. The output of the low-pass filtering was then resampled at whatever rate we wanted to run the simulated tracker, usually 1,000 Hz. Welch 2001 at Section 6.2. The simulator reads camera models describing the 26 views, the sensor noise parameters, the LED positions and their expected error, and the motion path described above. Before beginning the simulation, the LED positions are perturbed from their ideal positions by adding normally distributed error to each axis. Then, for each simulated cycle of operation, the "true" poses are up- dated using the input motion path. Next, a view is chosen and a visible LED within that view is selected, and the image-plane coordinates of the LED on the chosen sensor are computed using the camera model for the view and the LED as described in section 5.3. These sensor coordinates are then perturbed based on the sensor noise model (section 6.2.1) using the distance and angle to the LED. **These noise-corrupted sensor readings are then fed to the SCAAT filter to produce an up- dated position estimate. The position estimate is com- pared to the true position to produce a scalar error metric that is described next.** Welch 2001 at Section 6.2. The error metric we used combines the error in pose in a way that relates to the effects of tracker error on a head-worn display user. We define a set of points arrayed around the user in a fixed configuration. We compute two sets of coordinates for these points: the true position using the true pose and their estimated position using the estimated pose. The error metric is then the sum of the distances between the true and estimated positions of these points. **By adjusting the distance of the points from the user, we can control the relative importance of the orientation and the position error in the combined error metric. If the distance is small, then the position error is weighted most heavily; if the distance is large, then the orientation error is weighted most heavily.** Our two error metrics for the entire run are the square root of the sum of the squares of all the distances, and the peak distance. Welch 2001 at Section 6.2. *See also* Defendants' Invalidity Contentions for further discussion.
[47.h] receiving from said one or more sensor modules at the estimation module data based on measurements obtained	At least under Plaintiffs' apparent infringement theory, Welch 2001 discloses, either expressly or inherently, receiving from said one or more sensor modules at the estimation module data based on measurements obtained from the associated sensors, and the data passed to the sensor modules. In the alternative, this element would be

Exhibit D-6

CLAIM 47	Welch 2001
from the associated sensors, and the data passed to the sensor modules, and	obvious over Welch 2001 in light of the other references disclosed in Defendants' Invalidity Contentions and/or the knowledge of one of ordinary skill in the art. *See, e.g.*: Both parts of the camera model are determined using a calibration procedure that relies on a goniometer (an angular positioning system) of our own design. This device consists of two servo motors mounted together such that one motor provides rotation about the vertical axis while the second motor provides rotation about an axis orthogonal to vertical. An important characteristic of the goniometer is that the rotational axes of the two motors intersect at a point at the center of the HiBall optical sphere; this point is defined as the origin of the HiBall. . . . The rotational positioning motors were rated to provide twenty arc-second precision; we further calibrated them to six arc seconds using a laboratory grade theodolite—an angle measuring system. Welch 2001 at Section 5.1. To determine the mapping between sensor image-plane coordinates and three-space rays, we use a single LED mounted at a fixed location in the laboratory such that it is centered in the view directly out of the top lens of the HiBall. This ray defines the z or up axis for the HiBall coordinate system. We sample other rays by rotating the goniometer motors under computer control. We sample each view with rays spaced about every six minutes of arc throughout the field of view. We repeat each measurement 100 times to reduce the effects of noise on the individual measurements and to estimate the standard deviation of the measurements. Welch 2001 at Section 5.1. Given the tables of approximately 2,500 measurements for each of the 26 views, we first determine a 3 X 4 view matrix using standard linear least-squares techniques. Then, we determine the deviation of each measured point from that predicted by the ideal linear model. These deviations are resampled into a 25 X 25 grid indexed by sensor-plane coordinates using a simple scan-conversion procedure and averaging. Given a measurement from a sensor at runtime (section 5.2), we convert it to an "ideal" measurement by subtracting a deviation bilinearly interpolated from the nearest four entries in the table. Welch 2001 at Section 5.1. The online measurements (section 5.2) are used to estimate the pose of the HiBall during operation. The 1991 system collected a group of diverse measurements for a variety of LEDs and sensors, and then used a method of simultaneous nonlinear equations called collinearity (Azuma & Ward, 1991) to estimate the pose of the sensor

Exhibit D-6

CLAIM 47	Welch 2001
	fixture shown in figure 3 (bottom). Welch 2001 at Section 5.3. In contrast, the approach we use with the new HiBall system produces tracker reports as each new measurement is made, rather than waiting to form a complete collection of observations. **Because single measurements underconstrain the mathematical solution, we refer to the approach as single-constraint-at-a-time (SCAAT) tracking** (Welch, 1996; Welch & Bishop, 1997). **The key is that the single measurements provide some information about the HiBall's state, and thus can be used to incrementally improve a previous estimate. We intentionally fuse each individual "insufficient" measurement immediately as it is obtained.** With this approach, we are able to generate estimates more frequently, with less latency, and with improved accuracy, and we are able to estimate the LED positions online concurrently while tracking the HiBall (section 5.4). Welch 2001 at Section 5.3. **We use a Kalman filter (Kalman, 1960) to fuse the measurements into an estimate of the HiBall state x (the pose of the HiBall). We use the Kalman filter—a minimum-variance stochastic estimator—both because the sensor measurement noise and the typical user-motion dynamics can be modeled as normally distributed random processes, and because we want an efficient online method of estimation.** Welch 2001 at Section 5.3. The Kalman filter has been used previously to address similar or related problems. . . . A relevant example of a Kalman filter used for sensor fusion in a wide-area tracking system is given in Foxlin et al. (1998), which describes a hybrid inertial-acoustic system that is commercially available today (Intersense, 2000). Welch 2001 at Section 5.3. [O]ne key benefit warrants discussion here. There is a direct relationship between the complexity of the estimation algorithm, the corresponding speed (execution time per estimation cycle), and the change in HiBall pose between estimation cycles (figure 12). As the algorithmic complexity increases, the execution time increases, which allows for significant nonlinear HiBall motion between estimation cycles, which in turn implies the need for a more complex estimation algorithm. Welch 2001 at Section 5.3.

Exhibit D-6

CLAIM 47	Welch 2001
	 Figure 12. The SCAAT approach, on the other hand, is an attempt to reverse this cycle. Because we intentionally use a single constraint per estimate, the algorithmic complexity is drastically reduced, which reduces the execution time, and hence the amount of motion between estimation cycles. Because the amount of motion is limited, we are able to use a simple dynamic (process) model in the Kalman filter, which further simplifies the computations. In short, the simplicity of the approach means that it can run very fast, which means it can pro- duce estimates very rapidly, with low noise. Welch 2001 at Section 5.3. The Kalman filter requires both a model of the process dynamics and a model of the relationship between the process state and the available measurements. In part due to the simplicity of the SCAAT approach, we are able to use a simple position-velocity (PV) process model (Brown & Hwang, 1992). . . . We model the continuous change in the HiBall state with the simple differential equation

Exhibit D-6

CLAIM 47	Welch 2001

$$\frac{d}{dt}\bar{x}(t) = \begin{bmatrix} 0 & 1 \\ 0 & 0 \end{bmatrix}\begin{bmatrix} x_p(t) \\ x_v(t) \end{bmatrix} + \begin{bmatrix} 0 \\ \mu \end{bmatrix} u(t), \qquad (1)$$

where $u(t)$ is a normally distributed white (in the frequency spectrum) scalar noise process, and the scalar μ represents the magnitude or spectral density of the noise. We use a similar model with a distinct noise process for each of the six pose elements. We determine the individual noise magnitudes using an offline simulation of the system and a nonlinear optimization strategy that seeks to minimize the variance between the estimated pose and a known motion path. (See section 6.2.2.).

Welch 2001 at Section 5.3.

The differential equation (1) represents a continuous integrated random walk, or an integrated Wiener or Brownian-motion process. Specifically, we model each component of the linear and angular HiBall velocities as a random walk, and then use these (assuming constant intermeasurement velocity) to estimate the HiBall pose at time $t + \delta t$ as follows:

Exhibit D-6

CLAIM 47	Welch 2001

$$\bar{x}(t+\delta t) = \begin{bmatrix} 1 & \delta t \\ 0 & 1 \end{bmatrix} \bar{x}(t) \qquad (2)$$

for each of the six pose elements. In addition to a relatively simple process model, the HiBall measurement model is relatively simple. For any ceiling LED (section 4.2) and HiBall view (section 4.1), the 2-D sensor measurement can be modeled as

$$\begin{bmatrix} u \\ v \end{bmatrix} = \begin{bmatrix} c_x/c_z \\ c_y/c_z \end{bmatrix} \qquad (3)$$

where

$$\begin{bmatrix} c_x \\ c_y \\ c_z \end{bmatrix} = VR^T(\bar{l}_{xyz} - \bar{x}_{xyz}), \qquad (4)$$

V is the camera viewing matrix from section 5.1, $\bar{l}_{xyz}$ is the position of the LED in the world, $\bar{x}_{xyz}$ is the position of the HiBall in the world, and R is a rotation matrix corresponding to the orientation of the HiBall in the world. In practice, we maintain the orientation of the HiBall as a combination of a global (external to the state) quaternion and a set of incremental angles as described by Welch (1996) and Welch and Bishop (1997).

Welch 2001 at Section 5.3.

Exhibit D-6

CLAIM 47	Welch 2001
	Because the measurement model (3) and (4) is non-linear, we use an extended Kalman filter, making use of the Jacobian of the nonlinear HiBall measurement model to transform the covariance of the Kalman filter. Welch 2001 at Section 5.3. Along with the benefit of simplicity and speed, the SCAAT approach offers the additional capability of being able to estimate the 3-D positions of the LEDs in the world concurrently with the pose of the HiBall, online, in real time. This capability is a tremendous benefit in terms of the accuracy and noise characteristics of the estimates. The method we now use for autocalibration involves defining a distinct SCAAT Kalman filter for each LED. Specifically, for each LED, we maintain a state $\bar{l}$ (estimate of the 3-D position) and a 3×3 Kalman filter covariance. At the beginning of each estimation cycle, we form an augmented state vector $\hat{x}$ using the appropriate LED state and the current HiBall state: $\hat{x} = [\bar{x}^T, \bar{l}^T]^T$. Similarly, we augment the Kalman filter error covariance matrix with that of the LED filter. We then follow the normal steps outlined in section 5.3, with the result being that the LED portion of the filter state and covariance is updated in accordance with the measurement residual. At the end of the cycle, we extract the LED portions of the state and covariance from the augmented filter, and save them externally. The effect is that, as the system is being used, it continually refines its estimates of the LED positions, thereby continually improving its estimates of the HiBall pose. Again, for additional information, see Welch (1996) and Welch and Bishop (1997).

CLAIM 47	Welch 2001
	Welch 2001 at Section 5.4. The recursive nature of the Kalman filter (section 5.3) requires that the filter be initialized with a known state and corresponding covariance before steady-state operation can begin. Such an initialization (or acquisition) must take place prior to any tracking session, but also upon the (rare) occasion when the filter diverges and "loses lock" as a result of blocked sensor views, for example. Welch 2001 at Section 5.5. The acquisition process is complicated by the fact that each LEPD sees a number of different widely separated views (section 4.1). Therefore, detecting an LED provides at best an ambiguous set of potential LED directions in HiBall coordinates. Moreover, before acquisition, no assumptions can be made to limit the search space of visible LEDs. As such, a relatively slow brute-force algorithm is used to acquire lock. Welch 2001 at Section 5.5. As a result of a mechanical design tradeoff, each sensor field of view is less than six degrees. The focal length is set by the size of the sensor housing, which is set by the diameter of the sensors themselves. Energetics is also a factor, limiting how small the lenses can be while maintaining sufficient light-collecting area. As a result of these design tradeoffs, even a momentary small error in the HiBall pose estimate can cause the recursive estimates to diverge and the system to lose lock after only a few LED sightings. And yet the system is quite robust. In practice, users can jump around, crawl on the floor, lean over, even wave their hands in front of the sensors, and the system does not lose lock. During one session, we were using the HiBall as a 3-D digitization probe, a Hi-Ball on the end of a pencil-shaped fiberglass wand (figure 14, left). We laid the probe down on a table at one point, and were amazed to later notice that it was still tracking, even though it was observing only three or four LEDs near the edge of the ceiling. We picked up the probe and continued using it, without it ever losing lock.   Figure 13.

Exhibit D-6

CLAIM 47	Welch 2001

Figure 14.

Welch 2001 at Section 6.1.

To make measurements of the noise when the HiBall is in motion, we rely on the assumption that almost all of the signal resulting from normal human motion is at frequencies below 2 Hz. We use a high-pass filter (Welch, 1967) on the pose estimates, and assume the output is noise. The resulting statistics are comparable to those made with the HiBall stationary, except at poses for which there are very few LEDs visible in only one or two views. In these poses, near the edge of the ceiling, the geometry of the constraints results in amplification of errors. For nearly all of the working volume of the tracker, the standard deviation of the noise on measurements while the HiBall is still or moving is about 0.2 mm and 0.03 deg.
Welch 2001 at Section 6.1.

During the design of the HiBall system, we made substantial use of simulation, in some domains to a very detailed level. For example, Zemax (Focus Software, 1995) was used extensively in the design and optimization of the optical design, including the design of the filter glass lenses, and geometry of the optical-component layout.
Welch 2001 at Section 6.2.

To produce realistic data for developing and tuning our algorithms, we collected several motion paths (sequences of pose estimates) from our first-generation electro-optical tracker (figure 3) at its 70 Hz maximum report rate. These paths were recorded from both naive users visiting our monthly “demo days” and from experienced users in our labs. . . . we filtered the raw path data with a noncausal zero-phase-shift, low-pass filter to eliminate energy

CLAIM 47	Welch 2001
	above 2 Hz. The output of the low-pass filtering was then resampled at whatever rate we wanted to run the simulated tracker, usually 1,000 Hz. Welch 2001 at Section 6.2. The simulator reads camera models describing the 26 views, the sensor noise parameters, the LED positions and their expected error, and the motion path described above. Before beginning the simulation, the LED positions are perturbed from their ideal positions by adding normally distributed error to each axis. Then, for each simulated cycle of operation, the "true" poses are up- dated using the input motion path. Next, a view is chosen and a visible LED within that view is selected, and the image-plane coordinates of the LED on the chosen sensor are computed using the camera model for the view and the LED as described in section 5.3. These sensor coordinates are then perturbed based on the sensor noise model (section 6.2.1) using the distance and angle to the LED. **These noise-corrupted sensor readings are then fed to the SCAAT filter to produce an up- dated position estimate. The position estimate is com- pared to the true position to produce a scalar error metric that is described next.** Welch 2001 at Section 6.2. The error metric we used combines the error in pose in a way that relates to the effects of tracker error on a head-worn display user. We define a set of points arrayed around the user in a fixed configuration. We compute two sets of coordinates for these points: the true position using the true pose and their estimated position using the estimated pose. **The error metric is then the sum of the distances between the true and estimated positions of these points. By adjusting the distance of the points from the user, we can control the relative importance of the orientation and the position error in the combined error metric.** If the distance is small, then the position error is weighted most heavily; if the distance is large, then the orientation error is weighted most heavily. Our two error metrics for the entire run are the square root of the sum of the squares of all the distances, and the peak distance. Welch 2001 at Section 6.2. *See also* Defendants' Invalidity Contentions for further discussion.
[47.i] combining the data received from said one or more sensor modules and the estimates of the tracking parameters in	At least under Plaintiffs' apparent infringement theory, Welch 2001 discloses, either expressly or inherently, combining the data received from said one or more sensor modules and the estimates of the tracking parameters in the estimation module to update the tracking parameters. In the alternative, this element would be obvious over

CLAIM 47	Welch 2001
the estimation module to update the tracking parameters.	Welch 2001 in light of the other references disclosed in Defendants' Invalidity Contentions and/or the knowledge of one of ordinary skill in the art. *See, e.g.*: Both parts of the camera model are determined using a calibration procedure that relies on a goniometer (an angular positioning system) of our own design. This device consists of two servo motors mounted together such that one motor provides rotation about the vertical axis while the second motor provides rotation about an axis orthogonal to vertical. An important characteristic of the goniometer is that the rotational axes of the two motors intersect at a point at the center of the HiBall optical sphere; this point is defined as the origin of the HiBall. . . . The rotational positioning motors were rated to provide twenty arc-second precision; we further calibrated them to six arc seconds using a laboratory grade theodolite—an angle measuring system. Welch 2001 at Section 5.1. To determine the mapping between sensor image-plane coordinates and three-space rays, we use a single LED mounted at a fixed location in the laboratory such that it is centered in the view directly out of the top lens of the HiBall. This ray defines the z or up axis for the HiBall coordinate system. We sample other rays by rotating the goniometer motors under computer control. We sample each view with rays spaced about every six minutes of arc throughout the field of view. We repeat each measurement 100 times to reduce the effects of noise on the individual measurements and to estimate the standard deviation of the measurements. Welch 2001 at Section 5.1. Given the tables of approximately 2,500 measurements for each of the 26 views, we first determine a 3 X 4 view matrix using standard linear least-squares techniques. Then, we determine the deviation of each measured point from that predicted by the ideal linear model. These deviations are resampled into a 25 X 25 grid indexed by sensor-plane coordinates using a simple scan-conversion procedure and averaging. **Given a measurement from a sensor at runtime (section 5.2), we convert it to an "ideal" measurement by subtracting a deviation bilinearly interpolated from the nearest four entries in the table.** Welch 2001 at Section 5.1. The online measurements (section 5.2) are used to estimate the pose of the HiBall during operation. The 1991 **system collected a group of diverse measurements for a variety of LEDs and sensors, and then used a method of simultaneous nonlinear equations called collinearity (Azuma & Ward, 1991) to estimate the**

Exhibit D-6

CLAIM 47	Welch 2001
	pose of the sensor fixture shown in figure 3 (bottom). Welch 2001 at Section 5.3. In contrast, the approach we use with the new HiBall system produces tracker reports as each new measurement is made, rather than waiting to form a complete collection of observations. B**ecause single measurements underconstrain the mathematical solution, we refer to the approach as single-constraint-at-a-time (SCAAT) tracking (Welch, 1996; Welch & Bishop, 1997). The key is that the single measurements provide some information about the HiBall's state, and thus can be used to incrementally improve a previous estimate.** We intentionally fuse each individual "insufficient" measurement immediately as it is obtained. With this approach, we are able to generate estimates more frequently, with less latency, and with improved accuracy, and we are able to estimate the LED positions online concurrently while tracking the HiBall (section 5.4). Welch 2001 at Section 5.3. **We use a Kalman filter (Kalman, 1960) to fuse the measurements into an estimate of the HiBall state x (the pose of the HiBall).** We use the Kalman filter—a minimum-variance stochastic estimator—both because the sensor measurement noise and the typical user-motion dynamics can be modeled as normally distributed random processes, and because we want an efficient online method of estimation. Welch 2001 at Section 5.3. The Kalman filter has been used previously to address similar or related problems. . . . A relevant example of a Kalman filter used for sensor fusion in a wide-area tracking system is given in Foxlin et al. (1998), which describes a hybrid inertial-acoustic system that is commercially available today (Intersense, 2000). Welch 2001 at Section 5.3. [O]ne key benefit warrants discussion here. There is a direct relationship between the complexity of the estimation algorithm, the corresponding speed (execution time per estimation cycle), and the change in HiBall pose between estimation cycles (figure 12). As the algorithmic complexity increases, the execution time increases, which allows for significant nonlinear HiBall motion between estimation cycles, which in turn implies the need for a more complex estimation algorithm. Welch 2001 at Section 5.3.

Exhibit D-6

CLAIM 47	Welch 2001
	 Figure 12. The SCAAT approach, on the other hand, is an attempt to reverse this cycle. Because we intentionally use a single constraint per estimate, the algorithmic complexity is drastically reduced, which reduces the execution time, and hence the amount of motion between estimation cycles. Because the amount of motion is limited, we are able to use a simple dynamic (process) model in the Kalman filter, which further simplifies the computations. In short, the simplicity of the approach means that it can run very fast, which means it can pro- duce estimates very rapidly, with low noise. Welch 2001 at Section 5.3. The Kalman filter requires both a model of the process dynamics and a model of the relationship between the process state and the available measurements. In part due to the simplicity of the SCAAT approach, we are able to use a simple position-velocity (PV) process model (Brown & Hwang, 1992). . . . We model the continuous change in the HiBall state with the simple differential equation

Exhibit D-6

CLAIM 47	Welch 2001

$$\frac{d}{dt}\bar{x}(t) = \begin{bmatrix} 0 & 1 \\ 0 & 0 \end{bmatrix}\begin{bmatrix} x_p(t) \\ x_v(t) \end{bmatrix} + \begin{bmatrix} 0 \\ \mu \end{bmatrix} u(t), \qquad (1)$$

where $u(t)$ is a normally distributed white (in the frequency spectrum) scalar noise process, and the scalar μ represents the magnitude or spectral density of the noise. We use a similar model with a distinct noise process for each of the six pose elements. We determine the individual noise magnitudes using an offline simulation of the system and a nonlinear optimization strategy that seeks to minimize the variance between the estimated pose and a known motion path. (See section 6.2.2.).

Welch 2001 at Section 5.3.

The differential equation (1) represents a continuous integrated random walk, or an integrated Wiener or Brownian-motion process. Specifically, we model each component of the linear and angular HiBall velocities as a random walk, and then use these (assuming constant intermeasurement velocity) to estimate the HiBall pose at time $t + \delta t$ as follows:

Exhibit D-6

CLAIM 47	Welch 2001

$$\bar{x}(t+\delta t) = \begin{bmatrix} 1 & \delta t \\ 0 & 1 \end{bmatrix} \bar{x}(t) \qquad (2)$$

for each of the six pose elements. In addition to a relatively simple process model, the HiBall measurement model is relatively simple. For any ceiling LED (section 4.2) and HiBall view (section 4.1), the 2-D sensor measurement can be modeled as

$$\begin{bmatrix} u \\ v \end{bmatrix} = \begin{bmatrix} c_x/c_z \\ c_y/c_z \end{bmatrix} \qquad (3)$$

where

$$\begin{bmatrix} c_x \\ c_y \\ c_z \end{bmatrix} = VR^T(\bar{l}_{xyz} - \bar{x}_{xyz}), \qquad (4)$$

V is the camera viewing matrix from section 5.1, $\bar{l}_{xyz}$ is the position of the LED in the world, $\bar{x}_{xyz}$ is the position of the HiBall in the world, and R is a rotation matrix corresponding to the orientation of the HiBall in the world. In practice, we maintain the orientation of the HiBall as a combination of a global (external to the state) quaternion and a set of incremental angles as described by Welch (1996) and Welch and Bishop (1997).

Welch 2001 at Section 5.3.

Exhibit D-6

CLAIM 47	Welch 2001
	Because the measurement model (3) and (4) is non-linear, we use an extended Kalman filter, making use of the Jacobian of the nonlinear HiBall measurement model to transform the covariance of the Kalman filter. Welch 2001 at Section 5.3. Along with the benefit of simplicity and speed, the SCAAT approach offers the additional capability of being able to estimate the 3-D positions of the LEDs in the world concurrently with the pose of the HiBall, online, in real time. This capability is a tremendous benefit in terms of the accuracy and noise characteristics of the estimates. The method we now use for autocalibration involves defining a distinct SCAAT Kalman filter for each LED. Specifically, for each LED, we maintain a state $\bar{l}$ (estimate of the 3-D position) and a 3×3 Kalman filter covariance. At the beginning of each estimation cycle, we form an augmented state vector $\hat{x}$ using the appropriate LED state and the current HiBall state: $\hat{x} = [\bar{x}^T, \bar{l}^T]^T$. Similarly, we augment the Kalman filter error covariance matrix with that of the LED filter. We then follow the normal steps outlined in section 5.3, with the result being that the LED portion of the filter state and covariance is updated in accordance with the measurement residual. At the end of the cycle, we extract the LED portions of the state and covariance from the augmented filter, and save them externally. The effect is that, as the system is being used, it continually refines its estimates of the LED positions, thereby continually improving its estimates of the HiBall pose. Again, for additional information, see Welch (1996) and Welch and Bishop (1997).

CLAIM 47	Welch 2001
	Welch 2001 at Section 5.4. The recursive nature of the Kalman filter (section 5.3) requires that the filter be initialized with a known state and corresponding covariance before steady-state operation can begin. Such an initialization (or acquisition) must take place prior to any tracking session, but also upon the (rare) occasion when the filter diverges and "loses lock" as a result of blocked sensor views, for example. Welch 2001 at Section 5.5. The acquisition process is complicated by the fact that each LEPD sees a number of different widely separated views (section 4.1). Therefore, detecting an LED provides at best an ambiguous set of potential LED directions in HiBall coordinates. Moreover, before acquisition, no assumptions can be made to limit the search space of visible LEDs. As such, a relatively slow brute-force algorithm is used to acquire lock. Welch 2001 at Section 5.5. As a result of a mechanical design tradeoff, each sensor field of view is less than six degrees. The focal length is set by the size of the sensor housing, which is set by the diameter of the sensors themselves. Energetics is also a factor, limiting how small the lenses can be while maintaining sufficient light-collecting area. As a result of these design tradeoffs, even a momentary small error in the HiBall pose estimate can cause the recursive estimates to diverge and the system to lose lock after only a few LED sightings. And yet the system is quite robust. In practice, users can jump around, crawl on the floor, lean over, even wave their hands in front of the sensors, and the system does not lose lock. During one session, we were using the HiBall as a 3-D digitization probe, a Hi-Ball on the end of a pencil-shaped fiberglass wand (figure 14, left). We laid the probe down on a table at one point, and were amazed to later notice that it was still tracking, even though it was observing only three or four LEDs near the edge of the ceiling. We picked up the probe and continued using it, without it ever losing lock.   Figure 13.

CLAIM 47	Welch 2001

Figure 14.

Welch 2001 at Section 6.1.

To make measurements of the noise when the HiBall is in motion, we rely on the assumption that almost all of the signal resulting from normal human motion is at frequencies below 2 Hz. We use a high-pass filter (Welch, 1967) on the pose estimates, and assume the output is noise. The resulting statistics are comparable to those made with the HiBall stationary, except at poses for which there are very few LEDs visible in only one or two views. In these poses, near the edge of the ceiling, the geometry of the constraints results in amplification of errors. For nearly all of the working volume of the tracker, the standard deviation of the noise on measurements while the HiBall is still or moving is about 0.2 mm and 0.03 deg.
Welch 2001 at Section 6.1.

During the design of the HiBall system, we made substantial use of simulation, in some domains to a very detailed level. For example, Zemax (Focus Software, 1995) was used extensively in the design and optimization of the optical design, including the design of the filter glass lenses, and geometry of the optical-component layout.
Welch 2001 at Section 6.2.

To produce realistic data for developing and tuning our algorithms, we collected several motion paths (sequences of pose estimates) from our first-generation electro-optical tracker (figure 3) at its 70 Hz maximum report rate. These paths were recorded from both naive users visiting our monthly “demo days” and from experienced users in our labs. . . . we filtered the raw path data with a noncausal zero-phase-shift, low-pass filter to eliminate energy

CLAIM 47	Welch 2001
	above 2 Hz. The output of the low-pass filtering was then resampled at whatever rate we wanted to run the simulated tracker, usually 1,000 Hz. Welch 2001 at Section 6.2. The simulator reads camera models describing the 26 views, the sensor noise parameters, the LED positions and their expected error, and the motion path described above. Before beginning the simulation, the LED positions are perturbed from their ideal positions by adding normally distributed error to each axis. Then, for each simulated cycle of operation, the "true" poses are up- dated using the input motion path. Next, a view is chosen and a visible LED within that view is selected, and the image-plane coordinates of the LED on the chosen sensor are computed using the camera model for the view and the LED as described in section 5.3. These sensor coordinates are then perturbed based on the sensor noise model (section 6.2.1) using the distance and angle to the LED. **These noise-corrupted sensor readings are then fed to the SCAAT filter to produce an up- dated position estimate. The position estimate is com- pared to the true position to produce a scalar error metric that is described next.** Welch 2001 at Section 6.2. The error metric we used combines the error in pose in a way that relates to the effects of tracker error on a head-worn display user. We define a set of points arrayed around the user in a fixed configuration. We compute two sets of coordinates for these points: the true position using the true pose and their estimated position using the estimated pose. The error metric is then the sum of the distances between the true and estimated positions of these points. **By adjusting the distance of the points from the user, we can control the relative importance of the orientation and the position error in the combined error metric. If the distance is small, then the position error is weighted most heavily; if the distance is large, then the orientation error is weighted most heavily. Our two error metrics for the entire run are the square root of the sum of the squares of all the distances, and the peak distance.** Welch 2001 at Section 6.2. *See also* Defendants' Invalidity Contentions for further discussion.

L. DEPENDENT CLAIM 50

CLAIM 50	Welch 2001
[50] The method of claim 47 wherein providing the estimation module includes providing a module that is configurable to use different sets of sensor modules coupled to it.	At least under Plaintiffs' apparent infringement theory, Welch 2001 discloses, either expressly or inherently, the method of claim 47 wherein providing the estimation module includes providing a module that is configurable to use different sets of sensor modules coupled to it. In the alternative, this element would be obvious over Welch 2001 in light of the other references disclosed in Defendants' Invalidity Contentions and/or the knowledge of one of ordinary skill in the art. In all of the optical systems we have developed (see section 1.2), we have chosen what we call an inside-looking-out configuration, in which the optical sensors are on the (moving) user and the landmarks (for instance, the LEDs) are fixed in the laboratory. The corresponding outside-looking-in alternative would be to place the landmarks on the user and to fix the optical sensors in the laboratory. (One can think about similar outside-in and inside-out distinctions for acoustic and magnetic technologies.) The two configurations are depicted in figure 5. Welch 2001 at Section 2.

Exhibit D-6

CLAIM 50	Welch 2001

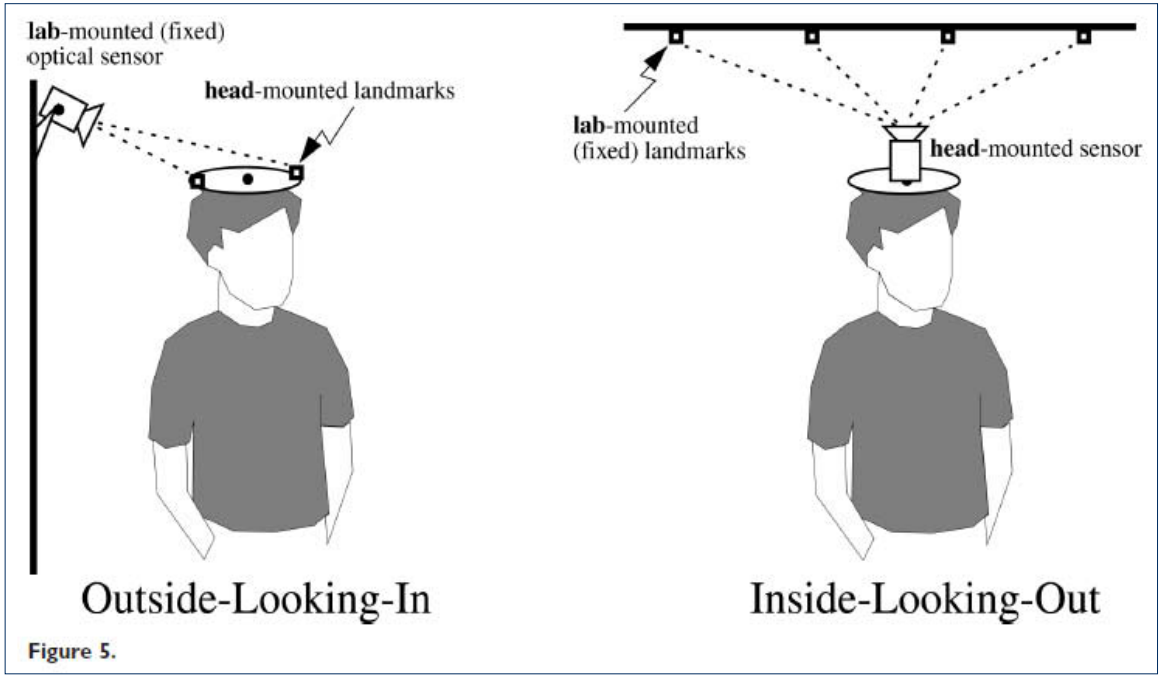

Figure 5.

[T]here are fewer mechanical considerations when mounting sensors in the environment for an outside-looking-in configuration. Because landmarks can be relatively simple, small, and cheap, they can often be located in numerous places on the user, and communication from the user to the rest of the system can be relatively simple or even unnecessary. This is particularly attractive for full-body motion capture.
Welch 2001 at Section 2.

However, there are some significant advantages to the inside-looking-out approach for head tracking. By operating with sensors on the user rather than in the environment, the system can be scaled indefinitely. . . . The inside-looking-out configuration is also motivated by a desire to maximize sensitivity to changes in user pose.
Welch 2001 at Section 2.

The Kalman filter has been used previously to address similar or related problems. . . . A relevant example of a Kalman filter used for sensor fusion in a wide-area tracking system is given in Foxlin et al. (1998), which describes

CLAIM 50	Welch 2001
	a hybrid inertial-acoustic system that is commercially available today (Intersense, 2000). Welch 2001 at Section 5.3 *See* Disclosures with respect to Claim 47, *supra*; *see also* Defendants' Invalidity Contentions for further discussion.

M. DEPENDENT CLAIM 51

CLAIM 51	Welch 2001
[51] The method of claim 47 wherein maintaining estimates of the tracking parameters in the estimation module includes using a stochastic model in the estimation module.	At least under Plaintiffs' apparent infringement theory, Welch 2001 discloses, either expressly or inherently, the method of claim 47 wherein maintaining estimates of the tracking parameters in the estimation module includes using a stochastic model in the estimation module. In the alternative, this element would be obvious over Welch 2001 in light of the other references disclosed in Defendants' Invalidity Contentions and/or the knowledge of one of ordinary skill in the art. Thanks to significant improvements in hardware and software, this HiBall system offers unprecedented speed, resolution, accuracy, robustness, and flexibility. The bulky and heavy sensors and backpack of the previous system have been replaced by a small HiBall unit (figure 4, bottom). In addition, the precisely machined LED ceiling panels of the previous system have been replaced by looser-tolerance panels that are relatively inexpensive to make and simple to install (figure 4, top; figure 10). Finally, we are using an unusual Kalman-filter-based algorithm that generates very accurate pose estimates at a high rate with low latency, and that simultaneously self-calibrates the system. Welch 2001 at Section 1.3.

Exhibit D-6

CLAIM 51	Welch 2001
	  Figure 4. Each HiBall observes LEDs through multiple sensor-lens views that are distributed over a large solid angle. LEDs are sequentially flashed (one at a time) such that they are seen via a diverse set of views for each HiBall. Initial acquisition is performed using a brute-force search through LED space, but, once initial lock is made, the selection of LEDs to flash is tailored to the views of the active HiBall units. **Pose estimates are maintained using a Kalman-filter-based prediction-correction approach known as single-constraint-at-a-time**

Exhibit D-6

CLAIM 51	Welch 2001
	(SCAAT) tracking. This technique has been extended to provide self-calibration of the ceiling, concurrent with HiBall tracking. Welch 2001 at Section 3. We use a Kalman filter (Kalman, 1960) to fuse the measurements into an estimate of the HiBall state x (the pose of the HiBall). We use the Kalman filter—a minimum-variance stochastic estimator—both because the sensor measurement noise and the typical user-motion dynamics can be modeled as normally distributed random processes, and because we want an efficient online method of estimation. Welch 2001 at Section 5.3. The Kalman filter has been used previously to address similar or related problems. . . . A relevant example of a Kalman filter used for sensor fusion in a wide-area tracking system is given in Foxlin et al. (1998), which describes a hybrid inertial-acoustic system that is commercially available today (Intersense, 2000). Welch 2001 at Section 5.3. The SCAAT approach, on the other hand, is an attempt to reverse this cycle. Because we intentionally use a single constraint per estimate, the algorithmic complexity is drastically reduced, which reduces the execution time, and hence the amount of motion between estimation cycles. Because the amount of motion is limited, we are able to use a simple dynamic (process) model in the Kalman filter, which further simplifies the computations. In short, the simplicity of the approach means that it can run very fast, which means it can pro- duce estimates very rapidly, with low noise. Welch 2001 at Section 5.3. The Kalman filter requires both a model of the process dynamics and a model of the relationship between the process state and the available measurements. In part due to the simplicity of the SCAAT approach, we are able to use a simple position-velocity (PV) process model (Brown & Hwang, 1992). . . . We model the continuous change in the HiBall state with the simple differential equation

CLAIM 51	Welch 2001
	$$\frac{d}{dt}\bar{x}(t) = \begin{bmatrix} 0 & 1 \\ 0 & 0 \end{bmatrix}\begin{bmatrix} x_p(t) \\ x_v(t) \end{bmatrix} + \begin{bmatrix} 0 \\ \mu \end{bmatrix} u(t), \qquad (1)$$ where $u(t)$ is a normally distributed white (in the frequency spectrum) scalar noise process, and the scalar μ represents the magnitude or spectral density of the noise. We use a similar model with a distinct noise process for each of the six pose elements. We determine the individual noise magnitudes using an offline simulation of the system and a nonlinear optimization strategy that seeks to minimize the variance between the estimated pose and a known motion path. (See section 6.2.2.). Welch 2001 at Section 5.3. The recursive nature of the Kalman filter (section 5.3) requires that the filter be initialized with a known state and corresponding covariance before steady-state operation can begin. Such an initialization (or acquisition) must take place prior to any tracking session, but also upon the (rare) occasion when the filter diverges and "loses lock" as a result of blocked sensor views, for example. Welch 2001 at Section 5.5. *See* Disclosures with respect to Claim 47, *supra*; *see also* Defendants' Invalidity Contentions for further discussion.

N. DEPENDENT CLAIM 52

CLAIM 52	Welch 2001
[52] The method of claim 51 wherein using a stochastic model	At least under Plaintiffs' apparent infringement theory, Welch 2001 discloses, either expressly or inherently, the method of claim 51 wherein using a stochastic model includes implementing some or all of a Kalman filter in the

CLAIM 52	Welch 2001
includes implementing some or all of a Kalman filter in the estimation module.	estimation module. In the alternative, this element would be obvious over Welch 2001 in light of the other references disclosed in Defendants' Invalidity Contentions and/or the knowledge of one of ordinary skill in the art. *See, e.g.*: Thanks to significant improvements in hardware and software, this HiBall system offers unprecedented speed, resolution, accuracy, robustness, and flexibility. The bulky and heavy sensors and backpack of the previous system have been replaced by a small HiBall unit (figure 4, bottom). In addition, the precisely machined LED ceiling panels of the previous system have been replaced by looser-tolerance panels that are relatively inexpensive to make and simple to install (figure 4, top; figure 10). Finally, we are using an unusual Kalman-filter-based algorithm that generates very accurate pose estimates at a high rate with low latency, and that simultaneously self-calibrates the system. Welch 2001 at Section 1.3.

Exhibit D-6

CLAIM 52	Welch 2001
	  Figure 4. Each HiBall observes LEDs through multiple sensor-lens views that are distributed over a large solid angle. LEDs are sequentially flashed (one at a time) such that they are seen via a diverse set of views for each HiBall. Initial acquisition is performed using a brute-force search through LED space, but, once initial lock is made, the selection of LEDs to flash is tailored to the views of the active HiBall units. Pose estimates are maintained using a Kalman-filter-based prediction-correction approach known as single-constraint-at-a-time (SCAAT) tracking.

Exhibit D-6

CLAIM 52	Welch 2001
	This technique has been extended to provide self-calibration of the ceiling, concurrent with HiBall tracking. Welch 2001 at Section 3. **We use a Kalman filter (Kalman, 1960) to fuse the measurements into an estimate of the HiBall state x (the pose of the HiBall). We use the Kalman filter—a minimum-variance stochastic estimator—both because the sensor measurement noise and the typical user-motion dynamics can be modeled as normally distributed random processes, and because we want an efficient online method of estimation.** Welch 2001 at Section 5.3. **The Kalman filter has been used previously to address similar or related problems. . . . A relevant example of a Kalman filter used for sensor fusion in a wide-area tracking system is given in Foxlin et al. (1998), which describes a hybrid inertial-acoustic system that is commercially available today (Intersense, 2000).** Welch 2001 at Section 5.3. The SCAAT approach, on the other hand, is an attempt to reverse this cycle. Because we intentionally use a single constraint per estimate, the algorithmic complexity is drastically reduced, which reduces the execution time, and hence the amount of motion between estimation cycles. Because the amount of motion is limited, we are able to use a simple dynamic (process) model in the Kalman filter, which further simplifies the computations. In short, the simplicity of the approach means that it can run very fast, which means it can pro- duce estimates very rapidly, with low noise. Welch 2001 at Section 5.3. **The Kalman filter requires both a model of the process dynamics and a model of the relationship between the process state and the available measurements.** In part due to the simplicity of the SCAAT approach, we are able to use a simple position-velocity (PV) process model (Brown & Hwang, 1992). . . . We model the continuous change in the HiBall state with the simple differential equation

Exhibit D-6

CLAIM 52	Welch 2001

$$\frac{d}{dt}\bar{x}(t) = \begin{bmatrix} 0 & 1 \\ 0 & 0 \end{bmatrix}\begin{bmatrix} x_p(t) \\ x_v(t) \end{bmatrix} + \begin{bmatrix} 0 \\ \mu \end{bmatrix} u(t), \qquad (1)$$

where $u(t)$ is a normally distributed white (in the frequency spectrum) scalar noise process, and the scalar μ represents the magnitude or spectral density of the noise. We use a similar model with a distinct noise process for each of the six pose elements. We determine the individual noise magnitudes using an offline simulation of the system and a nonlinear optimization strategy that seeks to minimize the variance between the estimated pose and a known motion path. (See section 6.2.2.).

Welch 2001 at Section 5.3.

The online measurements (section 5.2) are used to estimate the pose of the HiBall during operation. The 1991 system collected a group of diverse measurements for a variety of LEDs and sensors, and then used a method of simultaneous nonlinear equations called collinearity (Azuma & Ward, 1991) to estimate the pose of the sensor fixture shown in figure 3 (bottom).
Welch 2001 at Section 5.3.

In contrast, the approach we use with the new HiBall system produces tracker reports as each new measurement is made, rather than waiting to form a complete collection of observations. Because single measurements underconstrain the mathematical solution, we refer to the approach as single-constraint-at-a-time (SCAAT) tracking (Welch, 1996; Welch & Bishop, 1997). The key is that the single measurements provide some information about the HiBall's state, and thus can be used to incrementally improve a previous estimate. We intentionally fuse each individual "insufficient" measurement immediately as it is obtained. **With this approach, we are able to generate estimates more frequently, with less latency, and with improved accuracy, and we are able to estimate the LED positions online concurrently while tracking the HiBall (section 5.4).**
Welch 2001 at Section 5.3.

CLAIM 52	Welch 2001
	[O]ne key benefit warrants discussion here. There is a direct relationship between the complexity of the estimation algorithm, the corresponding speed (execution time per estimation cycle), and the change in HiBall pose between estimation cycles (figure 12). As the algorithmic complexity increases, the execution time increases, which allows for significant nonlinear HiBall motion between estimation cycles, which in turn implies the need for a more complex estimation algorithm. Welch 2001 at Section 5.3.  Figure 12. **The recursive nature of the Kalman filter (section 5.3) requires that the filter be initialized with a known state and corresponding covariance before steady-state operation can begin.** Such an initialization (or acquisition) must take place prior to any tracking session, but also upon the (rare) occasion when the filter diverges and "loses lock" as a result of blocked sensor views, for example. Welch 2001 at Section 5.5.

CLAIM 52	Welch 2001
	See Disclosures with respect to Claim 51, *supra*; *see also* Defendants' Invalidity Contentions for further discussion.

O. DEPENDENT CLAIM 53

CLAIM 53	Welch 2001
[53] The method of claim 52 wherein implementing some or all of the Kalman filter includes updating error estimates using linearized models of the sensor system.	At least under Plaintiffs' apparent infringement theory, Welch 2001 discloses, either expressly or inherently, the method of claim 52 wherein implementing some or all of the Kalman filter includes updating error estimates using linearized models of the sensor system. In the alternative, this element would be obvious over Welch 2001 in light of the other references disclosed in Defendants' Invalidity Contentions and/or the knowledge of one of ordinary skill in the art. *See, e.g.*: Thanks to significant improvements in hardware and software, this HiBall system offers unprecedented speed, resolution, accuracy, robustness, and flexibility. The bulky and heavy sensors and backpack of the previous system have been replaced by a small HiBall unit (figure 4, bottom). In addition, the precisely machined LED ceiling panels of the previous system have been replaced by looser-tolerance panels that are relatively inexpensive to make and simple to install (figure 4, top; figure 10). Finally, we are using an unusual Kalman-filter-based algorithm that generates very accurate pose estimates at a high rate with low latency, and that simultaneously self-calibrates the system. Welch 2001 at Section 1.3.

Exhibit D-6

CLAIM 53	Welch 2001
	  Figure 4. Each HiBall observes LEDs through multiple sensor-lens views that are distributed over a large solid angle. LEDs are sequentially flashed (one at a time) such that they are seen via a diverse set of views for each HiBall. Initial acquisition is performed using a brute-force search through LED space, but, once initial lock is made, the selection of LEDs to flash is tailored to the views of the active HiBall units. **Pose estimates are maintained using a Kalman-filter-based prediction-correction approach known as single-constraint-at-a-time**

Exhibit D-6

CLAIM 53	Welch 2001
	(SCAAT) tracking. This technique has been extended to provide self-calibration of the ceiling, concurrent with HiBall tracking. Welch 2001 at Section 3. **We use a Kalman filter (Kalman, 1960) to fuse the measurements into an estimate of the HiBall state x (the pose of the HiBall). We use the Kalman filter—a minimum-variance stochastic estimator—both because the sensor measurement noise and the typical user-motion dynamics can be modeled as normally distributed random processes, and because we want an efficient online method of estimation.** Welch 2001 at Section 5.3. **The Kalman filter has been used previously to address similar or related problems. . . . A relevant example of a Kalman filter used for sensor fusion in a wide-area tracking system is given in Foxlin et al. (1998), which describes a hybrid inertial-acoustic system that is commercially available today** (Intersense, 2000). Welch 2001 at Section 5.3. The SCAAT approach, on the other hand, is an attempt to reverse this cycle. Because we intentionally use a single constraint per estimate, the algorithmic complexity is drastically reduced, which reduces the execution time, and hence the amount of motion between estimation cycles. Because the amount of motion is limited, we are able to use a simple dynamic (process) model in the Kalman filter, which further simplifies the computations. In short, the simplicity of the approach means that it can run very fast, which means it can pro- duce estimates very rapidly, with low noise. Welch 2001 at Section 5.3. **The Kalman filter requires both a model of the process dynamics and a model of the relationship between the process state and the available measurements.** In part due to the simplicity of the SCAAT approach, we are able to use a simple position-velocity (PV) process model (Brown & Hwang, 1992). . . . We model the continuous change in the HiBall state with the simple differential equation

CLAIM 53	Welch 2001
	$$\frac{d}{dt}\bar{x}(t) = \begin{bmatrix} 0 & 1 \\ 0 & 0 \end{bmatrix}\begin{bmatrix} x_p(t) \\ x_v(t) \end{bmatrix} + \begin{bmatrix} 0 \\ \mu \end{bmatrix} u(t), \qquad (1)$$ where $u(t)$ is a normally distributed white (in the frequency spectrum) scalar noise process, and the scalar μ represents the magnitude or spectral density of the noise. We use a similar model with a distinct noise process for each of the six pose elements. We determine the individual noise magnitudes using an offline simulation of the system and a nonlinear optimization strategy that seeks to minimize the variance between the estimated pose and a known motion path. (See section 6.2.2.). Welch 2001 at Section 5.3. **The recursive nature of the Kalman filter (section 5.3) requires that the filter be initialized with a known state and corresponding covariance before steady-state operation can begin.** Such an initialization (or acquisition) must take place prior to any tracking session, but also upon the (rare) occasion when the filter diverges and "loses lock" as a result of blocked sensor views, for example. Welch 2001 at Section 5.5. *See* Disclosures with respect to Claim 52, *supra*; *see also* Defendants' Invalidity Contentions for further discussion.

P. DEPENDENT CLAIM 59

CLAIM 59	Welch 2001
[59] The method of claim 47 wherein providing configuration	At least under Plaintiffs' apparent infringement theory, Welch 2001 discloses, either expressly or inherently, the method of claim 47 wherein providing configuration information from the sensor modules includes providing information characterizing a type of a sensor associated with a sensor module. In the alternative, this element

CLAIM 59	Welch 2001
information from the sensor modules includes providing information characterizing a type of a sensor associated with a sensor module.	would be obvious over Welch 2001 in light of the other references disclosed in Defendants' Invalidity Contentions and/or the knowledge of one of ordinary skill in the art. *See* Disclosures with respect to Claim 47, *supra*; *see also* Defendants' Invalidity Contentions for further discussion.

Q. DEPENDENT CLAIM 60

CLAIM 60	Welch 2001
[60] The method of claim 47 wherein providing configuration information from the sensor modules includes providing information characterizing a position or an orientation of a sensor associated with a sensor module.	At least under Plaintiffs' apparent infringement theory, Welch 2001 discloses, either expressly or inherently, the method of claim 47 wherein providing configuration information from the sensor modules includes providing information characterizing a position or an orientation of a sensor associated with a sensor module. In the alternative, this element would be obvious over Welch 2001 in light of the other references disclosed in Defendants' Invalidity Contentions and/or the knowledge of one of ordinary skill in the art. *See, e.g.*: As part of his 1984 dissertation on Self-Tracker, Bishop put forward the idea of outward-looking tracking systems based on user-mounted sensors that estimate user pose by observing landmarks in the environment (Bishop, 1984). He described two kinds of landmarks: high signal-to-noise-ratio beacons such as light-emitting diodes (LEDs) and low signal-to-noise- ratio landmarks such as naturally occurring features. Bishop designed and demonstrated custom VLSI chips (figure 2) that combined image sensing and processing on a single chip (Bishop & Fuchs, 1984). The idea was to combine multiple instances of these chips into an outward-looking cluster that estimated cluster motion by observing natural features in the unmodified environment. Integrating the resulting motion to estimate pose is prone to accumulating error, so further development required a complementary system based on easily detectable landmarks (LEDs) at known locations. Welch 2001 at Section 1.2. In this article, we describe a new and vastly improved version of the 1991 system. We call the new system the HiBall Tracking System. Thanks to significant improvements in hardware and software, this HiBall system offers unprecedented speed, resolution, accuracy, robustness, and flexibility. The bulky and heavy sensors and backpack

CLAIM 60	Welch 2001
	of the previous system have been replaced by a small HiBall unit (figure 4, bottom). In addition, the precisely machined LED ceiling panels of the previous system have been replaced by looser-tolerance panels that are relatively inexpensive to make and simple to install (figure 4, top; figure 10). Finally, we are using an unusual Kalman-filter-based algorithm that generates very accurate pose estimates at a high rate with low latency, and that simultaneously self-calibrates the system. As a result of these improvements, the HiBall Tracking System can generate more than 2,000 pose estimates per second, with less than 1 ms of latency, better than 0.5 mm and 0.03 deg. of absolute error and noise, everywhere in a 4.5 m x 8.5 m room (with more than two meters of height variation). The area can be expanded by adding more panels, or by using checker-board configurations that spread panels over a larger area. The weight of the user-worn HiBall is approximately 300 grams, making it lighter than one optical sensor in the 1991 system. Multiple HiBall units can be daisy-chained together for head or hand tracking, pose-aware input devices, or precise 3-D point digitization throughout the entire working volume. Welch 2001 at Section 1.3. The LEPDs themselves are not imaging devices; rather, they detect the centroid of the luminous flux incident on the detector. The x-position of the centroid determines the ratio of two output y-position determines the ratio of two other output currents. The total output current of each pair are commensurate and are proportional to the total incident flux. Consequently, focus is not an issue, so the simple fixed-focus lenses work well over a range of LED distances from about half a meter to infinity. **The LEPDs and associated electronic components are mounted on a custom rigid-flex printed circuitboard (figure 8)**. This arrangement makes efficient use of the internal HiBall volume while maintaining isolation between analog and digital circuitry, and increasing reliability by alleviating the need for intercomponent mechanical connectors. Welch 2001 at Section 4.1.

Exhibit D-6

CLAIM 60	Welch 2001
	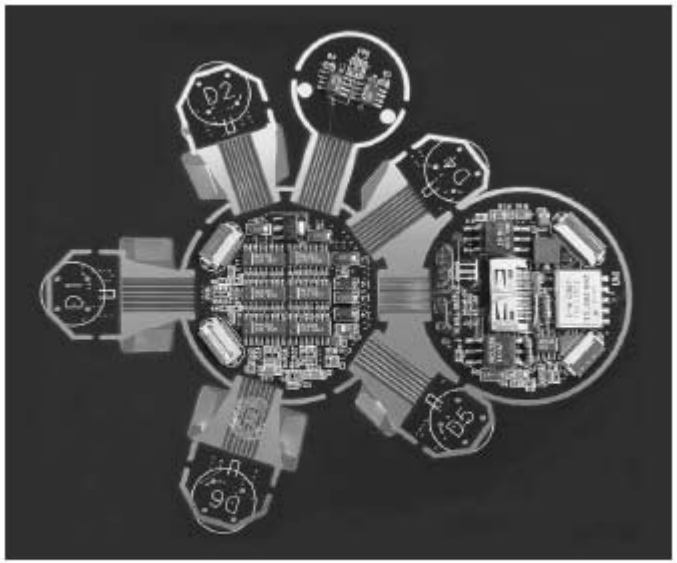 Figure 8. **Figure 9 shows the physical arrangement of the folded electronics in the HiBall. Each LEPD has four transimpedance amplifiers (shown together as one "Amp" in figure 9), the analog outputs of which are multiplexed with those of the other LEPDs, then sampled, held, and converted by four 16-bit Delta-Sigma analog-to-digital (A/D) converters.** Multiple samples are integrated via an accumulator. The digitized LEPD data are organized into packets for communication back to the CIB. The packets also contain information to assist in error detection. The communication protocol is simple, and, while presently implemented by wire, the modulation scheme is amenable to a wireless implementation. Welch 2001 at Section 4.1.

Exhibit D-6

CLAIM 60	Welch 2001

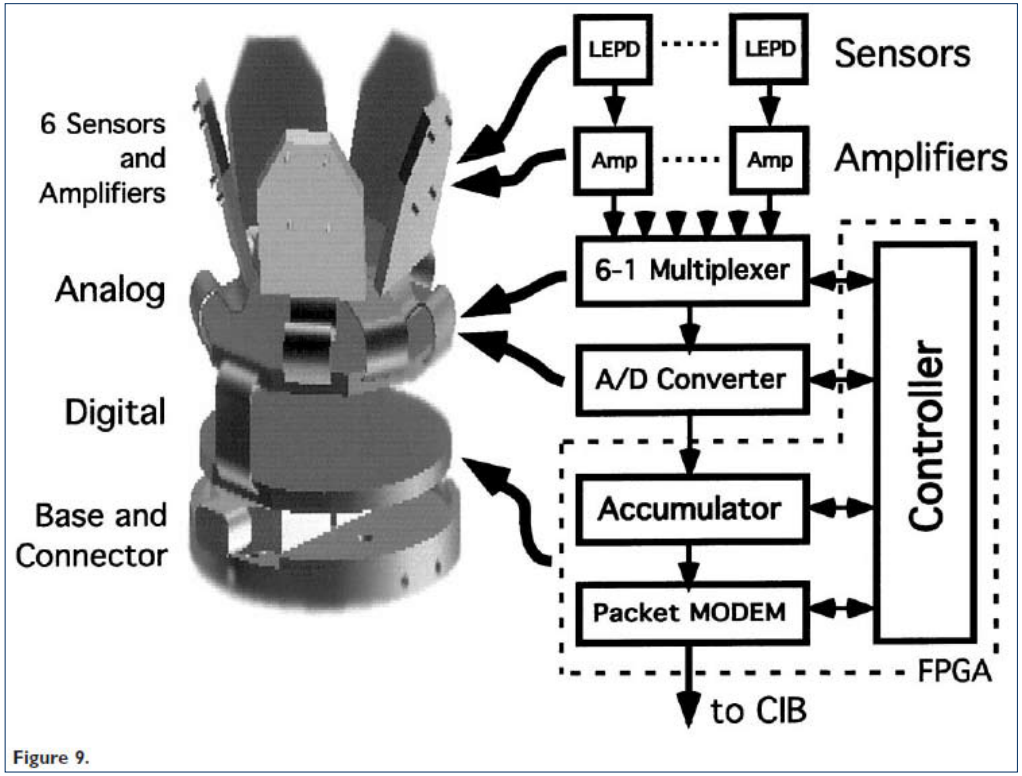

Figure 9.

The design results in a ceiling with a rectangular LED pattern with periods of 7.6 cm and 15.2 cm. This spacing is used for the initial estimates of the LED positions in the lab; then, during normal operation, the SCAAT algorithm continually refines the LED position estimates (section 5.4). The SCAAT autocalibration not only relaxes design and installation constraints, but provides greater precision in the face of initial and ongoing uncertainty in the ceiling structure.
Welch 2001 at Section 4.2.

The CIB comprises analog drive and receive components as well as digital logic components. The digital components implement store and forward in both directions and synchronize the timing of the LED "on" interval within the HiBall dark-light-dark intervals (section 5.2). The protocol supports full-duplex flow control. The data

Exhibit D-6

CLAIM 60	Welch 2001
	are arranged into packets that incorporate error detection. Welch 2001 at Section 4.3. **After each HiBall is assembled, we perform an off- line calibration procedure to determine the correspondence between image-plane coordinates and rays in space. This involves more than just determining the view transform for each of the 26 views. Nonlinearities in the silicon sensor and distortions in the lens (such as spherical aberration) cause significant deviations from a simple pinhole camera model. We dealt with all of these issues through the use of a two-part camera model.** The first part is a standard pinhole camera represented by a 3 X 4 matrix. The second part is a table mapping real image-plane coordinates to ideal image-plane coordinates. Welch 2001 at Section 5.1. Both parts of the camera model are determined using a calibration procedure that relies on a goniometer (an angular positioning system) of our own design. This device consists of two servo motors mounted together such that one motor provides rotation about the vertical axis while the second motor provides rotation about an axis orthogonal to vertical. An important characteristic of the goniometer is that the rotational axes of the two motors intersect at a point at the center of the HiBall optical sphere; this point is defined as the origin of the HiBall. . . . The rotational positioning motors were rated to provide twenty arc-second precision; we further calibrated them to six arc seconds using a laboratory grade theodolite—an angle measuring system. Welch 2001 at Section 5.1. **The online measurements (section 5.2) are used to estimate the pose of the HiBall during operation.** The 1991 system collected a group of diverse measurements for a variety of LEDs and sensors, and then used a method of simultaneous nonlinear equations called collinearity (Azuma & Ward, 1991) to estimate the pose of the sensor fixture shown in figure 3 (bottom). Welch 2001 at Section 5.3.

Exhibit D-6

CLAIM 60	Welch 2001

The method we now use for autocalibration involves defining a distinct SCAAT Kalman filter for each LED. Specifically, for each LED, we maintain a state $\bar{l}$ (estimate of the 3-D position) and a 3×3 Kalman filter covariance. At the beginning of each estimation cycle, we form an augmented state vector $\hat{x}$ using the appropriate LED state and the current HiBall state: $\hat{x} = [\bar{x}^T, \bar{l}^T]^T$. Similarly, we augment the Kalman filter error covariance matrix with that of the LED filter. We then follow the normal steps outlined in section 5.3, with the result being that the LED portion of the filter state and covariance is updated in accordance with the measurement residual. At the end of the cycle, we extract the LED portions of the state and covariance from the augmented filter, and save them externally. The effect is that, as the system is being used, it continually refines its estimates of the LED positions, thereby continually improving its estimates of the HiBall pose. Again, for additional information, see Welch (1996) and Welch and Bishop (1997).

Welch 2001 at Section 5.4.

The simulator reads camera models describing the 26 views, the sensor noise parameters, the LED positions and their expected error, and the motion path described above. Before beginning the simulation, the LED positions are perturbed from their ideal positions by adding normally distributed error to each axis. Then, for each simulated cycle of operation, the "true" poses are up- dated using the input motion path. Next, a view is chosen and a visible LED within that view is selected, and the image-plane coordinates of the LED on the chosen sensor are computed using the camera model for the view and the LED as described in section 5.3. These

CLAIM 60	Welch 2001
	sensor coordinates are then perturbed based on the sensor noise model (section 6.2.1) using the distance and angle to the LED. These noise-corrupted sensor readings are then fed to the SCAAT filter to produce an up- dated position estimate. The position estimate is com- pared to the true position to produce a scalar error metric that is described next. Welch 2001 at Section 6.2. The error metric we used combines the error in pose in a way that relates to the effects of tracker error on a head-worn display user. We define a set of points arrayed around the user in a fixed configuration. We compute two sets of coordinates for these points: the true position using the true pose and their estimated position using the estimated pose. The error metric is then the sum of the distances between the true and estimated positions of these points. By adjusting the distance of the points from the user, we can control the relative importance of the orientation and the position error in the combined error metric. If the distance is small, then the position error is weighted most heavily; if the distance is large, then the orientation error is weighted most heavily. Our two error metrics for the entire run are the square root of the sum of the squares of all the distances, and the peak distance. Welch 2001 at Section 6.2. *See* Disclosures with respect to Claim 47, *supra*; *see also* Defendants' Invalidity Contentions for further discussion.

R. DEPENDENT CLAIM 61

CLAIM 61	Welch 2001
[61] The method of claim 47 wherein providing configuration information from the sensor modules includes providing information characterizing one or more calibration parameters of a sensor	At least under Plaintiffs' apparent infringement theory, Welch 2001 discloses, either expressly or inherently, the method of claim 47 wherein providing configuration information from the sensor modules includes providing information characterizing one or more calibration parameters of a sensor associated with a sensor module. In the alternative, this element would be obvious over Welch 2001 in light of the other references disclosed in Defendants' Invalidity Contentions and/or the knowledge of one of ordinary skill in the art. *See, e.g.*: Thanks to significant improvements in hardware and software, this HiBall system offers unprecedented speed, resolution, accuracy, robustness, and flexibility. The bulky and heavy sensors and backpack of the previous system have been replaced by a small HiBall unit (figure 4, bottom). In addition, the precisely machined LED

CLAIM 61	Welch 2001
associated with a sensor module.	ceiling panels of the previous system have been replaced by looser-tolerance panels that are relatively inexpensive to make and simple to install (figure 4, top; figure 10). Finally, we are using an unusual Kalman-filter-based algorithm that generates very accurate pose estimates at a high rate with low latency, and that simultaneously self-calibrates the system. Welch 2001 at Section 1.3.  Figure 4.

Exhibit D-6

CLAIM 61	Welch 2001
	Each HiBall observes LEDs through multiple sensor-lens views that are distributed over a large solid angle. LEDs are sequentially flashed (one at a time) such that they are seen via a diverse set of views for each HiBall. Initial acquisition is performed using a brute-force search through LED space, but, once initial lock is made, the selection of LEDs to flash is tailored to the views of the active HiBall units. Pose estimates are maintained using a Kalman-filter-based prediction-correction approach known as single-constraint-at-a-time (SCAAT) tracking. This technique has been extended to provide self-calibration of the ceiling, concurrent with HiBall tracking. Welch 2001 at Section 3. The design results in a ceiling with a rectangular LED pattern with periods of 7.6 cm and 15.2 cm. **This spacing is used for the initial estimates of the LED positions in the lab; then, during normal operation,** the SCAAT algorithm continually refines the LED position estimates (section 5.4). The SCAAT autocalibration not only relaxes design and installation constraints, but provides greater precision in the face of initial and ongoing uncertainty in the ceiling structure. Welch 2001 at Section 4.2. The CIB comprises analog drive and receive components as well as digital logic components. The digital components implement store and forward in both directions and synchronize the timing of the LED "on" interval within the HiBall dark-light-dark intervals (section 5.2). The protocol supports full-duplex flow control. The data are arranged into packets that incorporate error detection. Welch 2001 at Section 4.3. After each HiBall is assembled, we perform an off- line calibration procedure to determine the correspondence between image-plane coordinates and rays in space. This involves more than just determining the view transform for each of the 26 views. Nonlinearities in the silicon sensor and distortions in the lens (such as spherical aberration) cause significant deviations from a simple pinhole camera model. We dealt with all of these issues through the use of a two-part camera model. The first part is a standard pinhole camera represented by a 3 X 4 matrix. The second part is a table mapping real image-plane coordinates to ideal image-plane coordinates. Welch 2001 at Section 5.1. Both parts of the camera model are determined using a calibration procedure that relies on a goniometer (an angular positioning system) of our own design. This device consists of two servo motors mounted together such that one motor provides rotation about the vertical axis while the second motor provides rotation about an axis orthogonal to vertical. An important characteristic of the goniometer is that the rotational axes of the two motors intersect at a point at the center of the HiBall optical sphere; this point is defined as the origin of the HiBall. . . .

Exhibit D-6

CLAIM 61	Welch 2001
	The rotational positioning motors were rated to provide twenty arc-second precision; **we further calibrated them to six arc seconds using a laboratory grade theodolite—an angle measuring system.** Welch 2001 at Section 5.1. The method we now use for autocalibration involves defining a distinct SCAAT Kalman filter for each LED. Specifically, for each LED, we maintain a state $\bar{l}$ (estimate of the 3-D position) and a 3×3 Kalman filter covariance. At the beginning of each estimation cycle, we form an augmented state vector $\hat{x}$ using the appropriate LED state and the current HiBall state: $\hat{x} = [\bar{x}^T, \bar{l}^T]^T$. Similarly, we augment the Kalman filter error covariance matrix with that of the LED filter. We then follow the normal steps outlined in section 5.3, with the result being that the LED portion of the filter state and covariance is updated in accordance with the measurement residual. At the end of the cycle, we extract the LED portions of the state and covariance from the augmented filter, and save them externally. The effect is that, as the system is being used, it continually refines its estimates of the LED positions, thereby continually improving its estimates of the HiBall pose. Again, for additional information, see Welch (1996) and Welch and Bishop (1997). Welch 2001 at Section 5.4. *See* Disclosures with respect to Claim 47, *supra*; *see also* Defendants' Invalidity Contentions for further discussion.